Self-organizing energy-autonomous systems

Liu, Qingzhi

DOI
10.4233/uuid:a30f03a2-ea65-44fe-9e63-1551e2722450

Publication date
2016

Document Version
Final published version

Citation (APA)
Liu, Q. (2016). *Self-organizing energy-autonomous systems*. [Dissertation (TU Delft), Delft University of Technology]. https://doi.org/10.4233/uuid:a30f03a2-ea65-44fe-9e63-1551e2722450

SELF-ORGANIZING ENERGY-AUTONOMOUS SYSTEMS

SELF-ORGANIZING ENERGY-AUTONOMOUS SYSTEMS

Proefschrift

ter verkrijging van de graad van doctor
aan de Technische Universiteit Delft,
op gezag van de Rector Magnificus prof. ir. K.C.A.M. Luyben,
voorzitter van het College voor Promoties,
in het openbaar te verdedigen op vrijdag 2 december 2016 om 12:30 uur

door

Qingzhi LIU

Master of Science in Embedded Systems, Delft, Nederland,
geboren te Xi'an, China.

Dit proefschrift is goedgekeurd door de

Promotor: Prof. Dr. F. M. Brazier
Promotor: Prof. Dr. K. G. Langendoen
Copromotor: Dr. M. E. Warnier
Copromotor: Dr. P. Pawełczak

Samenstelling promotiecommissie:

Rector Magnificus,	voorzitter
Prof. Dr. F. M. Brazier,	Technische Universiteit Delft
Prof. Dr. K. G. Langendoen,	Technische Universiteit Delft
Dr. M. E. Warnier,	Technische Universiteit Delft
Dr. P. Pawełczak,	Technische Universiteit Delft
Onafhankelijke leden:	
Prof. Dr. W. A. Serdijn,	Technische Universiteit Delft
Prof. Dr. M. Aiello,	Rijksuniversiteit Groningen
Prof. Dr. G. Dolmans,	Technische Universiteit Eindhoven
Dr. A. Bletsas,	Technical University of Crete

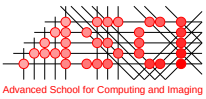

This work was carried out in the ASCI graduate school of TUDelft.
ASCI dissertation series number: 363

Cover design by: Qingzhi Liu

Printed by: Ipskamp Printing

ISBN/EAN: 978-94-6186-762-9

Science is a wonderful thing
if one does not have to earn one's living at it.

Albert Einstein

CONTENTS

SUMMARY

With the rapid development of mobile technology, more and more devices connect to the Internet of Things (IoT). The management of such large-scale networks becomes a challenge. Firstly, a large number of heterogeneous devices are distributed over a wide area, leading to a variation of the requirements of users, the performance of mobile devices, and the application scenarios. As the size of the IoT increases, the complexity of controlling such systems becomes a challenge. Most existing solutions choose global control, and are designed for a specific type of application scenario. However, any changes in the network, e.g. topology, node density, etc., affect the control schedule of the central node. Once the context changes beyond the adaptation ability, the system can hardly function anymore. Furthermore, the center node is the single break point in the control structure. Therefore, it is critical to find a solution with autonomous management, in which networks are organized and controlled by the local management of each node.

Secondly, maintaining the power supply for a large number of battery-operated mobile devices in the IoT becomes a challenge. The most direct solution is to replace batteries of devices periodically. However, this costs much money, time, and human resources. Increasing the size of the battery is another commonly used approach, but this enlarges the form and weight of devices, which is unsuitable for application scenarios where size and weight of devices should be minimized. Therefore, we need an approach where devices have autonomous energy, in which batteries of mobile devices can be wirelessly charged.

Based on the motivation above, the research of this dissertation is positioned in the area of autonomic computing. The proposed systems are self-adaptive self-organized and use radio-frequency based wireless power transfer. Specifically, nodes in the network can achieve global operation, based on local information exchange and control of each node, and increase battery lifetime by harvesting energy from transmitted radio waves and decreasing the duty cycle of radio in the communication protocol.

In the area of self-adaptive self-organization systems, we explore controlling networks based on local information exchange. The global operation of the whole network is controlled by local management of each node. The advantage is that nodes do not need to collect a large amount of global information, which largely decreases the communication complexity of the network. We leverage this mechanism in two case studies. First, we target data aggregation in mobile networks. Our algorithm uses evolutionary dynamics to select and spread the configuration of each node, and the network automatically adapts to the variation of application scenarios. The network can optimize configurations without predesigned setup for a specific scenario. In the second case study, we design an algorithm to achieve distance estimation with self-organization in large-scale mobile networks. The algorithm uses messages collected by local information exchange for statistical calculation, and the network collectively estimates distances between nodes in the network. This improves the accuracy and extends the application area of the existing

distance estimation approaches.

In the area of wireless power transfer systems, the main contribution is based on the exploration of increasing the efficiency of energy transmission and utilization in mobile devices using radio-frequency based wireless power transfer. First of all, we exploit the properties of active and backscatter radio for increasing the energy efficiency of harvesters. We demonstrate the world's first hybrid radio platform that combines the strengths of active radio (long range and robustness to interference) and backscatter radio (low power consumption). We design a switching mechanism that selects active radio or backscatter radio for different radio channel qualities. The measurement results on mobile devices prove that harvesting and saving radio energy is not the only choice to provide autonomous energy, and that backscatter radio for communication is more energy efficient for some applications on mobile devices. Second, we save energy on the charger side to make wireless power transfer green. Wireless power transfer based on radio frequency radiation and rectification is fairly inefficient due to power decaying with distance, antenna polarization, etc. To save energy in chargers, we monitor the idle charging state in wireless power transfer networks and switch off the energy transmitters when the received energy is too low for rectification. Although this system does not directly increase the efficiency of the radio harvesting process, the saved energy in chargers largely boosts the energy efficiency of the whole wireless power transfer network. The system is especially valuable for increasing the lifetime of mobile chargers powered by batteries. Finally, to demonstrate the value of energy autonomy in real applications, we select indoor localization using wireless power transfer as a case study. We design a battery-less indoor localization system that can operate perpetually under wireless power transfer. The novel localization method operates at energy levels that are within the energy budget provided by wireless power transfer today, and the communication schedule is well-designed to minimize the amount of idle listening. We use off-the-shelf devices to implement and deploy the system. It proves the feasibility of using long-range wireless power transfer for mobile systems.

SAMENVATTING

Met de snelle ontwikkeling van mobiele technologie staan steeds meer apparaten in verbinding met het Internet of Things (IoT, Internet der Dingen). Het beheren van zulke grootschalige netwerken wordt een uitdaging. In de eerste plaats zal er sprake zijn van een wijdverbreide verspreiding van een grote diversiteit aan apparaten. Dit zal leiden tot een variatie van de behoeften van gebruikers, van de prestaties van mobiele apparaten en van de toepassingsscenario's. Naarmate de omvang van het IoT toeneemt, wordt de complexiteit van het beheersen van dergelijke systemen een uitdaging. De meeste systemen kiezen voor een gecentraliseerde aanpak, en zijn toepassing specifiek. Echter veranderingen in het netwerk, zoals bijvoorbeeld de topologie, knooppuntdichtheid, etc., zijn van invloed op het schema van het centrale beheerseenheid. Maar wanneer de omstandigheden meer veranderen dan het aanpassingsvermogen kan verwerken, kan het systeem nauwelijks meer functioneren. Bovendien is het centrale knooppunt de zwakken schakel (breekpunt) in de beheersstructuur. Daarom is het van cruciaal belang een oplossing te vinden door middel van autonoom management waarbij netwerken worden georganiseerd en aangestuurd door het lokaal beheer van elk knooppunt.

In de tweede plaats zal het in stand houden van de stroomvoorziening voor een groot aantal mobiele apparatenwerkend op batterijen in het IoT een uitdaging worden. De meest directe oplossing is het regelmatig vervangen van de batterijen van een apparaat. Dit kost echter veel geld, tijd en personele middelen. Het vergroten van de batterijcapaciteit is een tweede, veel gebruikte methode. Hierdoor echter nemen het formaat en het gewicht van apparaten toe wat ongeschikt is voor applicatiescenario's waarbij de afmeting en gewicht tot een minimum beperkt moeten worden. Daarom hebben we een methode nodig waarbij apparaten een autonome stroomvoorziening hebben waarbij de batterijen van mobiele apparaten draadloos kunnen worden opgeladen.

Het in dit proefschrift beschreven onderzoek is gebaseerd op bovenstaande motivatie en ligt op het gebied van autonome systemen. De voorgestelde systemen passen zichzelf aan, organiseren zichzelf en maken gebruik van op radiofrequentie gebaseerde draadloze overdracht van energie. Meer specifiek kunnen knooppunten in het netwerk wereldwijd operationeel worden op basis van uitwisseling van lokale informatie en controle van elk knooppunt, en kan de levensduur van de batterij verlengd worden door het "oogsten" van energie uit de verzonden radiogolven.

Op het gebied van systemen die zichzelf kunnen aanpassen en organiseren, onderzoeken we netwerkbeheer gebaseerd op uitwisseling van lokale informatie. Het integrale functioneren van het gehele netwerk wordt geregeld door lokaal beheer van de individuele knooppunten. Het voordeel hiervan is dat knooppunten geen grote hoeveelheid netwerkwijde informatie hoeven te verzamelen wat de communicatiecomplexiteit sterk vermindert. We illustreren dit mechanisme middels twee casestudy's. Ten eerste kijken we naar de aggregatie van gegevens in mobiele netwerken. Ons algoritme maakt gebruik van evolutiedynamica om de configuratie van elk knooppunt te selecteren en te verspreiden.

Het netwerk past zich dan automatisch aan de variatie van applicatiescenario's aan. Het netwerk kan configuraties optimaliseren zonder dat er scenario-specifieke instellingen vooraf nodig zijn. In de tweede casestudy ontwerpen we een algoritme om door middel van zelforganisatie van grootschalige mobiele netwerken afstand te kunnen schatten. Het algoritme benut de door uitwisseling van lokale informatie verzamelde metingen voor statistische berekening, en het netwerk als geheel schat de onderlinge afstanden tussen de knooppunten. Dit leidt tot verbetering van de nauwkeurigheid en tot uitbreiding van het gebied waarbinnen de bestaande methodes voor het schatten van afstanden kunnen worden toegepast.

Op het gebied van systemen van draadloze energieoverdracht is de belangrijkste onderzoeksbijdrage de verhoging van het rendement van de energietransmissie en de benutting daarvan in mobiele apparaten die radiofrequentie gebaseerde draadloze energieoverdracht gebruiken. Allereerst benutten we de eigenschappen van actieve en passieve (backscatter) radiogolven om het rendement van zogeheten energy-harvesters te vergroten. We introduceren 's werelds eerste hybride platform dat de sterke punten van actieve (groot bereik en robuustheid tegen interferentie) en backscatter (laag energieverbruik) radio's combineert. We ontwerpen een schakelmechanisme dat actieve of backscatter radio selecteert afhankelijk van het kwaliteitsniveau van een radiokanaal. Dit systeem bewijst dat het ontvangen en opslaan van radiogolfenergie niet de enige keuze is om mobiele apparaten van autonome energie te voorzien en tevens dat backscatter radiocommunicatie voor bepaalde toepassingen energie-efficiënter is. In de tweede plaats besparen we energie in de laadstations zodat we de draadloze overdracht van energie groen kunnen maken. Draadloze radiofrequente-gebaseerde energieoverdracht is tamelijk inefficiënt als gevolg van het vermogensverlies over afstand, de polarisatie van de antenne, etc. Om het energieverbruik in opladers te minimaliseren houden we de status (active/idle) in het netwerk in de gaten, en of het ontvangen vermogen hoog genoeg is voor AC/DC-omzetting. Zo niet, dan schakelen we de laadstations af. Hoewel dit systeem de efficiëntie van de draadloze overdracht zelf niet vergroot, zorgt de besparing in de opladers voor een aanzienlijke toename van de energie-efficiëntie van het totale netwerk. Dit systeem is in het bijzonder van waarde voor het verhogen van de levensduur van batterij-gevoede mobiele laadstations. Om de waarde van energie-autonomie in praktische toepassingen te demonstreren, hebben we een casestudy voor plaatsbepaling binnen gebouwen (indoorlokalisatie) mbv. draadloze energieoverdracht uitgewerkt. We ontwierpen een systeem zonder batterijen dat permanent door draadloze energieoverdracht gevoed wordt. Deze nieuwe lokalisatiemethode werkt op energieniveaus die binnen het budget liggen dat vandaag de dag door draadloze energieoverdracht gerealiseerd kan worden en het communicatieschema is opgezet zodanig dat het inactief luisteren (idle listening) tot een minimum wordt beperkt. We maken gebruik van standaard verkrijgbare apparatuur om het systeem te implementeren en te testen. De resultaten bewijzen dat het inderdaad mogelijk is om draadloze energieoverdracht ook over lange afstanden te gebruiken om mobiele systemen van stroom te voorzien.

1

INTRODUCTION

1.1. RESEARCH MOTIVATION

In the current society our daily lives rely more and more on mobile devices. Mobile devices are widely used in medical care systems [126], environment monitoring [129, 207], emergency monitoring [121], traffic control [108], and navigation localization [127]. According to GSMA Intelligence [57], the number of mobile devices reached around 7.2 billion in October 2014, which is more than the total population of the world. In January 2016, this number has surpassed the 7.6 billion mark. At the same time, as the number of mobile devices increases, more Internet of Things (IoT) applications will be embedded in our lives. According to estimates of Gartner, Inc. [50], the number of IoT devices will reach more than 20 billion by the year 2020. More than 5 million new devices per day will connect into the IoT in 2016. The cost spent on IoT endpoints by the consumers and the industry will reach more than 3,000 billion dollars in 2020. A number of challenges related to mobile networks are discussed below.

1.1.1. CHANGING SCENARIO

As the number of mobile devices in networks increases, management of such networks becomes a challenge. Firstly, the capabilities of mobile devices vary widely. For example, communication range, data throughput, and battery lifetime all differ for specific devices. Secondly, as these devices are mobile, operation of these devices occurs over a wide array of scenarios in various geographical locations. Solutions for managing these devices need to be flexible. For example, GPS localization is available in some situations. However, as mobile devices move to the indoor areas, GPS becomes unavailable or can only provide coarse-grained accuracy. Thirdly, the requirements of mobile networks vary between different users in different situations. For example, even with the same type of temperature sensor, the required sampling period will differ between cities and countries, or between day and night.

Some research focuses on the challenge of context changing frequently [5, 51, 199]. Take weather monitoring networks for example: most existing systems and communi-

cation protocols are designed with a fixed network for monitoring a specific weather type [99, 142, 233]. The monitoring devices are deployed at fixed locations, and the data is transmitted back to a central processing station periodically. This central station produces the weather map and estimates the weather trend based on the aggregated data. The disadvantage of such a system is that the number of sampling positions are limited and the positions are fixed. Furthermore, the realtime weather conditions of small scale areas are unknown, such as rainfall conditions on the streets of a city. To solve these problems, more mobile devices need to be deployed in the monitoring area and more data needs to be aggregated in realtime [90, 140].

As the size of communication networks increases, centralized control organizing the whole network becomes the single break point. Any changes in the network, e.g. network topology, node density, etc., affect the control schedule of the central node. An approach to aggregate realtime data of high resolution from large numbers of heterogeneous devices, e.g. fixed monitoring stations, mobile and static sensors, etc. is required. Self-adaptive self-organization network control is an effective solution to solve this issue. *We propose that the control mechanism of communication networks is organized by each node itself, and not by a central node.* Each node only exchanges information locally with its neighbors, and schedules its actions based on these data. The behavior based on local information exchange of each node will jointly fulfill the requirements of the users. This approach thus builds autonomic management in each device, and the devices together meet the various requirements of users.

1.1.2. LIMITED LIFETIME

Another challenge comes from the maintenance cost of mobile devices, especially replacing batteries. Firstly, recharging the batteries of devices in some scenarios is expensive in terms of money and time. We take large-scale weather monitoring network and wearable health monitoring system as example scenarios. In the example of large scale weather monitoring network, the energy consumption of monitoring sensors is not balanced. Sensors in the hot spot areas, where more weather data should be collected, will consume more energy. The most common approach for lifetime maintenance is to predict the expected lifetime of the batteries in all devices, and then to change the batteries of all devices in a network based on a pre-calculated time schedule. This is suitable for devices in which power consumption is relatively stable and equally distributed in all devices of a network, and the lifetime of the device is relatively long, e.g. several years. However, if weather condition and the corresponding hot spot monitoring area in the network change frequently, the energy consumption and battery lifetime are difficult to predict. Further more, it is difficult to replace batteries of devices deployed deep sea, forest, or mountain area. In the example of wearable health monitoring system, the battery of most existing wearable devices can maintain only several days depending on the work load for monitoring. To guarantee the wearable system always works properly, devices must be recharged periodically, or devices have a long or even perpetual lifetime. Secondly, the batteries in some devices are irreplaceable. For example, in monitoring systems of building structure, sensors are often buried inside concrete, and required to work for many years [11]. As replacing the battery of a sensor device buried in concrete will destroy the building, most existing solutions therefore use a wired power supply [182]. However,

use of wires will negatively affect the strength of the concrete. To solve these problems, the battery lifetime needs to be longer.

As the number of devices increases and the deployment environment becomes more complicated, only increasing the battery lifetime can not fulfill the requirements. An approach that can increase the battery lifetime or even make the device have unlimited energy supply is required. Energy-autonomous systems [15] are an effective solution to these problems, in which mobile devices harvest energy from ambient energy sources to obtain the required power. The problem with this kind of system is that the amount of harvested energy from ambient energy sources is limited and can not always fulfill the energy requirement of mobile devices. *Therefore, we propose to purposely deploy power sources to supply energy by means of wireless power transfer.* The research of energy autonomy focuses on mobile devices with energy harvesting capabilities. It is important that energy sources and mobile devices cooperate to optimize the performance of wireless power transfer.

1.2. RESEARCH QUESTIONS

To solve the above challenges, this dissertation proposes that the key factor is to increase the autonomy of devices in mobile wireless networks. The autonomy includes two perspectives: autonomy of self-organizing communication networks by each node, and autonomy of energy supply from ambient wireless power transmission systems. The goal of the dissertation is thus to construct autonomic systems in mobile distributed networks. The research questions of this dissertation are defined as follows.

Main Research Question

Can self-organization based on local information exchange achieve global control of energy-autonomous systems?

To answer the main research question, we explore two fields: distributed mobile networks and energy-autonomous systems. Firstly, we use local information exchange among individual nodes to achieve global control in mobile distributed communication networks. Secondly, we construct energy-autonomous systems to increase the battery lifetime of mobile devices or make the battery lifetime perpetual.

These two fields are further classified into detailed research topics to answer the research question from various viewpoints. In the research of distributed mobile networks, we focus on two case studies: data aggregation and distance estimation. These two functions are achieved by self-organization mechanism using local information exchange among the nodes of large-scale mobile networks. In the research of energy-autonomous systems, we explore mobile systems with radio RF (frequency based) wireless power transfer using dedicated charging devices. Specifically, we design and implement a communication system using backscatter radio, a network for RF energy transmission, and localization services using harvested energy. The common challenge of these energy-autonomous systems is to increase the efficiency of power transmission and utilization. Chapter 2 explains the positioning of this dissertation and how the research is narrowed down to the topics of self-organizing networks and RF-based wireless power transfer

systems in detail. Based on the analysis above, the research question is categorized into the following sub-research questions:

Sub-Research Questions

- *Can local information exchange in mobile communication networks achieve self-organizing data aggregation?*
- *Can local information exchange in mobile communication networks achieve distance estimation?*
- *Can communication power efficiency be increased with backscatter radio?*
- *How can the performance of RF-based wireless power transfer networks be optimized?*
- *Can RF-based wireless power transfer supply enough energy to run a localization service?*

1.3. RESEARCH CONTRIBUTION

This dissertation studies autonomic computing properties in mobile devices from two perspectives: mobile distributed networks (Chapter 3 and Chapter 4) and energy-autonomous systems (Chapter 5, Chapter 6 and Chapter 7). In mobile distributed networks, self-configuration and self-optimisation properties of autonomic computing are explored, addressing the challenge of how to use distributed local information of each node to achieve self-adaptive control of the whole network. In two case studies, algorithms are designed for each individual node on how to exchange local information with neighbours by broadcasting, and organise the whole network in such a way that distance estimation and data aggregation, respectively, emerge as global properties. In energy-autonomous systems, self/context-awareness properties of autonomic computing are studied focusing on the challenge of how to use RF-based wireless power transfer to increase the battery lifetime of mobile devices. Three individual case studies of energy-autonomous systems are researched, including operation control in the energy transmission, efficiency control to the energy of backscatter radio communication, and the nodes' energy utilization of indoor localization. The research presents system designs with autonomy properties using local information exchange to achieve network-level global control, and using RF-based wireless power transfer to increase the lifetime of mobile devices. These studies demonstrate the approach to implement autonomy properties in application systems, and extend the existing application paradigms of autonomic computing. The detailed contributions of the dissertation are as follows.

1. A self-adaptive and self-organization algorithm using evolutionary theory for data aggregation. The network automatically selects different operation combinations to adapt to changing scenarios. (See Chapter 3)

2. A self-adaptive and self-organizing algorithm for distance estimation based on local broadcast. (See Chapter 4)

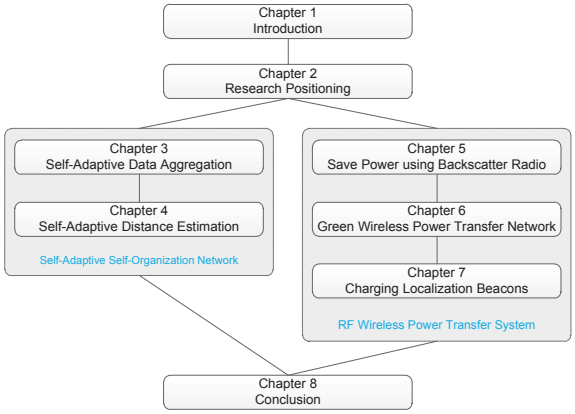

Figure 1.1: The structure of this dissertation.

3. Designing and implementing a communication device by merging active and backscatter radios. The device increases the power efficiency of wireless communication. (See Chapter 5)

4. Designing and implementing a wireless power transfer network. The system achieves high charging efficiency while providing the required amount of energy to mobile devices. (See Chapter 6)

5. Designing and implementing an indoor localization system using RF-based wireless power transmission. (See Chapter 7)

1.4. THESIS STRUCTURE

This dissertation consists of eight chapters. Figure 1.1 illustrates the structure of the thesis.

- Chapter 2 introduces the basics of autonomic computing, mobile distributed systems and energy-autonomous systems, and positions the research of this dissertation.
- Chapter 3 investigates data aggregation with self-adaptive self-organization properties.
- Chapter 4 uses local information exchange to achieve distance estimation with self-adaptive self-organization properties in large scale networks.
- Chapter 5 investigates the possibility to save communication energy by combining backscatter and active radios.
- Chapter 6 studies the effect of building chargers into a network, thereby saving energy not only from the user side, but also on the charger side.

- Chapter 7 explores an indoor localization algorithm using RF energy as a means for wireless power transfer.
- Chapter 8 concludes the thesis by answering the research questions, and proposing directions for future work.

The chapters of this dissertation are based on the following publications:

- Chapter 3: Qingzhi Liu, Stefan Dulman, Martijn Warnier. *AREA: an Automatic Runtime Evolutionary Adaptation Mechanism for Creating Self-Adaptation Algorithms in Wireless Networks.* In Proceedings of the Spatial Computing Workshop colocated with AAMAS, Saint Paul, Minnesota, USA, May 6-10, 2013.
- Chapter 4: Qingzhi Liu, Andrei Pruteanu, Stefan Dulman. *GDE: a Distributed Gradient-Based Algorithm for Distance Estimation in Large-Scale Networks.* In Proceedings of the ACM MSWiM, Miami Beach, FL, USA, Oct. 31- Nov. 4, 2011.
- Chapter 5: Ivar in 't Veen, Qingzhi Liu, Przemyslaw Pawelczak, Aaron N Parks, Smith Joshua. *BLISP: Enhancing Backscatter Radio with Active Radio for Computational RFIDs.* In Proceedings of the IEEE RFID, Orlando, FL, May 3-5, 2016.
- Chapter 6: Qingzhi Liu, Michal Golinski, Przemyslaw Pawelczak, Martijn Warnier. *Green Wireless Power Transfer Networks.* IEEE Journal on Selected Areas in Communications, 34(5): 1740 - 1756, 2016.
- Chapter 7: Qingzhi Liu, Wieger IJntema, Anass Drif, Przemysław Pawełczak, Marco Zuniga. *WiPLoc: Perpetual Indoor Localization with RF Wireless Power Transfer.* (Under submission).

2

Research Positioning and Related Work

This dissertation investigates properties of autonomic computing from the viewpoints of distributed mobile networks and energy-autonomous systems, respectively, as shown in Figure 2.1. The intersection area of distributed mobile systems and energy-autonomous systems is studied in this dissertation. Research is positioned in both self-adaptive self-organization (SASO) systems, which form a sub-category of distributed mobile systems, and wireless power transfer (WPT) systems, which forms a sub-category of energy-autonomous system.

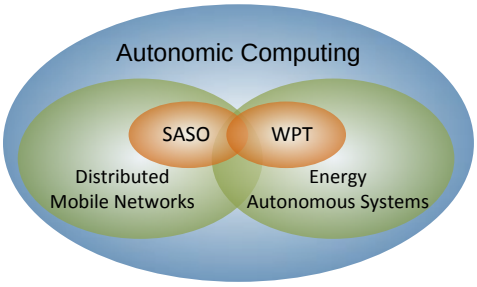

Figure 2.1: The research in this dissertation is positioned in the area of autonomic computing. Distributed mobile networks and energy-autonomous systems are further explored by studying self-adaptive and self-organization, and wireless power transfer properties.

This chapter first discusses the basics of autonomic computing, distributed systems and energy-autonomous systems, and then positions the research with respect to these fields.

2.1. Autonomic Computing, Distributed Mobile Networks and Energy-Autonomous Systems

This section presents the basics of Autonomic Computing (Section 2.1.1), Distributed Mobile Networks (Section 2.1.2) and Energy-Autonomous Systems (Section 2.1.3).

2.1.1. Autonomic Computing

As the complexity of computing systems increases, systems cannot only operate properly in predefined scenarios, but also need to be able to adapt to newly emerged application requirements. The goal of autonomic computing systems is to make it possible for each computing device in a system to manage itself in order to meet high-level application requirements. A computing device, the smallest unit of the autonomic computing system, is referred to as an autonomic element. Based on the definition of autonomic element [158], an element has a predefined input and output interface in system context. It should manage itself and interact with other autonomic elements according to the input context, predefined policies and requirements. The requirements for autonomic computing systems are first defined in [69]. Autonomic computing systems should have at least one of the following functions:

- **Self-Configuration:** Configuring parameters of operations to automatically cope with varying application scenarios.
- **Self-Optimization:** Improving the execution performance to achieve sub-optimized or optimized performance in any scenario.
- **Self-Healing:** Detecting, diagnosing and repairing problems in a system and maintaining performance at the required level.
- **Self-Protection:** Detecting any attack to a system, and protecting a system from failure.

Other properties of autonomic computing are required in some research [158]:

- **Context Awareness:** Detecting and monitoring the variation of the execution scenarios, and adapting self behavior.
- **Self-Awareness:** Detecting and monitoring the performance and system state of itself, and adapting self behaviors.
- **Open:** Have an interface that can be accessed by any heterogeneous system.
- **Anticipatory:** Anticipating the related data and system behavior of the above properties in any application scenario.

To achieve the properties above, IBM proposes the classic model of autonomic management for each autonomic element [93] as shown in Figure 2.2. Each autonomic element in the whole system operates its management process as follows: The *managed element* represents the entity to which the autonomic element is attached, e.g. a wearable

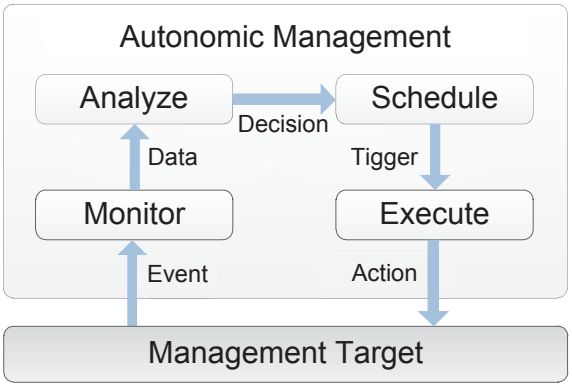

Figure 2.2: The management process of autonomic computing, adapted from [93].

device, a network server or a robot. The *monitor* component in the autonomic element observes the events that occur in the managed target and saves the observation results. This monitoring can be implemented by, for example, sensors or data logs. Then the *analyze* module filters and processes the data observed by the monitor module based on a predefined policy, and decides how to react/adapt to an event. The *schedule* module finds the suitable position and time to trigger the decided upon. And finally, the *execution* module manages the actuators to realize the action decided upon by the analyze module.

2.1.2. DISTRIBUTED MOBILE SYSTEMS

The concept of distributed systems is studied in many fields, including parallel computing, internet of things, and multi-agent systems. According to [186], distributed systems are defined as follows:

> *"A distributed system is a collection of independent computers that appears to its users as a single coherent system."*

According to this definition, independent computers can be autonomous elements. All autonomous elements together make up a distributed system. Elements cooperate with each other to realize the application requirements of a user. The key point is that all the elements together are considered as one single unit. The user only needs to access one interface of the system, and does not need to know how the elements in a system are organized.

This dissertation focuses on distributed systems in mobile wireless communication networks with the following requirements:

- **Communication:** Elements can wirelessly communicate with neighboring nodes, and the number of exchanged messages during a time period is limited.
- **Complexity:** Elements must use simple standard communication approaches, e.g. broadcast, to exchange information with neighbors. The elements do not consider the power consumption of communication.

- **Adaptive:** A network system should be adaptive to possible changes of the application scenarios. For example, a system must maintain a required performance when new users join and existing users leave a system, or when the topology of the mobile network changes, communication performance (e.g. data rate) changes.

2.1.3. ENERGY-AUTONOMOUS SYSTEMS

Limited lifetime of energy storage devices often forms a bottleneck when using wireless devices in application areas such as environmental monitoring, traffic monitoring and health care. To prolong the lifetime of electronic devices and to eliminate the problem caused by the limited energy of batteries lots of research explores the possibility to use harvested energy provided by the surrounding area. According to [15], energy-autonomous systems are defined as:

"*An electronic system that has been designed to operate and/or communicate as long as possible in known/unknown environments providing, elaborating and storing information without being connected to a power grid.*"

Many different resources are studied as the energy supply in energy-autonomous systems, including photovoltaic [168], vibration [13], thermal [185] and radio frequency [105]. Compared with using a fixed power supply, energy-autonomous systems have a larger spatial mobility range. And compared with using batteries, energy-autonomous systems can operate for a longer or even perpetual time. These advantages of energy-autonomous systems increase the application conditions of mobile wireless devices. For example, some sensors are randomly scattered in an large area [129]. The replacement of energy storage device is expensive. In the research, we categorize energy-autonomous system into two sub-fields: ambient energy harvesting [176] and wireless power transfer [71]. This dissertation focuses on RF-based wireless power transfer systems. Specifically, the wireless power transfer systems use dedicated energy transmitters to transfer the energy to the neighbor area, and mobile devices to harvest the energy transmitted from the transmitters. Energy-autonomous systems are designed with the following requirements in mind:

- **Energy Source:** Harvested energy is from a purposely deployed RF source, and energy sources are static.

- **Energy Storage:** Depending on different scenarios, received energy could be temporally stored and then used. If the amount of harvested energy is more than the required power consumption, the extra energy can be saved in an energy storage device.

- **Optimize energy consumption:** In most application scenarios, the harvested energy is quite limited compared to the power consumption of mobile devices in wireless communication. The system must be able to optimize the efficiency of energy consumption.

2.2. RESEARCH POSITIONING

Chapter 3 and 4 discuss new algorithms for data aggregation and localization in the area of distributed and energy-dependent. A centralized and semi-energy-autonomous system is proposed in Chapter 5 to decrease power consumption of communication by merging active and backscatter radios. In Chapter 6 and 7, communication protocols are proposed that achieve wireless power transfer networks and battery-less indoor localization, falling in the category of energy-autonomous systems and distributed mobile system. The research topics of each chapter are categorized in Figure 2.3.

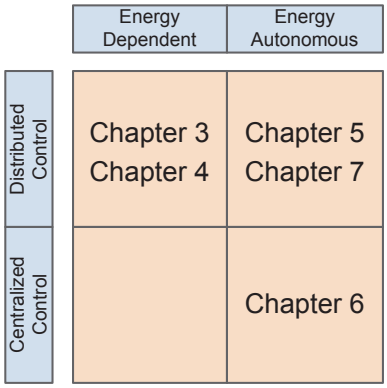

Figure 2.3: Categorization of the research fields of the chapters in the dissertation.

2.2.1. DISTRIBUTED MOBILE SYSTEMS: SELF-ADAPTIVE SELF-ORGANIZATION

In this section, we discuss the evaluation metrics, system properties, and system architecture of distributed mobile systems to position the research in self-adaptive self-organization systems.

EVALUATION METRICS

Distributed mobile systems studied in this dissertation are explored from two dimensions: communication complexity and system robustness. Communication complexity is considered as the difficulty in implementing a communication protocol, including the number of messages, packet size and the usage of historical data. System robustness captures how well a system adapts to variations in application scenarios. These two dimensions can be investigated from two research perspectives: global control and self-adaptive self-organization, as shown in Figure 2.4.

Most traditional approaches to manage distributed networks involve some kind of global control mechanism [49]. A central node collects global information of the whole network, makes decision and sends schedule back to each node. This approach is straightforward to implement in small-scale networks. However, as the size of the network increases, the communication load becomes prohibitive for data aggregation. Especially in ad-hoc networks, where nodes in hot spot areas must route an increased communication load from other parts of the network. To relax the communication load in a network,

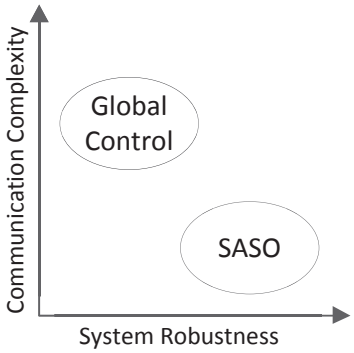

Figure 2.4: Evaluation metrics of distributed system. This dissertation focuses on the trade off between two evaluation metrics: communication complexity and system robustness. The case studies for comparison consider global control and self-adaptive self-organization.

a central node can increase the sampling period for collecting data. But in this case, it becomes much more challenging for a system to react to varying network scenarios in a timely manner. In addition, to make a network operate properly, the central node must select the network management approach based on network conditions, such as wireless communication range or node density. If the network conditions change, the central node must detect the new parameters and adjust its management strategy. Therefore, as the size of the network increases, the overload caused by detecting these network parameters accounts for a large percent of the total communication data. Further more, since the system operation relies on a centralized control node, there is a single point of failure that can cause the overall collapse of the system.

Compared to centralized control, more recent research focuses on self-adaptive and self-organizing systems [146] to address the above limitations. In such systems, each node only collects information from its neighboring nodes. Based on available local information, each node independently decides on its actions. The local behavior of all nodes together comprises the global behavior that is required on the system level. The complete management process occurs without any centralized control. Self-adaptive and self-organization systems have advantages in both communication complexity and robustness. Firstly, each node is required to only aggregate data from neighbors. This avoids the occurrence of hot spot nodes in the data aggregation realized by centralized control. Secondly, global behavior does not rely on decisions made by a central node. The behavior of each node, e.g. leaving the network, makes local affect and further converges to a global behavior. And as each node does not need to send information to the central node and wait for feedback, the system can quickly react to variations in application scenarios.

SYSTEM PROPERTIES

Compared to centralized control systems [16, 143, 184, 193], the properties and operations of each node in self-adaptive and self-organization networks have more influence on the global behavior of a system. Some works assume that all nodes in a network have

the same, homogeneous, performance [131, 146, 208]. For example, [146] constructs a global coordination system by nodes that only communicate with direct neighbors, and each node has the same communication mode. Some works consider the properties of nodes as more heterogeneous [25, 40, 70, 110, 141, 164]. For example, [40] deploys two types of robot nodes in a system, wheeled robots and flying robots. All robots reach their goal by the self-organized coordination among themselves. This dissertation focuses on homogeneous nodes in a network as shown in Figure 2.5. Some properties of the nodes are considered to be heterogeneous, e.g. mobility speed or transmission power.

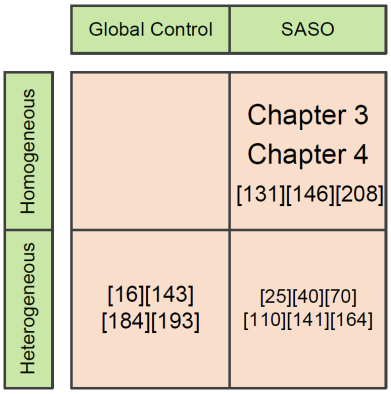

Figure 2.5: Positioning of the research in Chapter 3, Chapter 4 and related works using the properties: heterogeneous and homogeneous communication networks, communication with global control and self-adaptive self-organization with local broadcast.

The global behavior and communication approach are two other properties that are considered in this dissertation as categorized in Figure 2.6. Some works [131, 146] require each node in the network to have continuous idle listening and broadcast communication. Other works [23, 194, 206] use communication protocols requiring synchronization and handshakes, e.g. Zigbee [232], BLE [19] or Wifi [210]. Compared with idle listening and broadcasting, synchronization and handshakes increases the complexity of algorithm design. Although idle listening and broadcast approaches are sometimes not suitable in real system implementations, for example, power consumption for idle listening can be (too) large for low power devices, the advantage of the approach is its simple design, simulation and implementation. This dissertation assumes that nodes use the idle listening mode together with broadcast to exchange data.

Another dimension considered is the global behavior of self-adaptive self-organization systems. Most related work concentrates on a single global behavior. No matter when and where the user sends a request to the system, the system only displays one type of behavior in response to the user. For example, in [146], the global behavior of a network is estimating the distance from the user to an anchor node. Werner [208] organizes a network to achieve synchronization using self-organization. Some adaptive algorithms uses evolutionary theory in computing and optimization [10], which provides systems with the ability to organize multiple global behaviors. In [147], agents use an evolutionary adaptation mechanism to evolve their behavior to obtain a higher fitness value to the

changing environment. In this thesis Chapter 3 uses fixed global behavior and Chapter 4 uses evolutionary behavior.

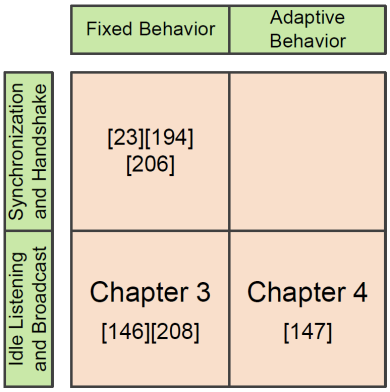

Figure 2.6: Positioning of the research in Chapter 3, Chapter 4 and related works using the properties: broadcast and unicast communication, fixed behavior and adaptive behavior.

SYSTEM ARCHITECTURE

The system architecture of distributed systems researched in this dissertation are self-adaptive and self-organizing systems as shown in Figure 2.7. All nodes have homogeneous communication and computing functions, e.g. communication transmission power, mobility model, radio propagation model, etc. Each node does not save historical communication data, and all communication is local using broadcast to neighboring nodes. Each node decides on actions based on information collected from neighboring nodes. The users are represented by a node that sends local request. All nodes together provide a global behavior to meet the requests from the users.

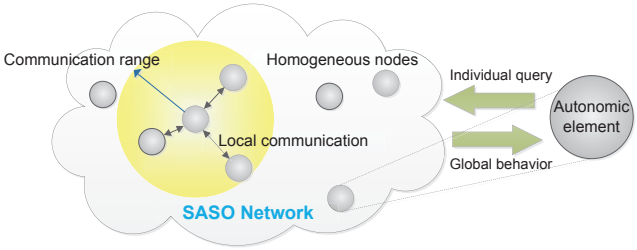

Figure 2.7: Architecture of self-adaptive self-organizing networks introduced in this dissertation. Homogeneous nodes use local information exchange to achieve global control for the queries of users.

According to the analysis of the properties and structures of mobile distributed systems, two self-adaptive self-organizing systems are designed in this dissertation: AREA (Chapter 3) and GDE (Chapter 4). AREA explores the evolutionary behavior of a network for data aggregation, and GDE focuses on fixed behavior for distance estimation. The implemented properties of autonomic computing are self-configuration, self-optimization

and self-healing. The advantages and disadvantages of various designs analyzed above, and the relation between the implemented systems and properties are shown in Figure 2.8.

Properties\Requirements	Communication complexity	System robustness
Centralized control	low	low
Distributed control	high	high
Heterogeneous	high	low
Homogeneous	low	high
Global information	high	low
Local information	low	high
Synchronization and handshake	high	low
Idle listening and broadcast	low	high
Fixed behavior	low	low
Evolutionary behavior	high	high

(a) Advantages and disadvantages of various designs.

Autonomic Computing	Research System
Self-configuration	Chapter 3, Chapter 4
Self-optimization	Chapter 3
Self-healing	Chapter 3, Chapter 4
Self-protection	/
Context aware	/
Self-aware	/
Open	/
Anticipatory	/

(b) Relation between the implemented systems and properties.

Figure 2.8: Based on the selected system design, AREA (Chapter 3) and GDE (Chapter 4) are constructed with autonomic computing properties, including self-configuration, self-optimization and self-healing. (Symbol / means the items are not discussed in this dissertation.)

2.2.2. ENERGY-AUTONOMOUS SYSTEMS: WIRELESS POWER TRANSFER

In this section, we discuss the evaluation metrics, system properties, and system architecture of energy-autonomous systems to position the research in RF-based wireless power transfer systems.

EVALUATION METRICS

Energy-autonomous systems are explored from two perspectives: mobility range and available energy. Mobility range is used to evaluate the size of the area that a device has enough energy for movement. Available energy is used to evaluate the amount of energy the device can harvest within a time period for various conditions, including distance, obstacles, direction, etc. Depending on the type of energy source, an energy-autonomous system can be categorized into either 'ambient energy harvesting' or 'wireless power transfer' as shown in Figure 2.9.

Available power is one of the most important evaluation parameters for energy-autonomous systems. Compared to battery powered systems and systems with a fixed

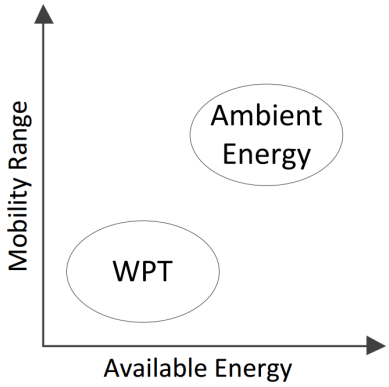

Figure 2.9: Evaluation metrics for energy-autonomous systems. This dissertation focuses on the trade off of two evaluation metrics: mobility range and available energy. The case studies for comparison are harvesting ambient energy and wireless power transfer.

power supply the available power is low and unstable. One possible solution to increase harvested energy is clustering multiple energy harvesting devices together and increasing the spatial size of the harvester, such as a solar panel power station. This dissertation focuses on mobile devices with only one energy harvester. Since the available harvested energy is limited, research focuses on application scenarios that do not require real time and/or continuous data flow, such as temperature sensing or position monitoring.

Compared with ambient energy harvesting, the disadvantage of wireless power transmission is that the available energy is less. And wireless power transfer make mobile devices harvest wireless energy from dedicated power sources. Therefore energy harvesting devices of wireless power transfer systems must be kept inside the effective power transmission range of their energy sources, which limits the mobility range of these devices.

The advantage of ambient energy harvesting is that there is no need to purposely deploy specific energy sources, therefore the mobility range of the device can be larger. The selection between ambient energy harvesting and wireless power transfer depends on the specific application requirements and scenarios. In this dissertation, wireless power transfer is studied as the energy source for mobile devices.

SYSTEM PROPERTIES

In the research field of energy-autonomous systems, many kinds of techniques are explored as energy sources. For ambient energy harvesting, the most widely-used techniques concern solar panels [169], wind [91], thermal energy harvesting [185], RF radio [21, 94, 105, 201] and vibration [14, 44]. For wireless power transfer, the most researched energy sources are RF radio [6, 7, 114, 116], magnetic resonance [24, 100], inductive charging [217] and ultra-sound [195]. The application target of this dissertation is on mobile wireless devices, which has the following requirements to the energy source:

- The system targets low-power mobile devices, therefore such devices must be able to harvest mW power.

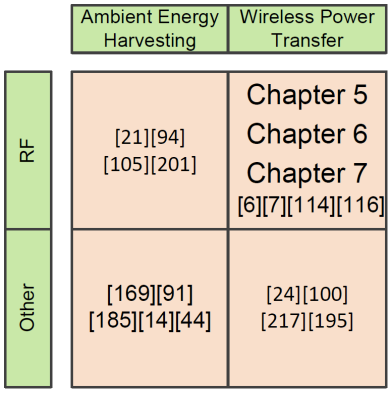

Figure 2.10: Positioning of the research in Chapter 5, Chapter 6, Chapter 7 and related work using the properties: harvesting RF energy and other sources, ambient energy harvesting and wireless power transfer.

- The process of harvesting energy must not rely on specific conditions of the user, e.g. movement, position, etc. The device should harvest energy without influencing the daily life of users.
- The mobility range covered by an energy source must be at least room level.

Based on these requirements, RF wireless power transfer technique is considered to be the most suitable for mobile devices. Furthermore, RF energy receivers can also harvest ambient radio signals. The research positioning related to this topic in this dissertation is shown in Figure 2.10.

RF-based wireless power transfer systems can be further classified into many subcategories [220], including antenna selection, and single or multi hop wireless charging [86]. Two sub-categorizations are used to illustrate the main difference between the research in this dissertation and existing related work as shown in Figure 2.11: mobile or static charger; simultaneous wireless information and power transfer (SWIPT) or parallel wireless information and power transfer (PWIPT).

Some related work focuses on mobile charger networks [31, 61, 161, 192, 205]. The common point in all these is that mobile chargers coordinate with nodes in the network to meet the charging requirements, such as minimizing the recharging route distance, maximizing the charging power or minimizing the number of mobile chargers. The application scenario of this dissertation targets mobile wireless devices. Mobile charger systems are considered to be unsuitable for our application for the following reasons: Firstly, as the chargers are mobile, it is difficult to guarantee that each receiver has long term constant harvested energy. Although the harvested energy can be stored for a long time, it is challenging to schedule mobile chargers to recharge every receiver in a large-scale network before receivers consumes all energy in the battery. Secondly, the harvested energy of the RF wireless power transfer is on the mW level, so the charger cannot charge each receiver in a short period. Thus the recharging period for all harvesters in the network will take too much time. However, static chargers can provide a stable charging range. Although the charging power of RF-type systems is only on the mW level and affected by

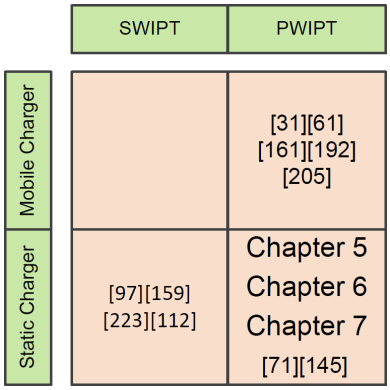

Figure 2.11: Positioning of the research in Chapter 5, Chapter 6, Chapter 7 and related works using the properties: static and mobile charger system, SWIPT and PWIPT.

obstacles, controlling for charger deployment positions, density, antenna directions, etc. can only partially compensate these constraints. Based on the observations above, static chargers are used in this dissertation.

SWIPT [97, 159] is proposed to transmit RF energy and communicate information at the same time with generally two approaches: In the first approach, the energy transmitter sends a radio signal, and the receiver harvests energy or listens for communication information from the radio signal depending on its schedule. For example, scheduling harvesting energy or listening for communication information in [223] is based on the receiver location. The receivers harvest energy if they are close enough to the energy transmitter, and they listen for communication information if they are further away. In the second approach, the time slot of energy harvesting and communication of information is split. For example, [112] allows the energy receiver to determine the amount of harvested energy and communication of information based on the dynamic radio channel conditions. The advantage of SWIPT is that the energy and information are transmitted at the same time, so the radio channel is efficiently used. Each device needs only one type of antenna and there is no need to deploy dedicated chargers. The disadvantage is that the optimization of scheduling harvesting energy and communication of information is complicated, and the performance of energy harvesting and radio communication cannot be maximized at the same time.

Compared to SWIPT, PWIPT uses two separate radio channels to transmit energy and information independently. Although PWIPT must use two antennas, the system is much easier to implement and the harvested energy is higher than SWIPT, since dedicated chargers are deployed. This dissertation uses the system model with static chargers and PWIFT [71, 145]. Chapter 5 researches an RFID system and although RFID is essentially SWIPT, another radio communication channel is purposely used for communication in this research, and backscatter radio is mainly used for saving power. Therefore, Chapter 5 is also classified as a PWIPT system.

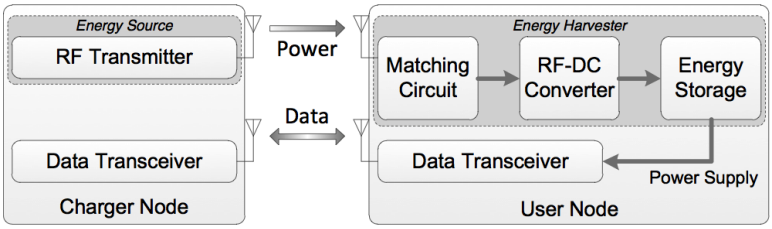

Figure 2.12: The operation process of the wireless power transfer system researched in this dissertation. Parallel RF channels are used to transfer energy and exchange data.

Properties\Requirements	Mobility range	Available energy
Non-energy autonomous	low	high
Energy autonomous	high	low
Other	/	/
Radio frequency	/	/
Ambient energy harvesting	high	low
Wireless power transfer	low	high
Mobile charger	high	high
Static charger	low	low
SWIPT	low	low
PWIPT	high	high

(a) Advantages and disadvantages of various designs.

Autonomic Computing	Research System
Self-configuration	/
Self-optimization	/
Self-healing	/
Self-protection	/
Context aware	Chapter 5, Chapter 6, Chapter 7
Self-aware	Chapter 6
Open	/
Anticipatory	/

(b) Relation between the implemented systems and properties.

Figure 2.13: Based on the selected system design, BLISP (Chapter 5), WPTN (Chapter 6) and WipLoc (Chapter 7) are constructed with autonomic computing properties, including context awareness and self-awareness. (Symbol / means the items are not discussed in this dissertation.)

SYSTEM ARCHITECTURE

The core operation process of wireless power transfer systems is shown in Figure 2.12. The data transmitting and receiving are done in parallel with energy transmission. The energy used in the radio transceiver of receiver nodes is used for energy harvesting. Energy sources transmit radio waves with a different frequency than data communication. The core component in the receiver is an RF-DC converter. It is used to rectify the radio waves into directional current. It consists of three components: resonant circuit, a rectifier and a power management unit (PMU). This thesis focuses on the communication control at the network level, the operation of these components is not discussed in detail. In [81] a detailed circuit components of the harvester is given. After the RF-DC converter, the harvester boosts the voltage of the harvested power to the required level.

Finally, the energy is used directly by the device or stored in a battery. The choice of antenna at the transmitter and the receiver, e.g. direction, polarization, gain, etc, are decided by application requirements. The frequency and transmission power must obey communication and safety regulations [116].

According to the analysis of the properties and structures of energy-autonomous system, the BLISP (Chapter 5), WPTN (Chapter 6) and WipLoc (Chapter 7) systems have been developed using RF-based wireless power transfer, static chargers and PWIPT. The implemented properties of autonomic computing are context-awareness and self-awareness. The advantages and disadvantages of various designs analyzed above, and the relation between the implemented systems and properties are shown in Figure 2.13.

3

AREA: AN AUTOMATIC RUNTIME EVOLUTIONARY ADAPTATION MECHANISM FOR CREATING SELF-ADAPTATION ALGORITHMS IN WIRELESS NETWORKS

Self-adaptive self-organization networks is a research branch of autonomic computing field. This chapter [1] researches data aggregation in the self-organizing network. The self-organization mechanism is based on local information exchange.

3.1. INTRODUCTION

Nowadays an increasing amount of research is focused on various wireless network applications, such as environment monitoring [207], traffic control [108] or navigation localization [127]. As the application complexity increases, more new research requirements are involved. However, most existing algorithms are designed with a specific type of (spatial) environment in mind, such as assumed bandwidth, node density, etc. Once the environment changes beyond the presumed domain, the algorithm will no longer be able to adapt: it will not function properly anymore. Therefore, it is necessary to design a mechanism that allows wireless networks to automatically self-create and self-evolve algorithms according to the changes in the (spatial) environment.

[1] This chapter is published as the paper:
Qingzhi Liu, Stefan Dulman, Martijn Warnier. *AREA: an Automatic Runtime Evolutionary Adaptation Mechanism for Creating Self-Adaptation Algorithms in Wireless Networks.* In Proceedings of the Spatial Computing Workshop colocated with AAMAS, Saint Paul, Minnesota, USA, May 6-10, 2013.

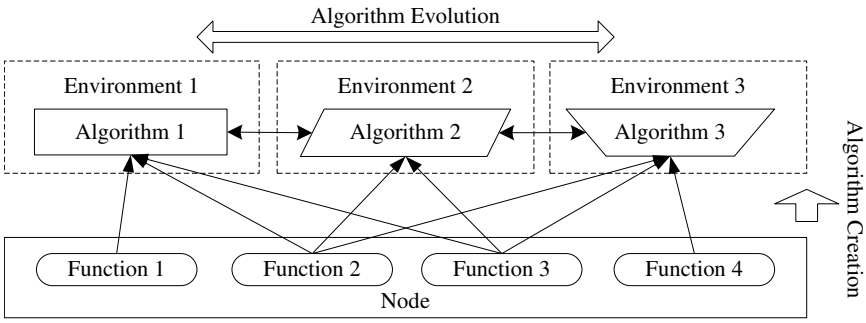

Figure 3.1: *AREA* lets each agent (node) self-create algorithms that adapt to different application requirements. The created algorithms self-evolve to other function combinations, self-adapting to their (changing) environment.

Based on this motivation, we propose a novel algorithm design mechanism called an *Automatic Runtime Evolutionary Adaptation (AREA)* mechanism. The *AREA* mechanism has three main properties, including automatic computing, runtime processing, and evolutionary adaptation.

The self-adaptation property has been widely recognized as an important performance metric for wireless networks. However, existing self-adaptive algorithms, based on design mechanisms such as swarm intelligence [92], stigmergy [39], and autopoiesis [149] only maintain the adaptation properties for specific environments. Once the deployment environment changes beyond the scope of the originally envisioned domain, the algorithm performance will decrease. The *AREA* mechanism allows the created algorithm not only to be adaptive but also to evolve to other adaptive abilities based on the variation of the application requirements and the spatial environment. In addition, *AREA* is totally distributed. Each agent only spatially coordinates with neighbors, uses runtime local information, and the whole processing flow is automatically executed in each agent during the runtime.

The *AREA* mechanism assumes that each agent has some basic functions, such as routing, forwarding messages, etc. Each agent mutates local function combinations and learns from neighbors. Finally, the function combination that meets the environment requirements emerges and spreads throughout the network. If the environment or the agent function parameters change, and the selected function combination no longer meets the application requirements, agents evolve the algorithm and converge to new function combinations. In this way, agents always use the function combinations that suit the application requirements and the spatial environment. We also present a stabilization algorithm that reduces the churning phenomenon in different function combinations while maintains fast convergence of function selection.

We validate the *AREA* mechanism by applying it to the simulation of a data aggregation example. In the simulation example, each agent is supposed to have four basic functions: forwarding messages, routing messages, joining into clusters, and increasing the transmission range. The application requirement for every agent is to maintain the message arriving rate above a predefined threshold. By changing the agent density and

transmission bandwidth parameters, agents in the network self-create and self-evolve various function combinations according to the spatial distribution. For the implementation of each component in *AREA*, we in detail illustrate how to select the parameters of fitness functions, etc. based on the requirement. We use three other algorithms with fixed strategies for comparison. According to the test results, the *AREA* mechanism always maintains the best performance even when the environment and agent parameters change.

The remainder of the chapter is organized as follows. Section 3.2 overviews the *AREA* mechanism and the application example. Section 3.3 illustrates *AREA*'s components in detail and the example implementation. We present the simulation results and evaluations in Section 3.4, related work in Section 3.5, and conclusions in Section 3.6.

3.2. THE *AREA* MECHANISM OVERVIEW

In this section, we present the design framework of the *AREA* mechanism, the working components and the processing flow. And we demonstrate the general implementation of the data aggregation example based on *AREA*.

3.2.1. MECHANISM FRAMEWORK

It is supposed that each agent has some basic functions in the function set, such as forwarding messages, routing, etc. The agents are given an application requirement, such as "the message arriving rate should be larger than a predefined value". The agents self-create algorithms by selecting suitable combinations from predefined basic functions. When the environment changes, the agents self-evolve to select a different function combination as the new algorithm. In the system, each agent is independent and distributed, and only accesses the information of neighboring agents. The working process is automatic and in realtime. Figure 3.1 demonstrates an example of the *AREA* design framework. In the environment 1, the agent (node) converges to select the combination of function 1, 2 and 3 as the algorithm to fulfill the requirement. As the environment changes from environment 1 to 2, the originally created algorithm cannot meet the application requirement any longer. The agent evolves the algorithm and converges to select the combination of function 2 and 3. No matter how the environment changes, the agent always evolves to the function combination that will fulfill the predefined application requirements. After these requirements are fulfilled, the algorithm selected by the agents converges to a spatially stable state.

The *AREA* mechanism has four working components as shown in Figure 3.2(a). The first component is the definition of the *basic functions* of the agents in the function set. All predefined basic functions should work independently of each other. The second component is *function mutation*. Each basic function has a mutation probability that can change between being used and unused. So each agent can use different function combinations. The third component is *environment selection*. The agents in the network need to meet application requirements, such as maximizing the message arriving rate, minimizing the power consumption, etc. Each agent calculates a fitness credit for every function in the environment, and learns the function usage rule (using or unusing) of the agent with the largest function fitness credit in the neighboring agents. This component allows the most suitable function combinations to be survived and diffused in the spatial

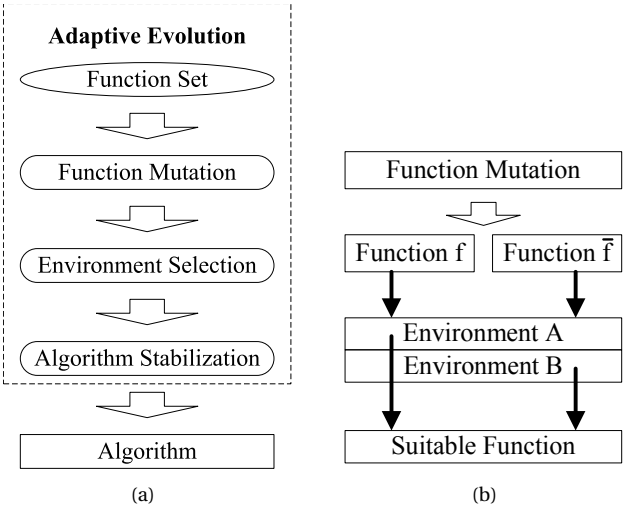

Figure 3.2: (a).The working flow components of the *AREA* mechanism combine the most suitable functions into an algorithm. (b).The function mutation component creates different function usage rules (f: use the function; $\overline{f}$: unuse the function), and the rule that best suits the environment (A or B) is selected as the suitable function.

network. To make the algorithm usable in practice, the algorithm needs to converge once the most suitable function combination is found. For this, the *algorithm stabilization* component is used. This component decreases the churn of selecting different function combinations in the network by each agent. The four components outlined above, make it possible for the agents in the network to select a suitable and stabilized function combination as the new algorithm. If the environment changes and the created algorithm can no longer fulfill the application requirements, the *AREA* mechanism will make the existing algorithm evolve to another function combination in order to meet the new application requirements.

3.2.2. APPLICATION EXAMPLE

The *AREA* mechanism is validated by implementing it in an application example: data aggregation. Data aggregation is a basic building block for spatial network application. Most of the existing data aggregation algorithms are designed for specific deployment environments. In deployment scenarios where the environment may change sometimes, these algorithms can no longer work properly. We use the *AREA* mechanism to implement data aggregation in changing environments.

Suppose agents are randomly scattered in an area. Each agent can only communicate with neighbors. A sink agent is predefined to aggregate messages from other agents. If new agents come into the network, the agent density increases. If existing agents leave the network, the agent density decreases. We define the bandwidth as the number of the messages that can be forwarded by a agent at one tick. The agent density and bandwidth are changeable in the environment. We suppose that each agent knows the number of messages that are sent out and arrive at the destination. The data aggregation implementation based on *AREA* allows the agents in the network to automatically find suitable function

combination that meet its application requirements. The created function combination for data aggregation maintains a high message arriving rate and low power consumption values.

In the simulation, the environment is changed by adapting the agent density and bandwidth. The different simulation scenarios are outlined in Figure 3.3. At the start of the experiment the agents are randomly deployed. Under standard agent density and bandwidth, agents self-create function combinations that use forwarding and routing functions, as shown in Figure 3(a). Then we change the environment by increasing the agent density. Because the bandwidth is limited, some messages are now dropped. So the agents start to evolve the existing data aggregation approach, and spatially self-organize to clusters to increase the message arriving rate in the network as shown in Figure 3(b). In case the agent density decreases, and the network becomes disconnected the message arriving rates of the agents that are not connected to the destination agent become 0. When this happens, some of the agents evolve their algorithm and increase the transmission range to connect the network as shown in Figure 3(c). The increased transmission range of the agents will increase their message arriving rates.

3.3. THE *AREA* COMPONENTS

Based on the overall design presented in Section 3.2, in the next subsections, we first define the content and structure of each component from *AREA*, and then present the detailed component implementation for the data aggregation example.

3.3.1. THE FUNCTION SET

Each agent has some basic functions in a function set. These basic functions, such as joining into a cluster, are predefined. For each agent, all the possible function combinations form the search space of the available algorithms. For the data aggregation application, we use four basic functions in the function set for each agent: forwarding messages, routing the messages via the shortest path, joining to a cluster with other neighbors and increasing the transmission range.

Firstly, each agent has the basic function that it can forward messages to a neighboring agent. The bandwidth of forwarding messages is limited. It is supposed that the agent can only forward a limited number of messages during one time slot. If the number of messages to be forwarded is larger than the bandwidth, the agent drops the excess messages.

For the second function it is assumed that each agent can calculate the next hop on the shortest path based on the gradient [115]. If the agent knows the next hop on the shortest path, the agent forwards the messages to the next hop. Otherwise, the agent forwards the messages to a random neighboring agent. We assume that if the message is forwarded to a hop that is further away from the destination agent, then next hop agent drops the message.

Agents also have the function to join in a cluster. In a cluster, the cluster leader represents all the members to send out messages. Because the bandwidth is limited, we suppose that the forwarding priority of the message from a cluster is higher than the message from a single agent. And it is assumed that the forwarding priority of the message

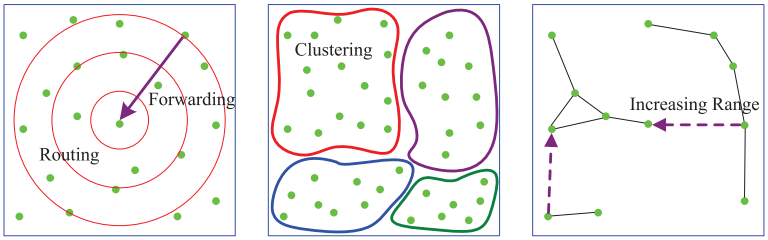

Figure 3.3: The application example of *AREA* for data aggregation. (a). Agents evolve to use forwarding and routing functions. (b). Agents form clusters to send out messages. (c). Agents unconnected to the destination agent increase their transmission range.

from a cluster with larger number of member agents is higher than the message from a cluster with smaller number of member agents. Agents forward messages from higher to lower priority.

Finally, agents have the basic function to increase their transmission range. Each agent has a default and an increased transmission range. If the agent cannot connect to the network with the destination agent using the default transmission range, then it can reconfigure (mutate) to use the increased transmission range.

3.3.2. FUNCTION MUTATION

In this section, we present how the function combinations are created for each agent. We define the function combination series $\{f_1, f_2, ..., f_i, ..., f_n\}$. Where n is the total number of functions. f_i represents the basic function i explained in Section 3.3.1. The value of f_i can be 0 or 1. $f_i = 0$ means that the function i is not used in the function combination, and $f_i = 1$ means that the function i is used. All the basic functions together form a function combination series. In the initial state, agents select a random value (0 or 1) for f_i ($i = 1, 2, ..., n$) of each basic function. In the function mutation component, *AREA* makes each agent change the function value f_i by setting $f_i = \overline{f_i}$ with a mutation probability.

In the application example, agent x has a $Switch_{xi}$ value 0 or 1 for each function i representing unused or used. We predefine a mutation probability P_m for all the basic functions. If a random value is smaller than P_m, then $Switch_{xi}$ does not change. Otherwise, $Switch_{xi}$ is changed to $\overline{Switch_{xi}}$.

3.3.3. ENVIRONMENT LEARNING

In this section, we demonstrate how agents learn from each other, and make the most suitable function combination spread throughout the network. We define the fitness credit of the function for each agent by $C_i = w_{i1}c_{i1} + w_{i2}c_{i2} + \cdots + w_{ik}c_{ik} + \cdots + w_{im}c_{im}$. Where i is the function number as defined in Section 3.3.2. k ($k = 1, 2, ..., m$) is the number of the evaluation criteria for the function, and m is the total number of evaluation criteria. For example, the performance of the network can be determined by the arriving rate, power consumption, etc. c_{ik} is the fitness credit of the function i evaluated by the criteria k. w_{ik} is the weight of the fitness credit with evaluation criteria k. In the learning

component, each agent records the fitness credit of each function. At the same time, each agent detects the fitness values of the functions from neighboring agents and learns the function usage strategy (used or unused) from the agent with the largest fitness credit. Finally, the function combination that has the largest fitness credit in the network survives and spreads. The mutation and learning process is shown in Figure 3.2(b).

For the application example, we define the fitness credit for every function as follows. The fitness credit of forwarding the messages is defined as $AR \cdot W_{AR} + FR \cdot W_{FR} + FC \cdot W_{FC}$. The AR value equals the percentage of the number of messages arriving at their destination. If the agent forwards messages of other agents, then $FR = 1$; otherwise, $FR = 0$. FC is the power consumption credit for forwarding messages. If the agent forwards messages, FC is 0; otherwise, FC is 1. W_{AR}, W_{FR} and W_{FC} are the weight values of AR, FR and FC. The value domain of AR is $[0,1]$. FR and FC can be 0 or 1. For different application requirements, AR, FR and FC can be set to different values. In the simulation, each agent sends out 10 messages for each communication round, so the precision accuracy is 0.1. The message arriving rate is assumed to be the most important evaluation criteria. Therefore, the weight value of the arriving rate is set as $W_{AR} = 1$. $W_{FR} = 0.02$ and $W_{FC} = 0.01$. Their sum is smaller than the arriving rate precision accuracy 0.1, so their weight values do not affect the distinction among different message arriving rate values. In the network, we suppose that forwarding messages is more important than saving energy. We set $W_{FR} = 0.02$, which is larger than $W_{FC} = 0.01$. The fitness credit of routing messages is defined as $AR \cdot W_{AR} + FR \cdot W_{FR} + RC \cdot W_{RC}$. RC is the power consumption credit for routing. If the agent calculates the next hop on the shortest path, $RC = 0$; otherwise $RC = 1$. The weight value $W_{RC} = 0.01$. The fitness credit of constructing a cluster is defined as $AR \cdot W_{AR} + CC \cdot W_{CC}$. CC is the power consumption credit for constructing and maintaining a cluster. If the agent joins in a cluster, $CC = 0$; otherwise $CC = 1$. The weight value $W_{CC} = 0.01$. The fitness credit of adjusting the transmission range is defined as $AR \cdot W_{AR} + RN \cdot RU \cdot W_{RU} + RC \cdot W_{RC}$. Where RN is the parameter that shows whether the agent has a connection route to the destination agent. If the agent cannot find a connection route to the destination agent, then RN is set to 1, which means that the agent has increased its transmission range to the maximum allowed value. RU is the usage value of increased transmission range. If the agent increases the transmission range, and the increased range is used to forward messages of other agents, then $RU = 1$; otherwise $RU = 0$. The weight value W_{RU} is set to 0.02. RC is the power consumption credit for using different transmission ranges. If the agent uses the default transmission range, $RC = 1$; if it uses the increased transmission range, $RC = 0$. The weight value $W_{RC} = 0.01$.

3.3.4. STABILIZATION

To make the selected function combination feasible, it must be stable. In this section, we introduce an algorithm that can stabilize the system. The mutation and learning probability are the main factors that affect churning in the selection and spread of the function combination among agents. First, we define a fitness credit threshold value T_i. This value equals the minimum acceptable fitness credit value by using or unusing the function i. Then we define a stabilization rate D, which equals the rate between the normal mutation or learning probability and the minimum acceptable mutation or

Algorithm 1 : Stabilization for Mutation and Learning

Mutation:
for all Agent x **do**
  if $(C_i \leq T_i \& R < P_M) ||| (C_i > T_i \& R < (P_M / D))$ **then**
    $Switch_{xi} = 1 - Switch_{xi}$
  end if

Learning:
for all Agent x **do**
  $maxC = max([C_i]\ of\ Nb)$
  if $maxC > C_i$ **then**
    if $(C_i \leq T_i \& R < P_L) ||| (C_i > T_i \& R < (P_L / D))$ **then**
      $Switch_{xi} = [Switch_{xi}]\ of\ Nb\ with\ [maxC]$
    end if

learning probability. If the fitness credit of the function i is smaller than T_i, then the agent selects learning probability P_L and mutation probability P_M. Otherwise, the agent selects learning probability $\frac{P_L}{D}$ and mutation probability $\frac{P_M}{D}$. So each agent uses low mutation and learning probabilities in the state with acceptable fitness credit to decrease churning of different function combinations. The detail processing flow is shown in Algorithm 1. Each agent x is given a $Switch_{xi}$ value for each function i. Where the switch values change between 0 and 1 representing unusing and using the function, R is the random probability from 0 to 1 and Nb is the neighbor agents.

To encourage the use of the forwarding and routing functions, in the data aggregation application, the threshold values of forwarding and routing are set to 1.01. So only agents with fitness credit 1.02 and higher can use $\frac{P_L}{D}$ and $\frac{P_M}{D}$ to learn and mutate. Whether to actually use the clustering and increasing the transmission range functions is based on the environment condition, such as agent density, bandwidth, etc., so the threshold value of clustering and ranging are set to 0.99 and 1.0 respectively.

3.4. TEST AND EVALUATION

We use NetLogo [211] for the simulation experiment. The deployment area is a 200×200 square region. Agents are static and randomly scattered across the area. Each agent sends out one message per one tick. After sending 10 messages, each agent waits 10 ticks for calculating the message arriving rate. We call the 20 ticks as one communication round. The default transmission range of each agent is 40 units. All the agents send messages to one specified destination agent. We run the experiment 10 times for each testing point.

3.4.1. ADAPTATION TO ENVIRONMENTS

In the experiments, the environment changes by varying the agent density and the bandwidth. The agent density ranges from 5 to 40, with 5 offset. The bandwidth is 5×2 units. m is from 0 to 7, with 1 offset. Three evaluation parameters are used: average message arriving rate, average power consumption unit and average arriving rate per power consumption unit. Three other data aggregation methods are used for comparison. The first method, named as *FR*, makes all agents forward and route the messages. The second method, named as *FRC*, makes all agents construct a fixed number of clusters. All agents can forward and route the messages, but only the cluster leader represents the cluster to send out messages. The cluster number is set to 20. The third method, named as *FRR*,

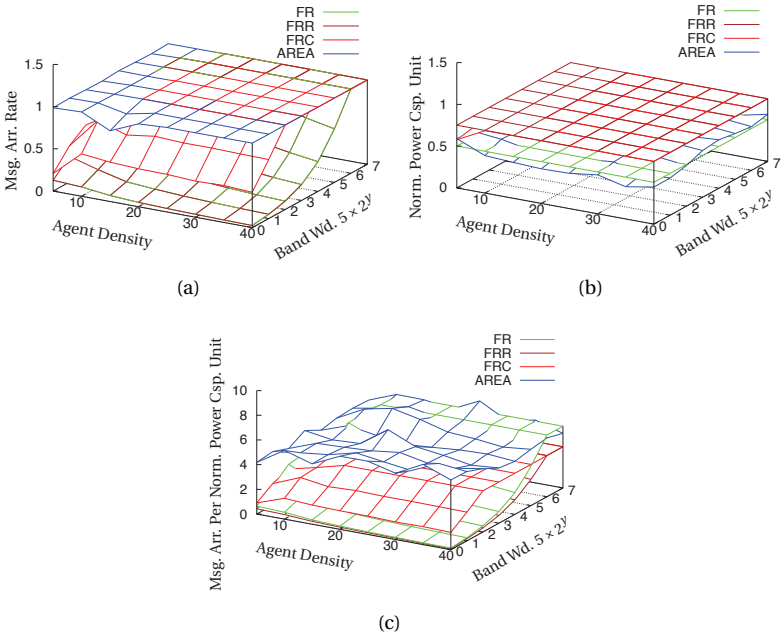

Figure 3.4: (a).Average message arriving rate for various agent densities and bandwidths. (b).Normalized average power consumption unit for various agent densities and bandwidths. (c).Average message arriving count per normalized power consumption unit for various agent densities and bandwidths.

makes all agents use the increased transmission range to forward and route the messages. The increased transmission range is 80 units. To evaluate the power consumption performance, we suppose that the running of each basic function consumes 1 unit power per round.

Figure 3.4(a) shows the average message arriving rate for various agent densities and bandwidths. The *AREA* mechanism has the best arriving rate in the low density area 5. This is because the network is generally unconnected with agent density 5. If the agents that are not connected to the destination agent do not increase their transmission range, they cannot send messages to the destination. Furthermore, the *AREA* mechanism makes some agents increase their transmission range to link the connected network. In the low bandwidth area from 0 to 2, the *AREA* mechanism constructs clusters to meet the bandwidth restrictions. The method *FRC* uses clusters to increase the message arriving rate. When the bandwidth is equal or larger than 20, which is equal to the fixed cluster number of *FRC*, the *FRC* method has the best arriving rate. But because it is construct with a fixed number of clusters, the method is not adaptive to the variation of the environment. If the environment has unconnected subnetwork or very low bandwidth, agents using the *FRC* method will drop messages. Agents that use the *FRR* method also use the increased transmission range all the time. In the connected network with low bandwidth, increasing the transmission range cannot always increase the message arriving rate. Although *AREA*

does not have the best arriving rate, the difference to the best arriving rate is very small. This is because agents need to keep a mutation rate to adapt to the new environments in *AREA*. When the bandwidth is larger than 6, the *FR* and *FRR* methods can also have near optimal message arriving rate. This is because that the bandwidth is larger than the total number of agents in the network. So no matter how the network topology is constructed, all the messages will finally arrive at their destination.

Figure 3.4(b) illustrates the power consumption for various agent density and bandwidth. Because there are four types of basic functions, the average power consumption unit is normalized to 4. It can be found that the *FRC* and *FRR* methods consume the same amount of energy in all the testing points. This can be explained because all agents always use clustering in the *FRC* method and increase their transmission range when using the *FRR* method. This is because it only uses two basic functions: forwarding and routing. The power consumption of *AREA* is larger than *FR*, because *AREA* sometimes increases its transmission range and constructs a cluster to increase the message arriving rate. But *AREA* makes all the agents in the network automatically adapt to the different environments.

In order to evaluate the efficiency of the *AREA* algorithm, we calculate the rate between the message arriving count and the power consumption unit for various agent densities and bandwidth values, as shown in Figure 3.4(c). It can be seen that the *AREA* algorithm is the most efficient method for almost all the testing points. Only in the very high bandwidth area, the *FR* method is slightly more efficient. This is again because the total bandwidth is larger than the total number of agents. Since the *AREA* algorithm always will mutate to other function combinations, its efficiency is slightly less at this point.

3.4.2. STABILIZATION EFFICIENCY

Agents in environments with a different spatial distribution could churn in different function combinations. Stabilization of the function selection is an important evaluation parameter. We test the stabilization algorithm presented in Section 3.3.4.

The testing results are shown in Figure 3.5. We initialize the environment with an agent density of 20 and bandwidth of 40. The y coordinates of Figure 3.5(a) and Figure 3.5(b) are the message arriving rate and the normalized power consumption unit respectively. The x coordinates in both figures are calculated by $x = \lg D$, in which D is the stabilization rate with value 1, 5, 10, 50, 100, 500, 1000, 5000, 10000. The other testing parameters are the same as the previous experiments. According to the results, as the stabilization rate D increases from 1 to 10000, the standard deviations of the message arriving rate and power consumption value decreases significantly. When the stabilization rate becomes 10000, which is 4 ($= \lg 10000$) in the figures, the standard deviations of the arriving rate and power consumption are 0.022 and 0.015. As the stabilization rate increases, the message arriving rate increases from 0.87 to 1. This is because the low stabilization rate D make the system unstable, and further decreases the message arriving rate. Therefore the stabilization Algorithm 1 can effectively stabilize the function mutation and learning.

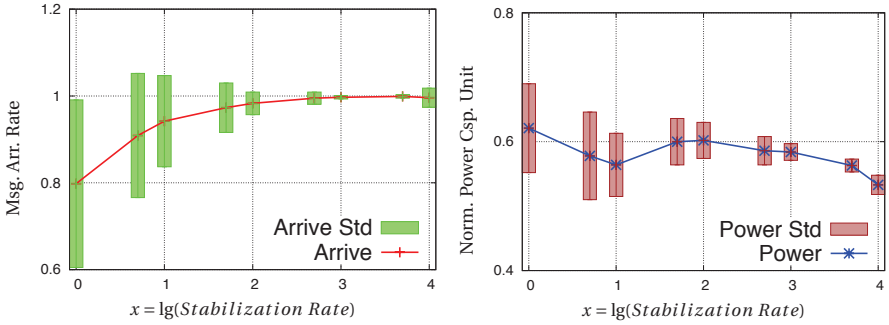

Figure 3.5: (a).The average message arriving rate and standard deviation with various stabilization rates D. (b).The normalized power consumption unit and standard deviation with various stabilization rates D.

3.5. RELATED WORK

Traditional spatial computing algorithms [12] [41] primarily focus on function implementation in a fixed environment. The spatial and temporal distribution of the agents in the network significantly affect the relations among agents. In this chapter, we make advantage of the coordination between agent interaction in the spatial network to promote the evolution of algorithms adapting to various changing environments.

Evolutionary dynamics [156] researches the power of advancing the system to evolves from one state to another on a global population level. Evolution dynamics theory forms the theoretical basis on which the *AREA* mechanism is founded. Evolutionary computing is widely researched for producing optimized systems [83]. Traditional evolutionary computation [132] selects members via centralized methods, which is not very efficient in distributed environments. Nakano and Suda [147] and Lee et al. [107] improve the adaptation mechanisms using evolutionary computing. They propose design structures that build adaptive network services using bio-inspired distributed agents. By evolutionary adaptation, agents can evolve and adapt their behavior to the changing environments. And Champrasert et al. [28] present a structure to self-optimize and self-stabilize cloud applications. It extends the biological evolutionary adaptation from agents to related platforms. But the above papers do not explain the influence of the parameters to the performance of the system. Moreover, these works focus on the construction of services using interacting agents, and the simulation is on a grid network, which does not map naturally (nor easily) to wireless networks. Mirko et al. [200] extends the tuple spaces by chemical-inspired model to coordinate spatially pervasive services. Although the mechanism can effectively make services diffuse and interact in a spatial network, it can not coordinate multiple different services together to cope with various problems.

3.6. CONCLUSIONS

We propose a new mechanism: *automatic runtime evolutionary adaptation (AREA)* for spatial algorithm design. It can effectively create and evolve the algorithms in wireless

networks to meet application requirements and adapt to the changing of the environment. The working process of *AREA* is automatically updated in every agent during runtime and the created algorithm works stably in the network. The mechanism is validated by simulation experiments of data aggregation.

4

GDE: A DISTRIBUTED GRADIENT-BASED ALGORITHM FOR DISTANCE ESTIMATION IN LARGE-SCALE NETWORKS

To further explore self-adaptive self-organization properties as researched in Chapter 3, this chapter [1] researches distance estimation as the case study. The common goal of this chapter and Chapter 3 is to achieve global control using local information exchange, and each node makes autonomic management.

4.1. INTRODUCTION

Nowadays, large-scale wireless networks are connecting most of the devices around us. Along with ubiquity comes also the problem of tremendous scale. The current approaches that enable services such as routing, data dissemination, context detection, etc. require new, radical changes, in order to assure scalability. When location information is needed, most of the current algorithms presume that node position information via GPS is available. For some application scenarios, such an approach is feasible (e.g., outdoors). Unfortunately, for most of the cases, GPS is either not available (e.g., indoors) or it is inaccurate and most likely consumes a lot of power. For all these reasons, there is a need for ways to estimate distances between nodes only based on local interaction with no additional information such as the one provided by GPS. In this chapter, we introduce *a gradient-based distance estimation algorithm*, called *GDE*, to estimate distances using very

[1] This chapter is published as the paper:
Qingzhi Liu, Andrei Pruteanu, Stefan Dulman. *GDE: a Distributed Gradient-Based Algorithm for Distance Estimation in Large-Scale Networks.* In Proceedings of the ACM MSWiM, Miami Beach, FL, USA, Oct. 31- Nov. 4, 2011.

simple, local interactions between nodes. The algorithm is based on a hop-count gradient that is smoothed to decrease the estimation error [146]. Additionally, we introduce two error compensation methods that improve its accuracy. Our approach is suited also for mobile networks and deployments having non-uniform spatial distributions.

The chapter is a theoretical study on the feasibility of such an approach for large-scale, dynamic systems. We validate our models via simulations with various environment parameter setups, such as node density, node speed, and propagation model. The testing results show that our algorithm has good performance in distance estimation accuracy. The rest of the chapter is organized as follows. Section 4.4 presents the *GDE* algorithm for a static, uniform deployment. Section 4.5 presents strategies making the algorithm work in real deployments. An in-depth simulation-based analysis of *GDE* for various parameter setups is presented in Section 4.6. We conclude the chapter in Section 4.7.

4.2. RELATED WORK

Distance estimation for wireless systems is one of the most important building blocks for various services such as routing [171], clustering [228], localization [66, 172], etc. For the case of geographic routing, nodes use locations as their addresses, and forward packets (when possible) in a greedy manner towards the destination. However, this approach demands for the nodes to be aware of their location information. While this is a feasible assumption in some settings (e.g., nodes have GPS modules attached), there are many cases (e.g., indoors) where node location information is either not available or it requires additional expensive equipments. For clustering algorithms [63] that require node position information, again, all nodes are assumed to be aware of their location information. To optimize for power, the GPS module has to be turned on for a very short time during bootstrapping. This approach does make sense when the nodes are either static or there are small changes of the network topology. When nodes are always moving for example, the localization system has to be turned on continuously, thus leading to a high power consumption.

Besides GPS, other methods suitable in particular for indoor deployments, make use of the wireless signal strength [9]. The main problem this class of algorithms is facing is the lack of accurate models for indoor radio propagation. Issues arise from various sources such as multi-path effects, reflection, and fading effects. Most of the time, there is limited correlation between the received signal strength indication and the real distance between devices.

The algorithm [146] serves as a starting point for our work and builds a self-organized, global coordinate system on top of a ad-hoc wireless sensor network. It relies only on distributed, simple computations and local communication. The distance estimation results can be used to calculate an estimated position, and the algorithm adapts to failures and additions of nodes. A remarkable aspect uncovered in the described scenarios (i.e., the presence of obstacles) is that greedy routing performs better when using virtual coordinates than when using the actual geographic coordinates.

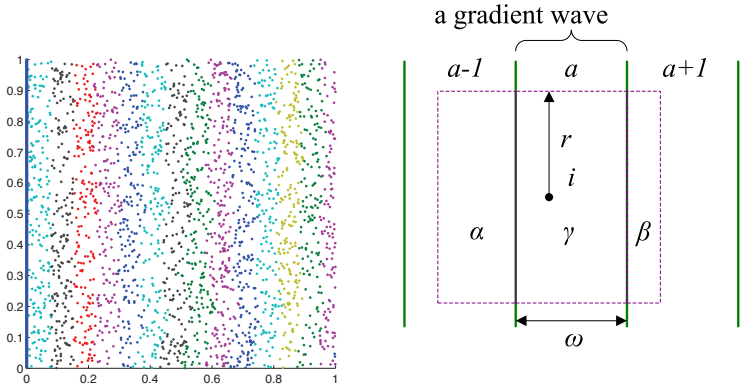

Figure 4.1: (a). Hop-count gradient triggered by a vertical line of seeds (left side of the area). (b). Adjacent hop-count gradient waves around node i.

4.3. EXISTING GRADIENT ALGORITHMS

In this section we briefly introduce the details of the related work, mainly the algorithm presented in [146]. Suppose all nodes are static and uniformly distributed in a deployment area, and the transmission range of each node is r. The node density is defined as the average number of nodes in the local transmission range of each node. Some nodes, called *seeds*, are placed at fixed positions, and take a constant counter value. Each node, except the seeds, listens to its neighbors and selects the largest counter value, and then rewrites the local counter value decreased by one. So the counter values of all nodes in the deployment area vary uniformly: the nodes closer to the seed nodes have larger counter values, and the nodes that are further from the seed nodes have smaller counter values. We refer to this variation trend as *gradient*. Figure 4.1(a) shows the resulting gradient when a straight line of seed nodes are vertically placed at the left side of the deployment area, and each node in the figure is colored according to its own counter value.

One can notice in Figure 4.1(a) that the obtained gradient is not smoothed but looks rather like stairs. This is because each node calculates the local counter value using only *the largest counter value* in its own transmission range, so based on this strategy, some adjacent nodes will finally take the same local counter values. We call the nodes with the same counter values a *wave* in the gradient. Because the width of each wave depends on the maximum number of hops from the seeds, we call this gradient the *hop-count gradient*.

4.3.1. SMOOTHED GRADIENT

The distance estimation produced by the hop-count gradient is a multiple of the width of the gradient wave ω. It produces an average error of approximately 0.5ω [146]. To improve the accuracy, the local neighborhood gradient values can be used to smooth the hop-count gradient. To simplify the equations, the transmission area of every node is approximated to a square with side length $2r$. Figure 4.1(b) shows the transmission

area of node i. By a we denote the integer hop-count gradient value of node i. α, β and γ are the ratio of the three areas in various hop-count gradient waves to the size of the transmission area as seen by node i. Because the nodes are uniformly distributed in the area, α, β and γ are supposed to be equal to the rates between the number of nodes in the adjacent three areas to the total number of nodes in the transmission range respectively. Suppose the width of each wave ω equals the transmission range r of the node. The smoothed gradient value of node i is:

$$\begin{aligned} G_\alpha &= (a-1)r + (r-2r\alpha) \overset{r=1}{=} a - 2\alpha \\ G_\beta &= ar - (r-2r\beta) \overset{r=1}{=} a + 2\beta - 1 \\ G_{\alpha\beta} = G_{SMG} &= \frac{G_\alpha + G_\beta}{2} \overset{r=1}{=} a - \alpha + \beta - \frac{1}{2} \end{aligned} \tag{4.1}$$

Another approach to calculate the smoothed gradient is to average the gradient values of the neighbor nodes [146]. The average gradient value is G_a (in which n_l is the number of nodes in the transmission range of node i) and the smoothed gradient value is G_{SMG}:

$$G_{avg} = \frac{n_l\alpha(a-1) + n_l\gamma a + n_l\beta(a+1)}{n_l} = a - \alpha + \beta \tag{4.2}$$

$$G_{SMG} = G_{avg} - \frac{1}{2} = a - \alpha + \beta - \frac{1}{2} \tag{4.3}$$

4.4. GDE ALGORITHM

In this section we introduce the main contribution of this chapter, the *GDE* algorithm. We introduce successively a series of improvements that make *GDE* a suitable algorithm to run in a distributed dynamic environment.

4.4.1. GRADIENT WIDTH REDUCTION

Suppose node i has transmission range r and node k has the largest distance to node i among all the nodes in the transmission range of node i. The number of nodes in the area is not infinite, thus there is high chance that the node k is not exactly on the border of the transmission range of node i, thus the distance between node k and node i is smaller than the transmission range r. This implies that the width of the hop-count gradient wave becomes smaller than r, next referred to as *width reduction of gradient waves*.

Figure 4.2 shows the phenomenon of width reduction of gradient waves. Suppose node n is at the border p_{bu} of hop-count gradient wave $a-1$, and node m at the border p_b of hop-count gradient a can just discover node n. Because the node density is not infinite, there is a high chance that there is no node on the line of border p_{bu}, and the nodes that are closer to the border p_{bu} are on the line p_{wu}. So the real border of the hop-count gradient wave $a-1$ moves from p_{bu} to p_{wu}. Suppose node n is replaced at position n'. The last node that can discover the node n' has to move from position m to m'. The border of the hop-count gradient wave a changes from p_b to p_w, because of the movement of the previous border from p_{bu} to p_{wu}. The nodes positioned between p_b and p_w, such as node v, can no longer discover the nodes with hop-count gradient value $a-1$, so updates the hop-count gradient value to $a+1$.

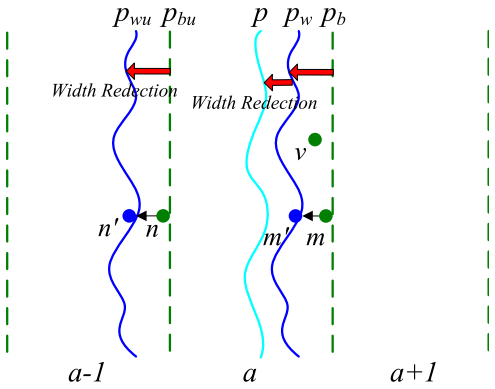

Figure 4.2: Width reduction of gradient waves.

At the same time, because of the nodes missing around border p_w, the nodes that are closer to the border p_w are on the line p. So the real border of the hop-count gradient wave a moves from p_b to p. As a result, the width of the hop-count gradient wave becomes smaller. At the same time, the movement of the border always influences the border positions of all the next hop-count gradient waves, so the movement distance of borders, such as p_b to p in hop-count gradient wave a, becomes larger and larger.

Suppose the estimated physical distance corresponding to a communication hop is d_{hop}. Equation 4.4 (taken from [96]) shows the relation between the real estimated distance and the node density n_l.

$$d_{hop} \overset{r=1}{=} (1 + e^{-n_l} - \int_{-1}^{1} e^{-\frac{n_l}{\pi}(\arccos t - t\sqrt{1-t^2})} dt) \tag{4.4}$$

Let $\Delta = 1 - d_{hop}$ be the width reduction of each hop-count gradient wave. As explained, the movement distance of borders has a cumulative characteristic and is related to the hop-count gradient value. The cumulative reduced width of the node with hop-count gradient value a is $S_i = (a-1)\Delta$ and the gradient width reduction value is $G_{si} = G_{SMG} - S_i$.

4.4.2. AVERAGING FOR REDUCED GRADIENT WIDTH

The width reduction of the gradient wave influences the result of the smoothed gradient. Each node in the one hop-count gradient wave could be placed at two positions. The first one is shown in Figure 4.3(a), where node n is not in the reduced width area of the gradient wave. The second place is shown in Figure 4.3(b), where node n is in the reduced width area of the gradient wave.

In the first case, as shown by Figure 4.3(a), the percentages of discovered nodes in α, β, γ become α', β', γ', as shown in Equation 4.5. In the second case, as shown by Figure 4.3(b), the percentages of discovered nodes in α, β, γ become α'', β'', γ'', as shown by Equation 4.6.

$$\begin{aligned}
\alpha' &= \frac{2r\alpha - S_i^{a-1}}{2r} \overset{r=1}{=} \alpha - \frac{1}{2}(a-1)\Delta \\
\beta' &= \frac{2r\beta + S_i^{a}}{2r} \overset{r=1}{=} \beta + \frac{1}{2}a\Delta \\
\gamma' &= \frac{2r\gamma + S_i^{a-1} - S_i^{a}}{2r} \overset{r=1}{=} \gamma - \frac{1}{2}\Delta
\end{aligned} \tag{4.5}$$

$$\begin{aligned}
\alpha'' &= \frac{2r\alpha + (r - S_i^{a-1})}{2r} \overset{r=1}{=} \alpha + \frac{1}{2} - \frac{1}{2}(a-1)\Delta \\
\beta'' &= \frac{2r\beta - (r - S_i^{a})}{2r} \overset{r=1}{=} \beta - \frac{1}{2} + \frac{1}{2}a\Delta \\
\gamma'' &= \frac{2r\gamma - (r - S_i^{a-1}) + (r - S_i^{a})}{2r} \overset{r=1}{=} \gamma - \frac{1}{2}\Delta
\end{aligned} \tag{4.6}$$

If the node is outside the reduced width area, the average gradient value is $G_{avg}^{out} = a - 2\alpha + \frac{1}{2} + (a\Delta - \frac{1}{2}\Delta)$ and the smoothed gradient value is $G_{si}^{out} = G_{avg}^{out} - \frac{1}{2} - (a-1)\Delta - \frac{1}{2}\Delta$. If the node is inside the reduced width area, the average gradient value is $G_{avg}^{in} = a - 2\alpha - \frac{1}{2} + a\Delta - \frac{1}{2}\Delta$ and the smoothed gradient value is $G_{si}^{in} = G_{avg}^{in} - \frac{1}{2} - (a-1)\Delta - \frac{1}{2}\Delta + 1$.

Due to the fact that nodes do not have position information and cannot tell whether they are inside or outside the reduced width area, we compute the expected average value of the gradients G_{si}^{out} and G_{si}^{in}. $R_{in} = \frac{(r - rd_{hop})}{r} \overset{r=1}{=} 1 - d_{hop}$ represents the percentage of the reduced width of one hop-count gradient wave normalized to r. $R_{out} = 1 - R_{in} \overset{r=1}{=} d_{hop}$ is the percentage of the not-reduced width of one hop-count gradient wave, normalized to r. The gradient value is given by $G_{esi} = G_{si}^{out} R_{out} + G_{si}^{in} R_{in}$.

4.4.3. OVERESTIMATED WIDTH REDUCTION

The gradient calculation in Section 4.4.1 uses the expected average value d_{hop}. But this expected average value will overestimate the width reduction of gradient waves. Suppose the gradient wave border moves as shown in the Figure 4.4(a). If the border moves from p_b to p, and node n is located in the area $(p + d_{hop})^+$, which means node n cannot discover the nodes on the border p, then the calculated hop distance d_{hop} is the expected width of hop-count gradient wave. But the real border that moves to p can not be a straight line, but a curved line like p_r. Node m' may move to the position of node m, to be inside the transmission range of the node n. As a result, node n can discover some of the nodes on the border p. This implies that the reduced width Δ is overestimated.

Assume the shape of the gradient waves is parallel lines, the node density is ρ and the transmission range of each node is r. The probability that k nodes are located in the area of size h is given by $\Pr(k \in h) = \frac{(\rho h)^k}{k!} e^{-\rho h}$ [146].

For example, in Figure 4.4(b), node n has d_{hop} as the real communication hop distance, which is given in Equation 4.4. Let p be the gradient wave border using d_{hop}, p_d

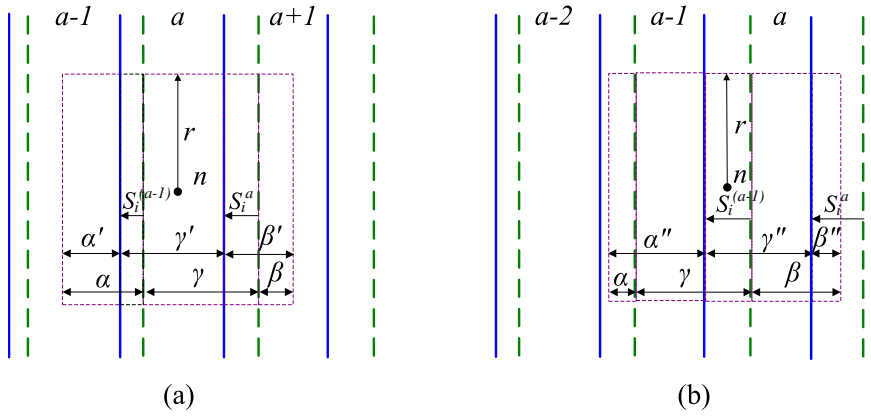

Figure 4.3: Average gradient for reduced width waves.

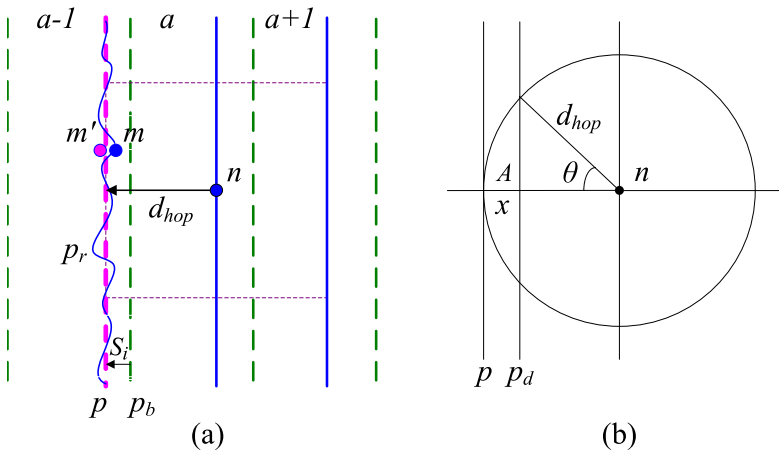

Figure 4.4: (a). Overestimation of gradient width reduction. (b). Expected reduced wave width.

the real border of the gradient wave, X is the overestimated reduced width, and A is the overlap area of the overestimated reduced width area and the transmission range. The probability that there are no nodes in the area A equals the probability that the gradient border p will have a shift larger than x: $\Pr(0 \in A) = \Pr(X > x) = e^{-\rho A}$.

Therefore, the probability distribution function of the overestimated reduced width X is given by:
$F(x) = \Pr(X \leq x) = 1 - e^{-\rho A}$.

Area A is computed using Equation 4.7 and the probability density function of X is shown in Equation 4.8. The expected overestimated reduced width Δr of the one hop-count gradient wave can be written as Equation 4.9. a being the hop-count gradient value

of the node, the gradient value for each node, the basic *GDE* value, can be calculated as:

$$A = 2[\pi r^2 \frac{\arccos\frac{r-x}{r}}{2\pi} - \frac{(r-x)\sqrt{r^2-(r-x)^2}}{2}] \tag{4.7}$$

$$f(x) = \mathrm{F}'(x) \overset{r=1}{=} \frac{\rho - 2x^2 + 4x - 1}{e^{(x-1)\sqrt{2x-x^2}+\rho\arccos(1-x)}\sqrt{2x-x^2}} \tag{4.8}$$

$$\begin{aligned}\Delta r = E(x) &= \int_0^1 x f(x)dx \\ &= \int_0^1 x \frac{\rho - 2x^2 + 4x - 1}{e^{(x-1)\sqrt{2x-x^2}+\rho\arccos(1-x)}\sqrt{2x-x^2}}dx\end{aligned} \tag{4.9}$$

$$G_{GDE} = G_{si}^{out} R_{out} + G_{si}^{in} R_{in} + (a-1)d_{hop}\Delta r \tag{4.10}$$

4.4.4. ERROR REFERENCE VALUE

This section introduces an error reference value, which can be used as a benchmark for the testing results of the distance estimation error.

If node density ρ tends to $+\infty$, then Δ and Δr converge to 0, as shown by Equations 4.11 and 4.12, which means gradient width reduction problem disappears for large node densities.

$$\lim_{\rho\to+\infty} \Delta \overset{r=1}{=} 1 - \lim_{\rho\to+\infty} d_{hop} = 0 \tag{4.11}$$

$$\lim_{\rho\to+\infty} f(x) = 0 \Rightarrow \lim_{\rho\to+\infty} \Delta r = 0 \tag{4.12}$$

The number of nodes n in the area of size h follows a $Poisson$ distribution with parameter λ (λ=ρh). If node density ρ goes to $+\infty$, then the probability distribution of n nodes in the area of size h tends to follow a $Normal$ distribution with a mean λ and a deviation of λ (Equation 4.13). Therefore, if node density ρ goes to $+\infty$, the number of nodes in various hop-count gradient waves of a transmission range obeys a $Normal$ distribution (Equation 4.14), in which n_α and n_β are the number of nodes in section α and β, and S_α and S_β are the area size of section α and β.

$$n \sim P(\lambda) = \frac{\lambda^n}{n!}e^{-\lambda} \overset{\lambda\to+\infty}{\Rightarrow} n \sim N(\lambda,\lambda) \tag{4.13}$$

$$n_\alpha \sim N(\rho S_\alpha, \rho S_\alpha),\ n_\beta \sim N(\rho S_\beta, \rho S_\beta) \tag{4.14}$$

The linear combination of $Normal$ distributions also follows a $Normal$ distribution. The computed gradient value using Equation 4.10 follows a $Normal$ distribution (Equation 4.15), in which n_l is the average number of nodes in the transmission range of a node.

$$\begin{aligned}\lim_{\rho\to+\infty} G_{GDE} &= \lim_{\rho\to+\infty}(a - \frac{n_\alpha}{n_l} + \frac{n_\beta}{n_l} - \frac{1}{2}) \\ &\sim N(a - \frac{\rho S_\alpha}{n_l} + \frac{\rho S_\beta}{n_l} - \frac{1}{2}, \frac{\rho(S_\alpha+S_\beta)}{n_l^2})\end{aligned} \tag{4.15}$$

If nodes are distributed on a grid and node density goes to infinity, then by using Equation 4.16 the gradient is computed as G^g_{GDE}. If nodes in the area are uniformly distributed and node density goes to infinity, then using Equation 4.17 the gradient is computed as G^u_{GDE}.

$$G^g_{GDE} \overset{\rho\to+\infty}{=} a - \frac{\rho S_\alpha}{n_l} + \frac{\rho S_\beta}{n_l} - \frac{1}{2} \tag{4.16}$$

$$G^u_{GDE} \overset{\rho\to+\infty}{=} a - \frac{n_\alpha}{n_l} + \frac{n_\beta}{n_l} - \frac{1}{2} \tag{4.17}$$

If all nodes are uniformly distributed, the error becomes ΔG, which is the absolute difference value between the gradient that is computed when nodes are distributed on a grid and the gradient computed when nodes are uniformly distributed (Equation 4.18), in which $S_l = \pi r^2$.

$$\Delta \mathrm{G} = G^u_{GDE} - G^g_{GDE} = (\frac{S_\alpha}{S_l} - \frac{n_\alpha}{n_l}) + (-\frac{S_\beta}{S_l} + \frac{n_\beta}{n_l}) \tag{4.18}$$

Equation 4.14 shows the probability distribution of the number of nodes n_α and n_β. While ΔG is the linear combination of the $Normal$ distributions of n_α and n_β, the ΔG also follows a $Normal$ distribution. The expected absolute error of distance estimation $E(|\Delta G|)$ is:

$$\begin{aligned} \Delta \mathrm{G} &\sim N(\tfrac{S_\alpha}{S_l} - \tfrac{\rho S_\alpha}{n_l}, \tfrac{\rho S_\alpha}{n_l^2}) + N(-\tfrac{S_\beta}{S_l} + \tfrac{\rho S_\beta}{n_l}, \tfrac{\rho S_\beta}{n_l^2}) \\ &\overset{n_l = S_l\rho}{\sim} N(0, \tfrac{\rho S_\alpha + \rho S_\beta}{n_l^2}) \overset{S_\alpha + S_\beta = \frac{1}{2}S_l}{\sim} N(0, \tfrac{1}{2n_l}) \end{aligned} \tag{4.19}$$

$$E(|\Delta G|) = \frac{1}{\sqrt{\pi n_l}} \tag{4.20}$$

It can be seen that as the node density tends to infinity, the error tends to zero (case not met in a reality). This result is the error of distance estimation in the ideal case, which can be used as a benchmark for the experimental results.

4.5. ALGORITHM PARAMETERS

So far we discussed about algorithms in more or less idealized conditions. However, for real deployments, wireless systems have to cope with many problems such as mobility, communication failures, non-uniform node distribution, influence on data dissemination speed by communication paradigms (unicast vs. multicast), etc. In this section we analyze all these aspects and see how the algorithm adapts to such conditions.

4.5.1. NODE MOBILITY

In the previous sections we described an algorithm for the case when the nodes are static. In this section, we introduce a compensation strategy for the case in which the nodes are mobile (i.e., we consider the Random Walk mobility model assuming a discrete time model).

In Figure 4.5(a), p_b is the border of a hop-count gradient wave. Node m can travel from position p to p' and p'' in one time step. The last node that can discover the border p_b changes from node n to node n', which enlarges the width of the hop-count gradient wave in the gradient. A strategy to compensate the enlarged width in the distance estimation value is needed.

We use the expected moving distance of one node in a given time step E_{dc} to compensate the enlarged width value, which equals the movement distance from p_b to p''. The translation of the hop-count gradient into x and y coordinates is shown by Figure 4.5(b), in which y coordinate is parallel to the line of the seed nodes.

When nodes move with various speeds, the average expected moving distance for a node in one time step is D which makes an angle θ with the y axis (V being the projection on it). Due to the fact that all the possible movement directions are symmetrical with respect to the x coordinate, only the movement for $y > 0$ is considered (θ ranging from $-\pi/2$ to $\pi/2$). The probability density function of V is given by Equation 4.21. Since we need the absolute expected moving distance of one node, the expected value is integrated from 0 to D as shown by Equation 4.22.

$$\left.\begin{array}{c}\theta \sim U(-\frac{\pi}{2}, \frac{\pi}{2}) \\ V = D\sin\theta\end{array}\right\} \Rightarrow f(v) \overset{-D<v<D}{=} \frac{1}{\pi\sqrt{D^2 - v^2}} \tag{4.21}$$

$$E_{dc} = E(v) = \int_0^D v f(v) dv = \int_0^D \frac{v}{\pi\sqrt{D^2 - v^2}} dv \tag{4.22}$$

The enlarged width of each gradient wave is accumulating from one hop-count gradient to the next. For a node with hop-count gradient value a and transmission range r, the mobility compensation value C_d and the gradient value G_i is given by Equations 4.23 and 4.24.

$$C_d = [(a-1)d_{hop}E_{dc}]/r \tag{4.23}$$

$$G_{GDE}^{comp\,mob} = G_{GDE} + C_d \tag{4.24}$$

4.5.2. MULTICAST COMMUNICATION

GDE algorithm does not require each node to communicate with all its neighbors. Multicast can be used for each node to decrease the number of messages in the network. Suppose the nodes are uniformly distributed in the area. If each node only selects a fraction of its neighbors as the communication targets, then the selected nodes can also construct a network. The only difference to the original network is that the new network has lower node density. According to the formulas in Section 4.4, *GDE* can make distance estimation in the network with different node densities. Therefore, each node can use multicast to communicate with neighbors. The equations of *GDE* algorithm introduced in Section 4.4 can still be used, the only difference being that the node density n_l needs to be adjusted with the percentage of neighborhood size considered.

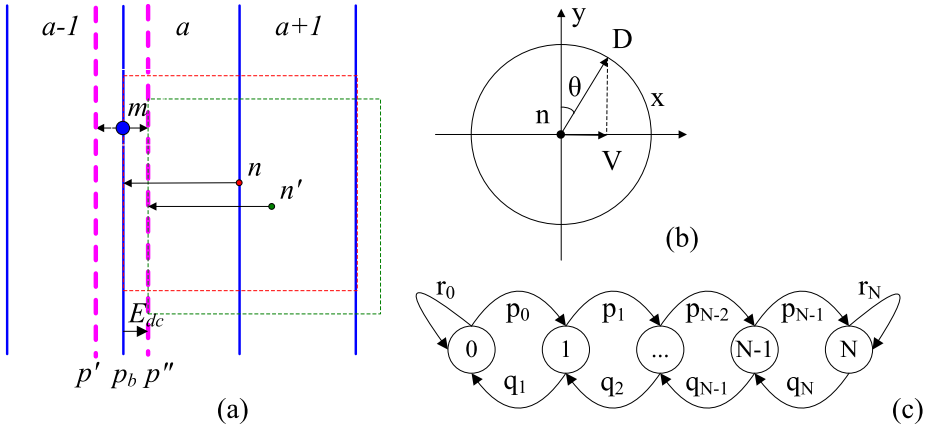

Figure 4.5: (a). Influence of node mobility to the border of the hop-count gradient wave. (b). Expected moving distance. (c). Moving distances of each time step of a round in the Markov Chain.

4

4.5.3. ROUND LENGTH

GDE assumes a discrete time model, with un-synchronized communication rounds of size P. Each node acts once in each round, in a different time slot. The rounds are not synchronized and are being used to mimic the asynchronous nature of communication. Suppose all nodes follow a Random Walk mobility model, the transmission range is r and the expected moving distance at one time step is E_{dc}. We model the motion segments with a Markov Chain in order to calculate the expected moving distance (see Figure 4.5(c)). In the model we only consider nodes moving in one dimension (i.e., towards the next hop-count gradient). Suppose that state j, $j = 0, ..., N$, is the state that describes a node moving forward for a distance $j \cdot E_{dc}$. p_j represents the probability that the node moves further from the original position, while q_j the probability of the node to move closer to the original position. Let N be the maximum number of moving steps in one round of length P. Let r_0 be the probability that a node does not move out of the initial state and is equal to $\frac{1}{2}$, and let p_0 be the probability that a node moves out of the initial state and is equal to $\frac{1}{2}$. In the inner processes, the backward and forward motion probabilities of a node in one time step are the same, so the node moves to the next state or to the previous state with $p_j = q_j = \frac{1}{2}$. For the final state N, due to the fact that there are nodes that can move to the previous state or start a new calculation round, let r_N be the probability that a node starts a new round (equal to $\frac{1}{2}$), and q_N be the probability that a node moves backward (equal to $\frac{1}{2}$). Due to the fact that there is a large number of nodes, the probability of each steady state can be used as the probability that a node stays in that state of P steps. Considering the mathematical properties of the Random Walk [136] , the model that describes the steady states π_j $(0 \leq j \leq N)$ is given by Equation 4.25. One can notice that all states converge to the same probabilities.

Algorithm 1: Calculate Gradient by Propagation

1: **select** $\{SN\}$
2: **calculate** D_{hop}, E_{sc}, E^p_{dc}
3: $E_c = (1 - D_{hop}) + E_{sc} + E^p_{dc}$
4: **for each element** $\{SN\}$
5: **if** $\mathrm{HCG}_i = (\mathrm{HCG} - 1)$
6: **sum** $(PE_{c\_i} + E_{c\_i})$
7: **end if**
8: **end for**
9: PE_c =**average**$(PE_{c\_i} + E_{c\_i})$
10: $G^{adp}_{GDE} = G_{SMG} - PE_c$

$$\begin{aligned}
&\pi_0 = r_0\pi_0 + q_1\pi_1 \overset{r_0=q_1=\frac{1}{2}}{\Rightarrow} \pi_0 = \pi_1 \\
&\pi_N = p_{N-1}\pi_{N-1} + r_N\pi_N \overset{p_{N-1}=r_N=\frac{1}{2}}{\Rightarrow} \pi_N = \pi_{N-1} \\
&\pi_j = \frac{\prod_{m=0}^{j-1}\frac{p_m}{q_{m+1}}}{1+\sum_{j=1}^{N}\prod_{m=0}^{j-1}\frac{p_m}{q_{m+1}}} \overset{p=q=\frac{1}{2}}{=} \frac{1}{1+N} \quad (1 \le j < N)
\end{aligned} \tag{4.25}$$

The node in state 0 does not affect the gradient of nodes in the next hop-count gradient. For this reason, we ignore state 0. For each state in the Markov Chain, it represents the expected moving distance from the original place. For state j, the moving distance is $j \cdot E_{dc}$. Because every steady state has the same probability as proved by Equation 4.25, the expected value for the moving distance of all states can be calculated by Equation 4.26. It can be found that if the length of the round becomes 1, Equation 4.26 is the same as Equation 4.22. The compensation value for the round length is given in Equation 4.27, and the computation for the gradient value is given in Equation 4.28.

$$E^p_{dc} = \frac{\sum_{j=1}^{P} jE_{dc}}{P} = \frac{(1+P)E_{dc}}{2} \tag{4.26}$$

$$C^p_d = [(a-1)d_{hop}E^p_{dc}]/r \tag{4.27}$$

$$G^{comp\,round}_{GDE} = G_{GDE} + C^p_d \tag{4.28}$$

4.5.4. INTEGRATED PARAMETERS INFLUENCE

For real deployments, the node distribution is not uniform. Furthermore, node speed, the neighborhood interaction and the communication periods may vary. Therefore, we introduce an algorithm that can calculate the gradient value for the nodes with various deployment conditions as shown in Algorithm 1. Each node communicates with parts of the neighbors to calculate its own gradient values as in Section 4.4, and propagates average values of the gradient reduced width value Δ, the static compensation value E_{sc} and the dynamic compensation value E_{dc}, from itself and the nodes in the previous hop-count gradient wave, to the nodes belonging to the next hop-count gradient wave. Each node uses the received width reduction values and compensation values to calculate its own gradient value.

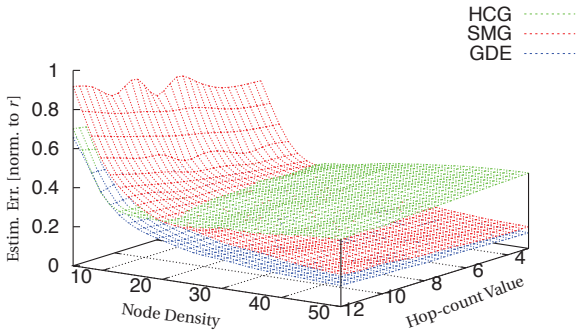

Figure 4.6: Absolute error for various node densities and hop-count gradient values.

For Algorithm 1, HCG is the hop-count gradient value, $\{SN\}$ is the subset of the neighbors to communicate, D_{hop} is the real one hop distance, E_{sc} is the compensation for the static case which equals Δr as shown in Equation 4.9, E_{dc}^{p} is the compensation for the mobile case given by Equation 4.26. E_c is the sum of reduced width $(1 - D_{hop})$, E_{sc}, and E_{dc}. PE_c is the sum of E_c for the nodes in all the previous hop-count gradients. PE_{c_i}, E_{c_i} and HCG_i are the PE_c, E_c and HCG values of node i in the neighbor subset $\{SN\}$. G_{SMG} is the gradient value computed using the simple smooth algorithm and G_{GDE}^{adp} is the final computed gradient value.

4.6. GDE ALGORITHM ANALYSIS

To validate our algorithms, we run simulations in Matlab. The nodes are placed randomly in a square area of 1000×1000 meters. The transmission range r of each node is 80 meters. The seed nodes are placed on the left border of the square. The resulting hop-count gradient looks like parallel waves. For the dynamic case, each node moves a step in every second. We run experiment 20 times for each testing point. Each node makes a distance estimation from itself to the line of seed nodes. The error for each node is computed as $\varphi = \frac{|\xi - \theta|}{r}$, in which ξ is the estimated distance to the line of seed nodes using different algorithms, θ is the real distance towards the line of seed nodes, r is the transmission range of each node and φ is the error normalized to the transmission range r. The Hop-Count Gradient (HCG) and Smoothed Gradient (SMG) algorithms calculate the gradient values G_{HCG} and G_{SMG}, and the estimated distance is calculated by $\xi_{HCG} = G_{HCG} \cdot d_{hop}$ and $\xi_{SMG} = G_{SMG} \cdot d_{hop}$ respectively. The Gradient-based Distance Estimation (GDE) algorithm uses algorithms provided in the previous sections to compute the gradient value G_{GDE}, and the estimated distance is calculated by $\xi_{GDE} = G_{GDE} \cdot r$.

4.6.1. NODE DENSITY

With the first set of experiments we want to find what are the effects of node density and the network diameter on the accuracy of the algorithm. All nodes are static and uniformly distributed. Each node broadcasts locally to their neighbors.

The qualitative analysis about the average absolute error of the distance estimation of

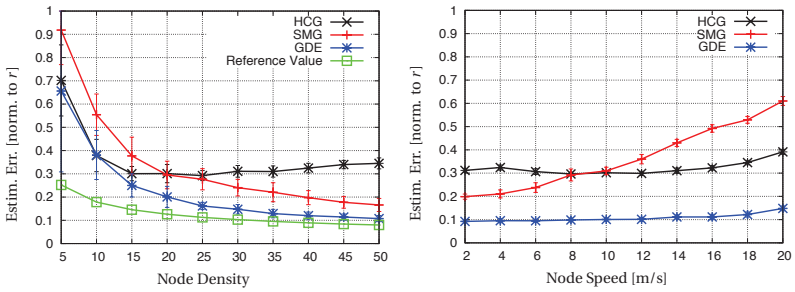

Figure 4.7: (a). Absolute error for various node densities. (b). Absolute error for various node speeds.

HCG, *SMG* and *GDE* algorithms is given out in Figure 4.6 for various node densities and network diameters. On the x axis we see the node density and, on the y axis the network diameter. The z coordinate is the average absolute error. The results show that the *HCG* has almost no decrease of the error after node density 15. The distance estimation error using *SMG* and *GDE* algorithms decreases when node density n_l increases. The error of *GDE* is always smaller than the one of *SMG*. When node density n_l is constant, and the network diameter increases, the errors of both *SMG* and *GDE* show a small increase. This is mainly caused by the cumulative effect of the distance estimation error of the nodes in the previous hop-count waves. Still, the error of *GDE* is much smaller than the error of *HCG*. Finally, the increasing error rate of *GDE* is smaller than the one of *SMG*.

The quantitative analysis about the average absolute error of the three algorithms is given out in Figure 4.7(a) for various node densities. The network diameter is 12. The *GDE* method reduces the error of *HCG* and *SMG* significantly for densities higher than 15. The standard deviations of the errors for both *SMG* and *GDE* decrease when the average node density increases. The standard deviation of the estimation error for *GDE* is always smaller than the one of *SMG* for node density higher than 15. For an average node density 30 the average estimation error for *HCG*, *SMG* and *GDE* are 0.31, 0.24 and 0.15. While the standard deviation is 0.025, 0.036 and 0.020 respectively. Figure 4.7(a) also shows out the error reference value according to Equation 4.20. As the node density increases, the error of *GDE* algorithm becomes smaller compared to the error reference value.

4.6.2. NODE SPEED

The second set of experiments is intended to quantify the effects various node speed levels and node densities has on the accuracy of *GDE*. Nodes are uniformly distributed, and use broadcast to communicate with their neighbors. They use the Random Walk model with network diameter 12.

The qualitative analysis about the average absolute error of the distance estimation of *HCG*, *SMG* and *GDE* algorithms is given out in Figure 4.8 for various node speeds and densities. The x axis shows the node density, the y axis the node speed, and the z axis the average absolute error. On the y axis, the speed is increased in step of 2 m/s. The estimation error of *GDE* decreases as node density increases. On the other hand, it

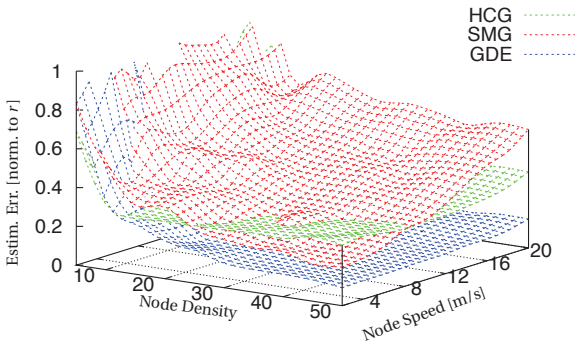

Figure 4.8: Absolute error for various node densities and node speeds.

increases slightly when the average node speed increases. Also, when the node speed increases, the error of *HCG* and *SMG* increases. For node speeds higher than 8 m/s, the error of *SMG* increases greatly and is even larger than the one of *HCG*. This is mainly caused by the fact that *SMG* is designed for the static environments and it does not consider the influence of node mobility.

The quantitative analysis about the average absolute error of the three algorithms is given in Figure 4.7(b) for various node speeds. Node density is set to 50. The network diameter is 12. As the speed increases, the error of *GDE* increases slightly, but *SMG* increases significantly. When the node speed is 20 m/s, the average error of distance estimation by *GDE* is 0.148, while the error levels for *HCG* and *SMG* are 0.391, 0.610 respectively. The standard deviation for *SMG* is 0.019. The standard deviation for *HCG* and *GDE* are 0.011 and 0.010 respectively. The test results show that the *GDE* algorithm has a good performance in a dynamic environment. *HCG* and *SMG* are not suitable in a dynamic environment especially at high node speed.

4.6.3. SPATIAL NODE DISTRIBUTION

We check next the influence of different spatial node distribution to the accuracy of the algorithms. Nodes follow again a Random Walk mobility pattern with speed of 2 m/s. The seed nodes are placed on the left border of the square. This time the placement of the nodes is not uniformly distributed. Instead, the y coordinates of nodes are uniformly distributed from 0 to 1000 meters, while the x coordinates of nodes are distributed following a normal distribution $|N(0,0.5)\cdot 1000|$, with maximum value 1000 and minimum value 0. So the field that is closer to the seed nodes has higher node density, and the field that is further to the seed nodes has lower node density. The *GDE* gradient is calculated using the algorithm shown in Section 4.5.4.

In Figure 4.9(a), the x axis represents the node density and the y axis the average distance estimation error. As shown by the graph, the errors of *HCG* and *SMG* increase significantly. For *GDE*, the average error of distance estimation is quite low, which is around 0.150 with node density 20 and 0.089 with node density 80. Thus, *GDE* is also suited for deployments with non-uniform node distributions.

4.6.4. MULTICAST PERCENTAGE

For wireless systems where nodes follow duty-cycled sleep schedules, nodes that transmit can only be heard by a subset of their neighbors. The percentage of nodes that take part determines the speed of information diffusion. For this experiment, nodes are uniformly distributed with an average density of 50. The network diameter is 12. The nodes use a Random Walk model with speed of 2 m/s.

In Figure 4.9(b), the x coordinate shows the multicast percentage, while the y coordinate shows the error level. Each node randomly selects a subset of its neighbors at each time step. The multicast percentage varies from 0.1 to 1.0. The error of both *SMG* and *GDE* algorithms decreases significantly. *GDE* always computes a better estimate than *SMG*. This is given in both the average error and the standard deviation. The estimation error of *HCG* decreases from the multicast percentage 0.1 to 0.5 and shows almost no improvement afterward. For an average multicast percentage of 0.6, the error and standard deviation of *GDE* are 0.122 and 0.009 respectively, and the values are almost the same as the results of Section 4.6.1 with node density 30. This experiment shows that even if each node cannot communicate with all its neighbors, *GDE* still shows good performance.

4.6.5. ROUND LENGTH

As previously described, *GDE* uses a discrete time model, with un-synchronized communication rounds of size P. In this section, we test the influence of the length of the communication round to the accuracy of distance estimation. For this experiment, nodes are uniformly distributed, with an average node density of 50. They use broadcasting to communicate with their neighbors, and the network diameter is 12. In Figure 4.9(c), on the x axis is shown the round length in seconds, while on the y axis the estimation error. As the round length increases, the error and standard deviation of *SMG* increases significantly. On the other hand, the error and standard deviation of *GDE* shows a much smaller increase from 0.097 and 0.006 to 0.113 and 0.014. The test results show that *GDE* algorithm offers good distance estimation without requiring very frequent communication with neighbor nodes.

4.6.6. ADAPTIVE BEHAVIOR

Previous experiments considered some simplified assumptions. In real deployments though, nodes are not uniformly distributed, node speed varies, local interaction is multicast communication, etc. In this section, we test all these aspects together. We consider nodes normally distributed, as in Section 4.6.3. The mobility model is Random Walk with node speed following a normal distribution with mean value of 2 m/s. The multicast percentage depends on the local node density. Nodes interact with a minimum 15 nodes to a maximum 30 nodes. The random variable of the number of neighbors for each node follows a Binomial distribution. For each neighbor, the probability of making successful communication is $p_s = (0.2 \cdot n_l + 15)/n_l$ (n_l is the node density). The communication round length P changes according to the node density as $P = |(p_s \cdot n_l)/15 - 1| \cdot 9 + 1$.

Figure 4.9(d) shows the experiment results. The x axis shows the distance to the seed nodes while y axis shows the error normalized to the transmission range r. It can be seen that, as the distance to the seed nodes increases, the distance estimation error also

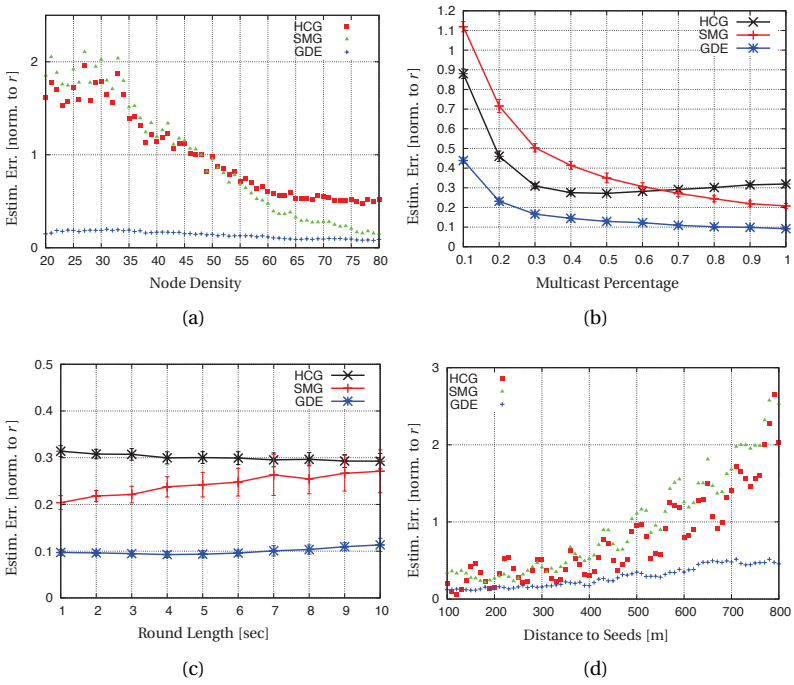

Figure 4.9: (a). Abs. error for normal distribution of nodes. (b). Abs. error for various multicast percentages. (c). Abs. error for various round lengths. (d). Abs. error for integrated parameters.

increases. When the distance is larger than 300 meters, the estimation error of *SMG* is even larger than that of *HCG*. The estimation error of the two algorithms increases significantly from 300 to 800 meters. As expected, *GDE* generally shows a small estimation error, with only a small increase from 0.120 to 0.456. So *GDE* can make acceptable distance estimation in the environment with integrated parameters.

4.7. CONCLUSIONS

Distance estimation in wireless networks is of tremendous importance for a lot of applications. The majority of the algorithms presume knowledge about node position via systems such as GPS. While this approach is feasible for some application scenarios, for a lot of cases it suffers from frequent unavailability and high costs in terms of energy consumption. For this reason, in this chapter we introduce a novel distributed algorithm called *GDE* for the estimation of distances in large-scale wireless networks. It is a mechanism which estimates distances between nodes using solely local interactions. The models and the theoretical evaluations by means of simulation show that *GDE* succeeds in evaluating the distances between nodes in both static and mobile scenarios with considerably high accuracy, even under the influence of some environment parameters.

5

BLISP: Enhancing Backscatter Radio with Active Radio for Computational RFIDs

In Chapter 3 and Chapter 4, we focus on self-adaptive self-organization properties of autonomy systems. In the two chapters, we use local information exchange to achieve global control in the network. In the next three chapters, including Chapter 5, Chapter 6, and Chapter 7, we focus on another branch of autonomy system: energy autonomous. As the first step, we explore backscatter radio for energy autonomous system in this chapter [1].

5.1. Introduction

Most low power wireless sensor nodes use active radio transmission techniques, such as Bluetooth Low Energy [54], to transport data. While active radios are becoming better with each year (in terms of throughput and range), the power consumption expenditure of radio communication can still be much larger than the power expended for computation [45]. This indicates that there is still a lot to be done to make wireless sensor nodes more power efficient, despite many years of research in low power electronics. One approach to reducing energy consumption of the wireless front end is by not actively transmitting, but instead modulating the reflection of power emitted by an external transmitter—as with Radio Frequency Identification (RFID)-based Computational RFIDs (CRFIDs) [175].

[1] This chapter is published as the paper:
Ivar in 't Veen, Qingzhi Liu, Przemyslaw Pawelczak, Aaron N Parks, Smith Joshua. *BLISP: Enhancing Backscatter Radio with Active Radio for Computational RFIDs.* In Proceedings of the IEEE RFID, Orlando, FL, May 3-5, 2016.

5.1.1. PROBLEM STATEMENT AND RESEARCH QUESTION

Unfortunately the transmission technique used by CRFIDs, i.e. backscatter, has non-ideal characteristics compared to active radio. Assume the backscatter radio is in the monostatic system. Compared with active radio, backscatter radio saves much power in communication of receiver side [197, 198, 203]. However, the radio propagation of backscatter radio is more susceptible to the environmental conditions [229, Fig. 4]. Additionally, the path loss for backscatter signals is very different than for active transmissions. Active transmissions have a signal-to-noise ratio which approximately decays with the square of distance. For backscatter radio, this decay approximates the fourth power of distance [229, Sec. 2.2]. Hence, the energy wasted due to lost data increases. At the same time, active radios, although more resistant to interference, consume more energy than backscatter radios. The difference in power consumption is mostly due to the need to actively emit RF power instead of reflecting preexisting signals. This robustness/energy efficiency trade-off of active and backscatter radio calls for connecting these platforms. Practically, many real-life situations call for an extension of backscatter by active radio.

Example: It is shown in [62] that cows have preferred regions (hotspots) within the paddock in which they spend the majority of their time. In [62, Fig. 3] the number of hotspots (covering less than 20 m^2) is limited to six, and is spread over a large area ($\approx$230 m^2). To monitor cattle movement (C)RFID would cover the hotspot area, while active radio would cover transitional movement.

The research question is then: *What energy consumption and transmission reliability improvements can one get by exploiting the combined benefits of active and backscatter radio?*

5.1.2. CONTRIBUTIONS OF THIS CHAPTER

To answer this question we design a new heterogeneous radio sensor node combining both active and passive radio in one device. We call this platform BLISP—a composition of **B**luetooth **L**ow Energy (state-of-the-art Commercial off-the-Shelf (COTS) active radio platform for consumer applications [54]) and W**ISP** [214] (state-of-the-art CRFID). We use WISP as the case study of CRFID to implement our BLISP system. This proposed platform consists both of low-cost experimental hardware combining the two radios in one system, and a radio selection technique (implemented in software) to choose the appropriate radio for the appropriate situation while trying to optimize both reliability and energy efficiency. To show the benefit of BLISP, the complete system is evaluated in replicable static and mobile scenarios using a COTS RFID reader and a modified smartphone-attached RFID reader.

The contributions presented in this chapter are:

Contribution 1: we provide a set of simple theories, supported by experiments, showing the benefit of connecting active and backscatter radio platforms;

Contribution 2: we show the benefit of using BLISP as an extension to CRFID applications by demonstrating that it is possible to transmit more data compared to an out-of-range CRFID while only increasing energy consumption per byte by $\approx$15 % compared to Bluetooth Low Energy (BLE).

Contribution 3: we show the benefit of using BLISP as an extension to BLE applications by demonstrating the possibility of transmitting the same amount of data compared

to BLE while decreasing energy consumption per byte by more than 50 %.

The rest of this chapter is organized as follows. Section 5.2 reviews related work. Research motivation is provided in Section 5.3, followed by Section 5.4 discussing a simple feedback-less radio switching method for BLISP. Section 5.5 presents experimental platform used to verify the quality of the proposed switching mechanism of which the results are discussed in Section 5.6. A discussion on limitations and future work is given in Section 5.7, and the chapter concludes with Section 5.8.

5.2. RELATED WORK

We start by reviewing literature pertaining to active and backscatter radios and connection thereof into an hybrid device.

5.2.1. COMPUTATIONAL RFID

The use of CRFID for wireless sensor applications has been advocated by many papers including [162, 226]. The only stable CRFID [175] implementation currently available is Wireless Identification and Sensing Platform (WISP). The communication protocol used by WISP is the industrial standard EPCglobal Class 1 Generation 2 (EPC C1G2) RFID protocol. Although completely battery-autonomous, CRFID has intrinsic limitations: Limited channel robustness, as evaluated by [229]; and limited RF power transfer efficiency results in an intermittent power supply. A solution to the continuous power supply problem proposed by [38] exercises a hybrid power solution based on RF power harvesting and an energy storage device. While this significantly improves CRFID energy supply stability, it does not solve the robustness problem.

5.2.2. BLUETOOTH LOW ENERGY

Active (low power) radio systems are less susceptible to interference compared to backscatter communication. However, they bring the disadvantage of higher energy consumption. There are multitudes of low power active radio platforms, and reviewing all options is not in the scope of this work. However, there is one believed to be broadly adopted, with more than 30 billion devices expected to reach the consumer market by 2020 [20]: BLE—the newest version of the Bluetooth protocol optimized for low energy applications[2]. Works by [54, 88] experimentally evaluate the performance of BLE, while [178] shows the energy consumption of BLE compared to other popular active radio technologies. No studies comparing the energy consumption of BLE with a backscatter-based CRFID have yet been published to the best of our knowledge.

5.2.3. MULTI-RADIO SYSTEMS

A combination of backscatter radio and active radio seems to be the logical step to solve the imperfections of both systems. Again, to the best of our knowledge, no such hybrid implementation exists. One obvious way of using BLE to extend the RFID range is to use multiple RFID readers which are coupled using BLE, as proposed for different radio types

[2] For example, recent standards like SigFox [179], LoRa [120] or IEEE 802.15.4k [216] could be used, and are expected to have even lower energy consumption than BLE. We will not use them in this work as they are not (yet) easily accessible for experimental evaluation, nor broadly adopted.

(with node-to-node communication) by [80]. This approach, unfortunately, cannot be used for BLISP because state of the art CRFIDs cannot communicate with other CRFIDs without the interrogator. The only hybrid active/backscatter platform we are aware of is [89], which uses BLE to reprogram a backscatter testbed, and does not use the active radio to improve reliability.

Authors of [22] propose a method of using BLE as a physical transport layer for an RFID protocol. A backscatter-BLE method is proposed in [43], which allows a backscatter device to synthesize BLE packets but which has similar channel constraints as conventional backscatter. In the non-backscatter context, an approach to combine multiple heterogeneous radios by [59] uses acknowledgement delay and machine learning mechanisms to optimize system performance. All above-mentioned multi-radio platforms rely on acknowledgements from the receiving party and/or active radio transmissions.

5.2.4. RF POWER HARVESTING

Considering literature related to energy storage in CRFID, we need to mention [38] again proposing to store energy in battery/capacitor for future use and [183] where energy storage from rectifying Wi-Fi signals has been proposed.

5.3. MOTIVATION FOR COMBINING ACTIVE AND BACKSCATTER RADIO

To understand why backscatter is not always the most efficient radio technique, we introduce a simple analytical basis to bring insight into the design of BLISP. The theoretical model is followed by experimental results verifying the theory.

5.3.1. DIFFERENCE IN WISP AND BLE RADIO EFFICIENCY

We start with the analytical model.

ANALYSIS

Assume a hybrid radio platform composed of $i = \{1, \ldots, n\}$ independent radio technologies (such as backscatter and active radio). We characterize the energy per successful transferred byte for radio i as $E_{\text{byte},i}(d) = E_{\text{tx},i}/B_{\text{rx},i}(d)$, where $E_{\text{tx},i}$ is the total amount of energy spent in transmitting data and $B_{\text{rx},i}(d)$ is the number of received bytes for distance $d \in [0, d_{\max})$. Generalizing [109, Sec. III-A]

$$B_{\text{rx},i}(d) \triangleq \frac{L}{L+H}\left[1 - \text{erfc}\left(f_i(d)\right)\right]^{L+H}, \tag{5.1}$$

where L and H are the payload size in bits and the amount of overhead in bits, respectively, and erfc(.) is the complementary error function. We define the signal quality decay function $f_i(d) = (d/a_i)^{-r_i}$, a_i as radio-intrinsic correction value and r_i as loss coefficient. For example, a typical value of $r_i = 2$ for active radio or $r_i = 4$ for backscatter radio. Now, based on the above model we pose the following lemma.

Lemma 1. *Any hybrid radio composed of n radios has limited range after which energy consumption per byte is infinite.*

Proof. $\forall n \lim_{d\to+\infty} B_{\mathrm{rx},i}(d) \to 0 \Rightarrow E_{\mathrm{byte},i} = E_{\mathrm{tx},i}/B_{\mathrm{rx},i}(d) \to +\infty$ which completes the proof. □

Corollary 1. *Defining* $\mathrm{E}(d) \triangleq \{E_{byte,1}(d), \cdots, E_{byte,n}(d)\}$ *if* $\exists_{E_{byte,i}(d)\in \mathrm{E}(d)} \forall_{E_{byte,j}(d), i\neq j} E_{byte,j}(d) < E_{byte,i}(d), \forall d$*, then radio* j *can be removed from designing a hybrid radio.*

Corollary 2. *The maximum range of a system is limited by the radio with the largest range.*

Corollary 3. *At distance* d *the lower bound of the hybrid radio energy consumption per byte is given by the radio with the lowest energy consumption at that distance.*

MEASUREMENT

To verify this simple analytical model we need to measure the consumed power of each radio as a function of the signal loss. We first introduce the selected hardware for BLE, WISP and finally the measurement setup.

Bluetooth Low Energy—Transmitter/Receiver We selected the Nordic Semiconductor PCA10005 evaluation module with an NRF51822 BLE System on Chip (SoC) [154] as BLE transmitter. The software used on the BLE radio is a customized firmware version (source code is available upon request or via [79]) transmitting only standard advertising messages [20] at a constant rate of 120 Byte/s=0.96 kbit/s, which is comparable to 0.65 kbit/s of [36, Sec. III-B]. BLE has a maximum packet size smaller than the selected payload (i.e. 24 Byte) therefore each transmission consists of multiple packets. A second identical NRF51822 module is used as BLE receiver—continuously logging advertisement messages send by the BLE transmitter.

Computational RFID—Transmitter/Receiver We select WISP 5 as a state-of-the-art CRFID platform [214]. The WISP 5 used for experiments has the RF energy harvester disabled by desoldering the output pin of the buck converter. This modification simplifies the energy measurement, as the energy provided to WISP 5 is not fluctuating in time as in the case of harvested energy. The WISP 5 firmware is adapted (see again [79]) to transmit with the same data rate as BLE. Again, as in the case of BLE, since the maximum payload of WISP 5, i.e. 12 Byte, is smaller than 120 Byte each message consists of multiple packets. The RFID reader is an Impinj Speedway R420 [76], controlled via SLLURP Low-Level Reader Protocol (LLRP) library [180], and connected to a panel antenna [101].

Based on observations by [60, Sec. 4.1] we have chosen to use the EPC C1G2 Electronic Product Code (`EPC`) field as our data carrier instead of the `Read` command. Using the `EPC` field cuts down on the protocol overhead because it halves the amount of roundtrips [56, Sec. 6.3.2.12.3]. According to [56, Sec. 6.3.2.1.2.2] the length of the `EPC` field may be set between zero and thirty one words. While it is possible to have WISP transmit longer `EPC` values to reduce the overhead, this increases the probability of corrupted messages [109].

Measurement Setup We measure energy per byte at the receiver (separately for BLE and WISP) as a function of signal attenuation. This is realized with two signal attenuators [82] connected in series. These attenuators limit the signals bi-directionally, and therefore both uplink and downlink are attenuated at the same time. Both BLE transmit/receive

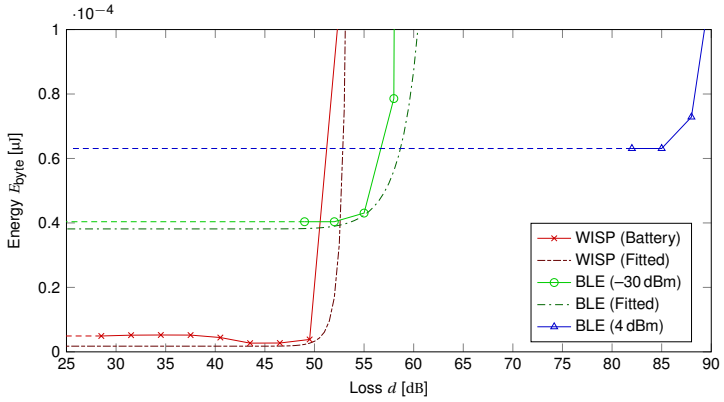

Figure 5.1: **Energy per byte over distance for WISP and BLE.** The dashed data points are extrapolated, the constant power consumption for the BLE radio and all data being received, yields constant energy per byte. Fitted plots are based upon (5.1). Parameters for fitted WISP curve: $a_i = 30$, $d_i = 4$, $E_{\text{tx},i} = (L+H)5\,\mu\text{J}$ with $L = 96$ and $H = 320$. Parameters for fitted BLE curve: $a_i = 87$, $d_i = 2$, $E_{\text{tx},i} = (L+H)21\,\mu\text{J}$, L and H are equal to WISP.

5

evaluation boards used are equipped with an antenna connector allowing attenuators to be inserted directly into the transmission channel. WISP, on the other hand, does not provide such an antenna connector and therefore it is positioned at a fixed distance of 50 cm from the interrogator antenna which is then connected to the RFID interrogator via the attenuators.

The BLE module [154] has an uncalibrated transmission power setting via the API of the S110/S120 (transmitter/receiver, respectively) softdevice. The highest (4 dBm) and lowest (–30 dBm) transmission power are tested. The RFID reader is tested at its maximum transmission power (32.5 dBm).

We measure the power consumption of both radios using a self developed, buffered, differential, sensing circuit monitoring the voltage drop over a 100 Ω shunt resistor in series with the Device Under Test (DUT). This circuit is coupled to a Tektronix MDO4054B–3 oscilloscope [187] to measure power over time which is used to calculate the energy consumption. Schematics of this device are available upon request or at [79].

MEASUREMENT RESULTS

The relationship between energy per byte and signal loss, as measured for both active and backscatter radio and complementary fitted plots, is shown in Fig. 5.1. As expected, the WISP—while more energy efficient in good channel conditions—also has a shorter range of operation. Instead of a gradual increase in energy consumption per received byte, at one point the energy per byte metric starts to rapidly increase for both platforms. This "brick wall" effect [109, Sec. V] is caused by an increase in bit errors, causing whole packet loss and therefore requiring more transmit attempts per successfully received byte.

5.3.2. DO ALTERNATIVES EXIST TO HYBRID ACTIVE/BACKSCATTER RADIO?

The question remains of whether, in the light of this observation, the hybrid radio platform is the only solution which improves energy efficiency and transmission range of CRFID.

We review the alternatives and provide our answer.

LOW POWER ACTIVE RADIO WITH BATTERY

The simplest alternative to the hybrid platform would be a connection of a sufficiently large battery and BLE radio.

Limitation: Unfortunately, all batteries will eventually deplete, leading to expensive battery (or even whole device) replacement. For battery replacement, the device must be physically accessible, as it is impossible to wirelessly restore the energy level of the empty battery without an energy harvester.

POWER HARVESTER WITH ACTIVE RADIO

Wireless RF power harvesters solve the physical accessibility and battery constraint.

Limitation: Inefficiencies in RF power harvesters, energy storage, energy conversion, and energy transmission through RF waves, mean that no power harvester and active radio combination will be as energy efficient as a backscatter radio.

BACKSCATTER RADIO WITH IMPROVED CHANNEL CODING

The operational reliability and robustness of communication of CRFIDs could be improved by adding a more extensive channel coding mechanism. For example: WISP is currently limited to the FM0 coding [56, Sec. 6.3.1.3.2.1], in which each bit is represented by one signal alternation for each symbol. Miller coding methods [56, Sec. 6.3.1.3.2.3] have redundant alternations within each symbol, reducing the possibility of lost messages.

Limitation: Channel coding would make CRFID more robust (i.e. shift the WISP curve to the right in Fig. 5.1), still keeping CRFID susceptible to reflections and destructive interference. Finally, we conjecture, this would still not make WISP as energy efficient as BLE in a broad attenuation range.

5.4. CHANNEL ESTIMATION METHODS FOR HYBRID ACTIVE/BACKSCATTER RADIO PLATFORMS

We propose a method of estimating the backscatter channel and use this estimation to select between backscatter and active radio on-the-fly. We start with revising unsuitable solutions.

5.4.1. BACKSCATTER CHANNEL QUALITY ESTIMATION METHODS: REVIEW OF UNSUITABLE SOLUTIONS

Backscatter channel quality estimation is the key factor to achieve scheduling of backscatter and active radio. However, some widely used channel estimation methods are not suitable for our solution.

EPC C1G2 PROTOCOL FEEDBACK

The de facto standard method of assessing packet reception rate is to query the receiving party if it indeed received a packet. Most protocols rely on receive acknowledgments for (all) packets.

Limitation: Within the EPC C1G2 [56] protocol there are no standard ways to guarantee the successful reception of `EPC` values transmitted by a tag. The default method of awaiting an Acknowledgement (`ACK`) message for each transmitted data message is therefore not possible. The exclusion of this functionality is logical for standard RFID tags, as they are computationally limited, transmit unchanging identifier, and most likely could not handle retransmissions. Transmitting data back to a CRFID also implies that CRFID should handle computationally hard, and a protocol-wise large overhead inducing EPC C1G2 `write` accesses.

BLE PROTOCOL FEEDBACK

The more responsive BLE channel could be used to provide a feedback for the reception of RFID packets transmitted by CRFID.

Limitation: The use of a separate radio channel could increase RFID reliability because the channels might break down under different circumstances. However, it might also decrease reliability because the BLE channel might be broken while the RFID channel is working. Practically, including a BLE radio in receiving mode will also dramatically decrease the energy efficiency of a hybrid platform, as the radio has to listen for an extended (worst case: continuous) time.

RSSI STRENGTH FEEDBACK

Neither CRFID hardware nor EPC C1G2 protocol has a built-in support for Received Signal Strength Indication (RSSI) measurement on the RFID transmission. A coarse method to estimate the vicinity of RFID reader is by measuring the amount of energy harvested by the CRFID. If a tag is close to a reader, it is easily possible to harvest energy, while if a tag is far away it would be almost impossible to harvest it. The BLE radio has native support for RSSI measurements on the received messages.

Limitation: Measuring RSSI for the signal originating from the interrogator and received by the backscatter radio does not directly correlate with the channel quality for backscatter data (as there is no constructive interference, as explained in Section 5.1.1). While the interrogator knows the RSSI, the backscatter device cannot reliably determine it. A CRFID could query the RFID reader for its RSSI as measured by the reader but this would induce a lot of overhead on both sides. I BLE should be placed into listening mode in order to retrieve RSSI values, which is more power consuming than the transmission mode. Therefore, enabling BLE only for channel estimation without using it for data transfer is a loss of energy.

5.4.2. PROPOSED CHANNEL QUALITY ESTIMATION METHOD

For the BLISP system we propose a novel, less standard, way of estimating the channel.

Proposition 1. *Tracking the number of EPC C1G2 `RN16` `ACK` messages in handshake can be used to estimate the backscatter channel quality.*

Proof. (Sketch) If RFID interrogator and tag perform a multipart handshake, the backscatter channel is usable to transfer data. Work of [229] proposed an approach for setting an interrogator to its optimal settings based on both measured RSSI and packet loss. However, packet loss-based, estimations can also be performed on the tag instead of

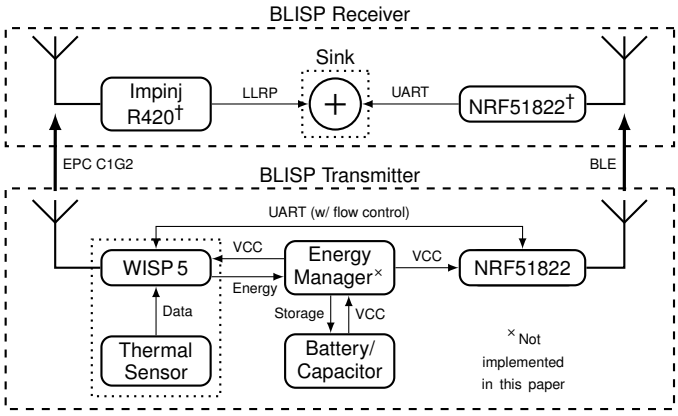

Figure 5.2: **Overview of the BLISP system consisting of one transmitter and one receiver.** The temperature sensor providing data is part of WISP but displayed separately for clarity and completeness. All displayed connections depict a flow of energy or data and do not directly correspond to physical connections. For a detailed description of the physical connections see [79]. †For the mobile reader experiments the Impinj R420 is replaced by an MTI MINI ME, and the NRF51822 by the BLE receiver of a Samsung Galaxy S3.

5

the interrogator. Part of this handshake is the tag sending the reader a random number (`RN16`), which the reader should acknowledge by an `ACK` message containing this random number. To reach the `ACK` both channels (to and from) the CRFID tag need to be in a state good enough to transmit a payload. By measuring the number of handshakes and testing this number to be at least the same as the amount of packets we expected to transmit, we are able to estimate quality of the backscatter channel. □

5.5. BLISP DESIGN

We are now ready to introduce BLISP, our hybrid backscatter and active radio platform, to help exploit the main trade-offs as proposed in Lemma 1 and Corollaries 1 to 3. The BLISP infrastructure mainly consists of two parts:

(i) a COTS RFID interrogator combined with a BLE receiver; and

(ii) our multi-radio sensor node—the BLISP.

To provide a flexible platform we opt to combine two readily available radios instead of developing our own, single silicon, platform.

A complete system level overview of the BLISP is shown in Fig. 5.2. The main design principle behind BLISP is the absence of any algorithm on the host side: the host only merges the multiple data streams received by the different radios.

5.5.1. BLISP HARDWARE ARCHITECTURE

The chosen radio modules for this platform are the same as described in Section 5.3.1. PCB has been designed to ease the connection of the two separate radio platforms, see Fig. 5.3. The PCB connects the active and passive radio, and provides means for radio collaboration and energy distribution.

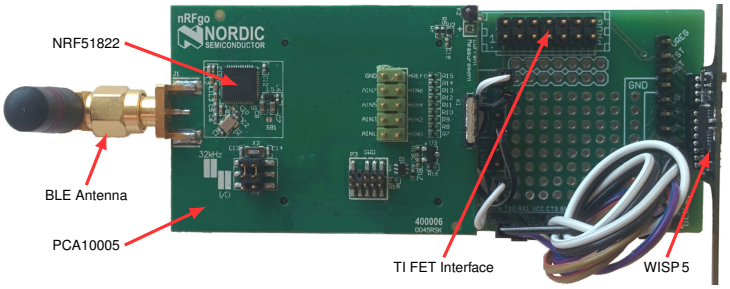

(a) The top side of the BLISP with annotations for the most important components. Please note that the WISP antenna is not fully shown.

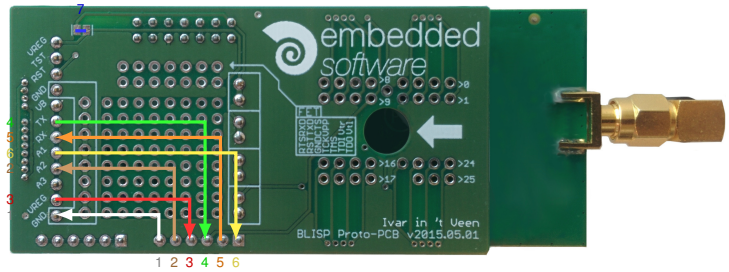

(b) Bottom side of the BLISP. Symbolicaly illustrated directional connections by color, as numbered: (1) **white**: ground; (2) **brown**: clear to send; (3) **red**: power supply; (4) **green**: WISP to BLE serial channel; (5) **orange**: BLE to WISP serial channel (unused); (6) **yellow**: ready to send, and (7) **blue**: power supply.

Figure 5.3: **The BLISP Printed Circuit Board (PCB) as seen from top (Fig. 5.3(b)) and bottom (Fig. 5.3(a)).** PCB design files are available upon request or from [79].

Table 5.1: Setup Parameters of Data Aggregators

Component	Parameter	Mobile BLISP RX	Static BLISP RX
Host Device	Model	Samsung Galaxy S3	Lenovo T530
	Software	Android 4.3	Linux 3.13.0
RFID Reader	Model	MTI MINI ME	Impinj R420
	TX Power	18 dBm	32.5 dBm
	RX Sensitivity	–84 dBm	–82 dBm
	Antenna Gain	2 dBi	9 dBi
	Link Frequency	640 kHz	640 kHz
	Coding	FM0	FM0
	Session	2	2
	Q-value	5	n/a
	Duty Cycle	100%	100%
BLE Receiver	Model	Samsung Galaxy S3	Nordic NRF51822
	Duty Cycle	100%	100%

ACTIVE RADIO

We use the same NRF51822 BLE module as described in Section 5.3.1.

BACKSCATTER RADIO

As backscatter radio we also use the same WISP 5 as described in Section 5.3.1.

RADIO COLLABORATION

A communication channel is needed to convey desired state information for the active radio and to share sensor values between the two separate radios. The NRF51822 BLE module has a silicon bug causing high power consumption by perpetually keeping non-vital microcontroller peripherals enabled [155, Id 39]. This bug unfortunately affects all conventional (digital) communication channels including General Purpose Input/Output (GPIO)-interrupts rendering them useless as low power wake-from-sleep devices. The low power analog comparator peripheral is not affected by this bug, therefore this peripheral is used as wake-up signal enabling the high throughput Universal Asynchronous Receiver/Transmitter (UART). The BLE radio also uses digital output as CTS signal.

BLISP RECEIVER/SINK

The receiving side of BLISP consists of two receiving radios matching the two transmitting radios on the BLISP. In contrast to [59], the BLISP receiver is as simple as possible and only merges the data streams from the receiving radios. Because the host does not make decisions about which radio to use, the BLISP can switch without synchronization mechanism. We present two host setups: (i) a fixed receiver; and (ii) a mobile smartphone setup.

Fixed Receiver The fixed receiver consists of a host computer with an Ethernet connected Impinj Speedway R420 [76] and an USB/UART connected Nordic Semiconductor NRF51822 [154]. This setup is again described in Section 5.3.1.

Mobile Receiver To test BLISP with a mobile reader, comparing to the fixed reader case, we have a prepared the following setup. Smartphone is selected as platform for mobile host, which consists of BLE and RFID reader. We developed an Android application

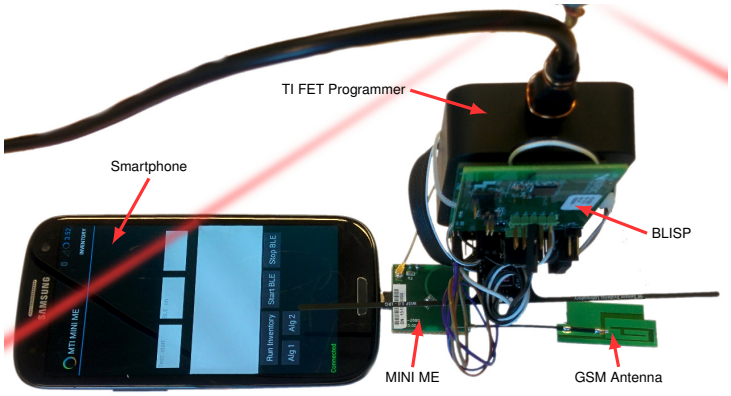

Figure 5.4: **Mobile receiver BLISP test setup.** BLISP and TI FET programmer/power monitor are hanging from an overhead crane (the red diagonal wires) [27] as described in Section 5.6.1. MINI ME mobile RFID reader is shown without plastic housing, easing connection of a different antenna.

(available upon request or via [79]) for the smartphone to scan the BLE channel and log all advertising data originating from the BLISP. As a smartphone-attachable RFID reader we selected the MTI MINI ME [135]. Based on the low level command set Application Programming Interface (API) provided by MTI, we log all inventory data.

Unfortunately, the MINI ME can only inventory WISP with fixed power supply up to a maximum range of 2 cm. To increase the inventory range of MINI ME, we replace the embedded antenna with a 2 dBi GSM band omnidirectional antenna [1]. By replacing the antenna, the maximum range is extended to 10 cm. Table 5.1 shows parameters for the two reader platforms, while Fig. 5.4 shows the MINI ME reader with GSM antenna connected to a smartphone running our application.

5.5.2. BLISP SOFTWARE ARCHITECTURE

The WISP component of the BLISP software consists of 1700 lines of C code and 1900 lines of assembly code of which 600 lines C and 50 lines assembly were written in the BLISP development process. The remaining part is based upon [213]. The BLE element consists of a 500 line C coded program and the NRF51822's API. The fixed BLISP host currently consists of various Bash and Octave scripts with varying lengths. The mobile host consists of 750 lines of customized Java code.

WIRELESS IDENTIFICATION AND SENSING PLATFORM

Because of the low power requirements and therefore our preference for backscatter communication we choose to have WISP acting as master over BLE radio. Between the periodic sensing and transmission rounds WISP is put into a low power state.

For all following experiments WISP measures temperature and a timestamp since the startup[3]. The timestamp is included for evaluation purposes, as this value enables to evaluate the number of missing and/or duplicate packets. To ensure a constant data

[3] Other possible sensors are the accelerometer, already available on WISP, or any other (low power) electronic sensor.

Algorithm 2 BLISP Control Protocol

```
1:  x ← Maximum backoff window, see Section 5.5.2
2:  each PERIOD_n do
3:      a ← #ACK_{n−1}                          ▷ Received ACKs
4:      r ← #FRAME_{n−1}                        ▷ Frames planned to transmit
5:      WISP_ok ← (a = r)                       ▷ Expect ACK for each frame
6:      if WISP_ok then
7:          backoff ← 0                         ▷ No backoff on success
8:      if 0 = backoff then                     ▷ Is (re)try slot?
9:          WISP_TX ← true                      ▷ Transmit using WISP
10:         if ¬WISP_ok then
11:             backoff ← 𝒰(0, x)               ▷ New uniformly random backoff
12:     else
13:         WISP_TX ← false                     ▷ Not transmit using WISP
14:         backoff ← backoff − 1               ▷ Shift backoff
15:     BLE_TX ← ¬WISP_ok                       ▷ Use BLE if not use WISP
```

stream in case of radio switching the sensor data is periodically shared with the BLE radio as described in Section 5.5.1. The BLE radio and the WISP are both set to have 12 Byte payload per message and ten messages are combined into a single transmission. As the temperature data combined with the timestamp only uses 4 Byte the message is padded with 8 Byte of constant data.

Because of incompatibilities between WISP and the MINI ME RFID reader used for the mobile host experiments the EPC C1G2 `tag select` mechanism [56, Sec. 6.3.2.3] is disabled for all fixed and mobile reader experiments.

BLUETOOTH LOW ENERGY

BLE module (as decribed in Section 5.3.1) is programmed as slave under WISP. As described in Section 5.5.1 the BLE radio is periodically awaken by the WISP to receive new data. When not wirelessly transmitting nor receiving (UART) data from WISP BLE module is put into a low power sleeping state.

RADIO SWITCHING

The software implements feed-forward channel estimation as proposed in Section 5.4.2. The circumstances and environmental influences affecting the RF performance of the WISP might change in a very irregular and most likely unpredictable way. We therefore propose and evaluate two switching approaches.

Random ($< x$) Making the switching mechanism depend on past results will decrease the number of unnecessary backscatter channel evaluations, thereby reducing overhead and improving energy efficiency. Because we assume the environment to have random unpredictable behavior we opt that it does not make sense to include a sophisticated self-learning algorithm. Our *random backoff* approach implements an ALOHA-inspired random backoff window with a maximum value of x. A low value of x will make the system more responsive while a high value will make the system more stable in the long run. A pseudo-code representation of this switching algorithm in shown in Algorithm 2.

Naïve Limiting the maximum random value to zero will generate a constant as-short-as-possible backoff window resulting in the *naïve* approach. This approach (used as a

reference) assures that we use WISP as much as possible which increases energy efficiency. At the same time, checking a perpetually broken WISP communication channel induces an overhead compared to other maximum backoff window sizes.

5.6. EXPERIMENTAL EVALUATION

To test the performance of BLISP we executed the following experiments measuring both goodput and energy consumption.

5.6.1. EXPERIMENT SETUP

Our experimental setup consists of hardware components and methodologies for replicable and traceable measurements. For this test the BLISP (built as described in Section 5.5.1) was running software as described in Section 5.5.2.

HARDWARE

The measurement and evaluation setup we use for these experiments is based on the setup described in Section 5.3.1. In addition we use an automatic three-dimensional positioning crane [27] situated in a lab environment to automate the experiments involving a mobile BLISP.

REPLICABILITY

According to Fig. 5.1 wireless radios have two main ranges of operation:

(i) within the first range most of the packets get received and therefore the energy per byte ratio stays rather constant,

(ii) within the second range almost no packets are received and the energy spend on transmitting a byte therefore increases drastically.

For the BLISP performance tests we limit the transmission power and sensitivity of RFID reader and define two static positions, one in WISP-range and one outside WISP-range. The experiments were performed by placing the BLISP in the in-range spot, placing the BLISP in the out-range spot, and alternating the BLISP location between the in- and out-range positions on a predefined constant time interval (10 s). The BLE radio was in range for all experiments, otherwise the system would fail according to Corollary 2. The time duration for each experiment was 2 min and each experiment was repeated five times. We run baseline experiments with a battery powered WISP and a BLE radio transmitting at 4 dBm as used in Section 5.3.1.

DATA COLLECTION

In the experiments we log the number of received packets for RFID and BLE receivers. The power consumption is measured by the programmer interface using the EnergyTrace platform[4] [188]. Due to random startup delays of each platform, we match the start and stop of an experiment by asynchronously starting all platforms and logging their state after a fixed (empirically found) delay of 3 s.

[4] Because of the limited API for the EnergyTrace platform we use synchronously timed screen shots and Optical Character Recognition (OCR) to log the energy measurements for experiments using the EnergyTrace.

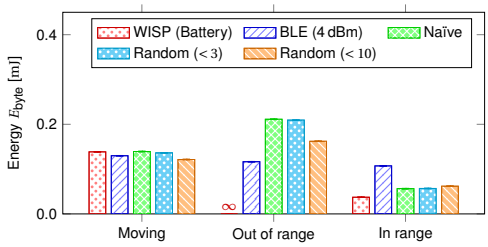

(a) Energy per byte comparison for all setups in different scenarios

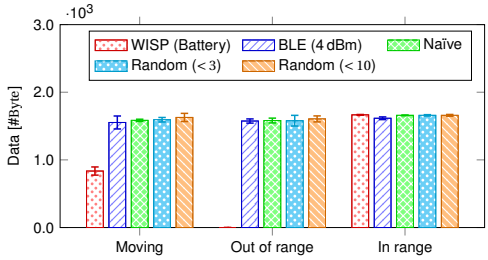

(b) Number of received messages for all setups in different scenarios

Figure 5.5: **Results of the WISP, BLE and BLISP evaluation using Impinj R420 RFID reader.** Because of WISP not being able to transmit data in the long range, see Fig. 5.5(b), effectively wasting energy, the energy per byte is infinite for this situation, see Fig. 5.5(a). We show the only WISP, only BLE, naïve BLISP and random BLISP for random backoff windows up to three and ten slots. These experiments have been normalized to *unique* messages eliminating messages transmitted by both radios around switching moments.

5.6.2. STATIC RFID READER EXPERIMENT

Measurements of energy per byte and transferred data, are shown in Fig. 5.5(a) and Fig. 5.5(b), respectively. Due to normalization to unique messages, the values in Fig. 5.5(a) are around ten times larger than the ones shown in Fig. 5.1.

Our experiments show that BLISP increases goodput almost infinitely in the long range compared to WISP (see Lemma 1) while not severely increasing power consumption over WISP in the short range. On the other hand BLISP almost halves energy consumption in the short range compared to a normal BLE radio while for Random ($x < 10$) increasing energy consumption by ≈25% on the long range. For the remaining two switching methods this difference is much larger. This is presumably caused by the amount of unneeded channel sensing operations and the overhead of redundant micro-controllers. As we add a mobility to the experiment we see WISP loosing a share of messages corresponding to the relative out of range time, this increases the energy per byte to the same level as the active BLE radio which is able to transfer data in all positions. The combined system cannot be more energy efficient than the most efficient radio for a certain position (see Corollary 3).

For an uniformly distributes in-/out-range mobility pattern the energy profit the BLISP has over the BLE radio in short range and the energy cost in the long range zero out. BLISP improves energy efficiency and throughput for situations in which the WISP

can be used for half of the time.

5.6.3. MOBILE RFID READER EXPERIMENT

The experiment setup parameters on the BLISP side is the same as using fixed RFID reader in Section 5.6.1. The detail setup parameters of mobile data aggregator are as in Table 5.1.

Results for the mobile host experiments as shown in Fig. 5.6 show comparable results among WISP, BLE and BLISP compared with fixed reader experiments from Section 5.6.2. The relative improvement from BLE to WISP and *naïve*-BLISP using a mobile reader is even larger while in-range. This relative improvement is mainly because the performance of the smartphone's BLE module has worse performance than the NRF51822 receiver. Interestingly, for in-range measurements, a large backoff window shows worse performance than the *naïve* and small backoff experiments. We suspect that this is caused by the hardware limitation of MINI ME. Based on our experiments, the MINI ME reader has trouble with rapidly moving, or only shortly available, RFID tags. Fortunately, the BLISP algorithm detects the failing RFID reader and correctly enables the BLE radio which results in continuous data availability.

5.7. LIMITATIONS AND FUTURE WORK

We list the limitations and action items for future work related to hybrid active/passive radio platforms:

1. **Improving platform switching mechanism:** Non-predictable mobility patterns require further research on learning mechanism to select the best backoff parameter x of Algorithm 2, or the complete redesign thereof.

2. **Reducing micro-controller overhead:** The current BLISP is built using two separate radio modules and therefore two micro-controllers. One micro-controller is a better approach, reducing energy consumption of BLISP.

3. **Extending to beyond two radio platforms:** By Corollary 2 and Corollary 3 adding radios with heterogenous characteristics to a hybrid system will increase the performance of BLISP, requiring research on radio selection.

5.8. CONCLUSION

In this chapter we design, implement, and evaluate a hybrid radio platform composed of Wireless Identification and Sensing Platform (WISP) and Bluetooth Low Energy (BLE), denoted as BLISP. Through experiments we show that BLISP, in situations in which this hybrid platform stays within the reception region of the lowest power radio, i.e. WISP, the energy efficiency is improved compared to BLE. At the same time the reliability of BLISP is larger than the reliability of WISP alone when BLISP moves frequently out of the RFID reader range.

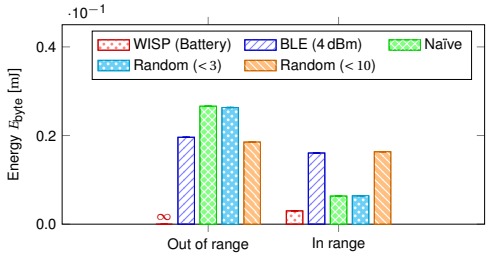

(a) Energy per byte comparison for all setups in different scenarios

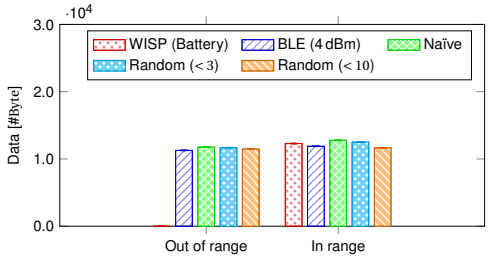

(b) Number of received messages for all setups in different scenarios

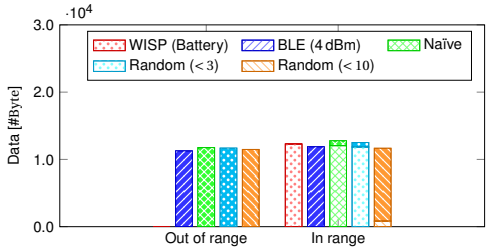

(c) Received messages per radio (BLE or WISP). Note: dark (top) part of bars—BLE messages, light (bottom) part—WISP messages

Figure 5.6: **Results of the WISP, BLE and BLISP evaluation using MiniMe RFID reader.** Again, in the long range the MINI ME reader is not able to receive data transmitted by the WISP. Fig. 5.6(c) shows the distribution of received messages per radio for completeness of the illustration. Because of the limited logging capabilities on the smartphone the number of messages is not normalized to number of unique messages.

6

GREEN WIRELESS POWER TRANSFER NETWORKS

Chapter 5 explores energy autonomous using backscatter radio. This chapter [1] researches energy management in charger networks.

6.1. INTRODUCTION

Edholm's law states that data rates offered by wireless communication systems will converge with wired ones, where forward rate extrapolation indicates convergence around the year 2030 [29]. As a result, the only cables that would require removal are the cables supporting power. In turn, wireless power (transfer) (WPT) is rapidly gaining momentum, see Fig. 6.1, and more companies are trying to capitalize on the wireless energy promise, refer for example to WiTricity [215], uBeam [195], Ossia [157], Artemis [4], Energous [42], or Proxi [167].

A natural next step is the deployment of *networks of WPT sources* (denoted throughout this work as WPTNs), i.e. deployed and dedicated WPT devices providing power to nearby energy receivers [33, 222] with numerous designs to be available, considering type of control and feedback mechanisms for power provision, localization services for power receivers, type of cooperation between individual WPTN elements, and channel feedback (e.g. for directing power to a specified device)—see also an example of a fully energy autonomous WPTN in [209, Fig. 1]. WPTNs are expected to find numerous applications, e.g. in sensing systems (vide rechargeable sensor network [65]), biology research (vide inSect fly monitoring [189] or animal inspection [87]), or implantable networks (vide brain-machine interface [68]). In all the above applications, the use of batteries is prohibitive (in biology-related applications—due to induced weight or prohibitive cabling, in implantable applications—due to necessity of surgical battery

[1] This chapter is published as the paper:
Qingzhi Liu, Michal Golinski, Przemyslaw Pawelczak, Martijn Warnier. *Green Wireless Power Transfer Networks.* IEEE Journal on Selected Areas in Communications, 34(5): 1740 - 1756, 2016.

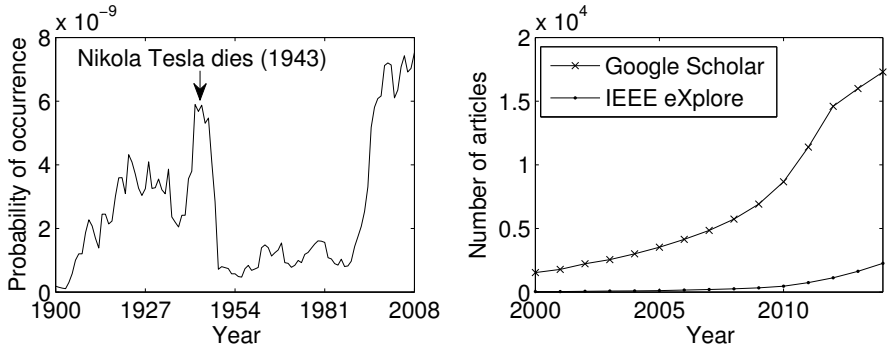

(a) Retrieved: 21 March 2015 (b) Retrieved: 21 March 2015

Figure 6.1: Probability of 'wireless power' n-gram occurrence extracted from Google digitalized books database [134] (left), and number of articles containing phrase 'wireless power' published in a given year according to Google Scholar and IEEE eXplore database (right) (see also [130, Fig. 1]).

replacement), thus WPT is the only long-term viable option. Finally, we conjecture that continuous decrease of energy consumption of embedded platforms [119, Fig. 1], [160, p. 87] over the coming years will allow for their full energy provision through WPTNs within a decade.

6

6.1.1. PROBLEM STATEMENT

The necessity of WPT becomes imminent as powering of battery-based platforms using energy harvesting alone is not enough [163, Section I]. For example, large-scale London, UK-based RF far field energy harvesting measurements at 270 London Underground stations demonstrate that in the best case only 45% of such locations can sustain the required minimum rectifying operation [163, Table VI] (for a single input source, considering digital TV, GSM 900/1800 and 3G transmitters).

However, WPT(N) has its own inherent deficiency. While there is a huge focus on making WPT(N) more efficient considering its hardware and physics, its energy conversion coefficient is still low [163, Section I] and absolutely not considered to be "green", i.e. waisting energy of the energy transmitter when the energy transmitted to the receiver is too low for rectification [64, Sec. II].

CASE STUDY—COST OF UPTIME FOR STATE-OF-THE-ART WPT NODES

Let us consider the green WPTN from a monetary perspective. Taking the energy conversion efficiency into account, let us assume that the energy conversion coefficient at a given distance for wired and wireless system are $\eta_{\text{CPT}} = 0.99$ (e.g. almost perfect) and $\eta_{\text{WPT}} = 0.01$ (e.g. almost zero), respectively. Then, an extra cost of providing an equal amount of energy by WPT-based compared to a conventional cable-based energy supply during a period of 1 year for a device consuming $\Gamma = 12.5\,\text{Wh/day}$[2] is $365 \times C_e\Gamma(1/\eta_{\text{WPT}} - 1/\eta_{\text{CPT}}) = 103.87\,€$, where $C_e = 0.23\,€/\text{kWh}$ denotes the energy cost.

[2] Approximate smartphone daily energy consumption.

Table 6.1: Energy Consumption of various WPTN transmitters, see Section 6.1.1

	R1000	S420	PWC	TI
Consumed power (idle state) [W]	24.31	5.57	4.13	≈0[a]
Consumed power (charge state) [W]	45.20	12.68	4.13	1.59

R1000—Impinj Speedway R1000 RFID reader [77] (firmware: Octane 3.2.4.240, hardware revision: 030-02-00001); S420—Impinj Revolution R420 RFID reader [78] (firmware: 4.8.3.240, hardware version: 250-004-000); PWC—Powercast TX91501-3W transmitter [165, Powercast]; TI—Texas Instruments BQ500410AEVM-085 transmitter evaluation board [190, /product/bq500410a]. Both RFID readers were controlled by [170], charge state induced in the inventory state of EPC Gen2 protocol.

[a] Value was too small to be measured by Energino.

In consequence, an equally important aspect is the cost of running the WPT source. Suppose that 50% of the day the harvester cannot harvest energy even if the receiver is inside the charging range (due to obstacles between the charger and receiver, mis-polarization of the receiver antenna, etc.). Even if the person is near the charger for eight hours only but the charger is switched on continuously without any uptime control then $1 - 8/24 \times 50\% = 83\%$ of power is wasted at the charger.

It is, therefore, of paramount importance to keep the chargers active only when the nearby receivers are requesting energy, and to forbid energy provision when charging (rectification) becomes ineffective. Finally, it is a truism to note that control of charging uptime minimizes unnecessary exposure to any WPT technology, including RF [123, Sec. IX-H] and magneto-inductive WPT [74, Sec. V] which is one of the critical aspects of any WPT technology making the approach of WPT to the market difficult.

Now, to provide concrete results on how much power can be wasted we measured the power consumption of several WPT nodes using the Energino platform [55]—a realtime power consumption monitoring device for DC-powered devices. In the experiment, the Energino is connected between the mains power source and a WPT source to measure the power consumed by the charger. The set of example WPTN chargers is provided in Table 6.1 representing (i) induction-based (short range) WPTN, i.e. TI board, (ii) RFID readers for transient computing/energy harvesting platforms [53], i.e. R1000 and S420, and (iii) long-range RF power transfer, i.e. PWC. We observe that all of the above devices consume a non-negligible amount of energy, both RFID readers in particular, even in the idle state, consume a lot of energy (except for the TI board).

RESEARCH QUESTION—HOW TO MAKE WPTN "GREEN"?

In majority of cases the energy receiver cannot harvest energy, or can only harvest a very small amount of it, even though the charger is switched on. In these cases the charger will waste energy, see again the example measured values Table 6.1, which makes the energy conservation at the WPT charger important especially if the chargers are battery-powered, e.g. mobile chargers [106]. Therefore, the aim of a "Green" WPTN (following our definition) is to *avoid WPT chargers wasting energy when the receiver cannot harvest energy (or can only harvest a very small amount of it) while maintaining the harvested*

energy at the receiver as high as possible.[3]

In the most obvious WPTN topology (which naturally resembles cellular communication networks, where recent work proposed to overlay a WPTN on top of a cellular one[4] [72]) chargers are static but the energy receivers are moving and chargers and receivers are able to communicate with each other. Thus for energy receiver discovery and control of charger uptime, there needs to be a well designed control plane (and communication protocol) that turns on chargers only when the charging conditions are favorable—thus "greenifying" the WPTN, as suggested in [64, Sec. II].

Unfortunately, to the best of our knowledge, the problem of provision of energy to mobile energy receivers in such WPTN topology, guaranteeing fast charger discovery without the unnecessary energy waste at the charger has been overlooked. We conjecture that solving such problem is not a trivial task.

6.1.2. OUR CONTRIBUTION

1. In this chapter we prove that making a WPTN "green" is *an NP-hard problem*. I.e., we show that it is algorithmically difficult to maximize harvested energy at the receiver and minimize idle time of the energy transmitters at the same time;

2. We then *propose two heuristics, called Beaconing and Probing, that control the WPTN charge uptime* aiming at (i) maximization of the harvested energy, charge accuracy and charge efficiency and (ii) minimization of the energy consumed by the communication between energy receivers and energy transmitters and by the chargers;

3. Finally, *we build (to the best of our knowledge) the worlds-first green WPTN*. In our experiments, compared to a baseline case (all chargers being constantly on), the proposed system saves at most ≈80% of energy with only ≈17% less energy possibly harvested.

6.1.3. CHAPTER ORGANIZATION

The rest of the chapter is organized as follows. Related work is discussed in Section 6.2. The WPTN module considered in this chapter is introduced in Section 6.3. A simple system model to assess green WPTN metrics is presented in Section 6.4. Two proposed WPTN "Green" charge control protocols are briefly introduced in Section 6.5, with their implementation details (and their performance evaluation) given in Section 6.6. Experimental results are presented in Section 6.7. Limitations of this work and future challenges are presented in Section 6.8. Finally, the chapter is concluded in Section 6.9.

6.2. RELATED WORK: WPTN CHARGERS UPTIME CONTROL

A plethora of papers consider an information theoretic, or 'classical' communications approach to analyze WPTNs, e.g. through the Shannon capacity formulation of energy

[3] We speculate that in the future other definitions of WPTN greenness will appear in the literature, as has happened for cellular networks. For more in-depth discussion on various existing "green" cellular network metrics we refer to [64].

[4] Which is a conceptual extension of powering wireless networks via renewable energy sources, refer e.g. to [73].

transfer, see e.g. [85], or optimization of transmission parameters of WPT sources to maximize considered objectives such as (i) harvested power [98, 224], (ii) interference to collocated transmission sources [191], (iii) energy outage [72, 150], (iv) charging delay [47] and (v) quality of service [117]. In the majority of those studies a continuous energy source is assumed, i.e. energy transmitters (ETx(s)) are always on/up, despite of the absence of energy receivers (ERx(s)) in the vicinity [117, 191] or are triggered at predefined intervals [133, Sec III-A]. Minimizing energy consumption while maximizing energy supply mostly limits itself to power control of the ETx.

On-demand energy provision has been considered in [204] (in case of mobile ETx and static ERx), [145, 209] (for static ETx/ERx). In all of these works no actual protocol for controlling ETx uptime has been introduced. Papers that do propose ETx uptime control are [219] (controlling power flow in an inductive-based WPT), [227] (although considered only architecturally without further investigation), [209, Fig. 4] (without any discussion on the details of the protocol), or [34] (in the context of electromagnetic exposure minimization). The most relevant work [145], proposes a new medium access control protocol for WPTN-enabled sensor networks, which controls (among other things) ETx uptime, (i) considers both static ETx/ERx, and (ii) is ETx-centric, i.e. receivers must take care of requests for energy (ETxs never offer to send energy). Another relevant protocol has been considered in [209, Fig. 4], but without analysis of the protocol parameters and its influence on the WPTN performance.

It is important to state that in all the above works the number of ETx and ERx is always constant and an ERx/ETx discovery mechanism has been overlooked. Furthermore, as none of the above works (except for [145]) propose an actual charge control protocol for WPTNs, it is unknown how control and signaling affects provisioned energy for topologies other than that of [145]. We thus conclude that ETx charge control with discovery mechanism, saving energy due to signaling, has not been considered. This chapter will fill this gap.

6.3. WPTN MODULE

We now present the classification of the existing WPTNs. Based on this classification we shall select a WPTN model.

6.3.1. WPT CLASSIFICATION

WPTN APPLICATIONS

Wireless Power Transfer Network can be used in numerous situations where charging of batteries in (mobile) devices by physical contact is undesired (e.g. charging implanted cardiac pacemakers), impossible (e.g. charging sensors embedded in concrete for the entire lifetime of the building, including wireless sensor networks [138, 144]), or causing obstructions in day to day life (e.g. charging of small consumer electronic devices)[5]. For a separate discussion on the applications of WPTN we refer to e.g. [123, Section II-D].

[5] On the other hand we need to remark that current state-of-the-art consumer-grade WPT technologies are targeting small low-power devices, charged at small devices, e.g. via contact-based inductive charging. For example, we are not aware of long range WTP technology available on the consumer market that would be able to charge a smartphone in time comparable to a cable-based charging. For a discussion on RF-based charging duration versus charging distance we refer to [137].

WPT PHYSICAL LAYER TECHNIQUES

The obvious classification in WPT relates to the source of energy which is later converted to electric current—please refer to recent surveys of WPT considering far field [202] (through various radio frequency (RF) ranges), [181] (through microwave RF), and through inductive coupling [174] (near field[6]), [67] (mid-field). The majority of WPTN that we are aware of are RF conversion-based—refer also to a recent survey of [122, 123] considering design issues in RF rectification conversion for wireless networks, or recent implementation examples [138].

WPTN TOPOLOGY

A WPNT topology is composed of m ETx and n ERx. Consequently, four special cases WPNT are observed in the literature: with (i) $m = 1$, $n > 1$ e.g. [85, 230], (ii) $m > 1$, $n > 1$ e.g. [145, 191], (iii) $m = 1$, $n = 1$ e.g. [117, 224], and (iv) $m > 1$, $n = 1$ (which to the best of our knowledge has not been considered so far).

Considering mobility, a WPTN topology is categorized into: (i) static ETx/static ERx [117, 145], (ii) mobile ETx/static ERx [204, 230], (iii) static ETx/mobile ERx [33, 65, 133], and (iv) mobile ETx/mobile ERx (which also has not been considered so far in the literature to the best of our knowledge). A related categorization on WPTN mobility can be found in [123, Table IX] considering routing algorithms in energy harvesting sensor networks. In addition, WPTN topologies can be categorized into (i) planned, e.g. [85, 117, 191, 230] and (ii) unplanned, e.g. [98].

WPTN ENERGY/COMMUNICATION SEPARATION

Separation of energy provision and communication/control in WPTN can be categorized into (i) joint energy and information transmission (through power splitting) [72, 113, 191], (ii) time division approach [85, 117], and (iii) frequency division [204, 219] (often in relation to inductive-based WPT). For an in-depth survey we again refer to [123, Sec. III-E] and [18].

6.3.2. SELECTED WPT TECHNOLOGY

As we show above, due to the large design space it is prohibitive to consider all WPTN topologies in one work. Therefore, we constrain ourselves to the following WPTN model, due to simplicity and resemblance to a cellular topology (see Section 6.1.1)—forming a baseline for further studies.

WPTN NODES

We utilize RF-based energy transfer, as it is the (i) least invasive, (ii) and its hardware is the smallest of all WPT techniques (allowing for implantation in biological organisms while keeping the charging distance long range [68]).

ETx ETxs are assumed to be static, with their locations planned such as to guarantee a minimum needed energy supply at any place in space (which nevertheless does not

[6] For the example papers that optimize circuit parameters of inductive-based WPT to maximize energy conversion efficiency we refer, e.g. to [103, 148].

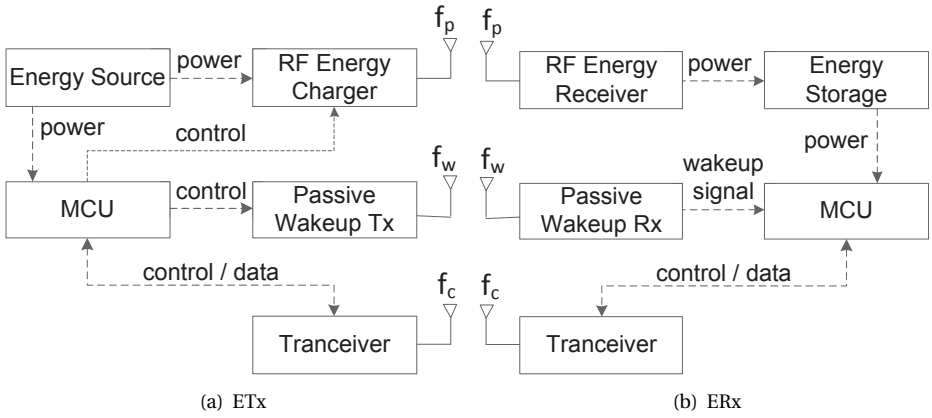

Figure 6.2: WPTN components: ETx (left) and ERx (right).

preclude energy being below the rectification threshold for any ERx at any point of space-time).

No central controller coordinating a set of ETx is considered (in contrast to [30, Sec. III]). Charging is performed at a frequency f_p MHz, e.g. $f_p = 915$ Mhz in case of Powercast TX91501-3W transmitter [165, /products/powercaster-transmitters]. ETxs do not posses MIMO capabilities, beam steering nor transmission power control, making an ETx (and a whole WPTN) design simple.

ERx Charge requests/charge control between ETx and ERx is performed at frequency f_c, e.g. $f_c = 2.4$ GHz (as used in the experimental WPTN measurement setup introduced in Section 6.6 using XBee motes [218]). The ERx aims at charging its internal battery/capacitor to the maximum level. ERxs are mobile and equipped with wake-up radio capability, as in [68, Sec. II], operating at frequency f_w MHz, e.g. $f_w = 915$ MHz [212]. Wake-up radio allows to conserve energy by the ERx by avoiding idle listening to information broadcasted by an ETx. In our WPTN charge protocol implementation we assume $f_w \neq f_c \neq f_p$ to avoid any interference scenarios (which does not preclude to design a WPTN charge control system with overlapping charge/wake-up/control frequencies). Note that the ETx and the ERx are schematically depicted in Fig. 6.2.

WPTN CHARGE CONTROL PROTOCOL

In general, as ERxs roam they are assumed to request a continuous flow of energy from neighboring ETx. To achieve the "green" WPNT presented in Section 6.1.1, ETxs will send power to an ERx only when (i) a formal connection at frequency f_c between ETx and ERx has been established and (ii) when the rectified energy at ERx is above the predefined threshold. Two attempts to introduce such protocols will be described in Section 6.5 and Section 6.6. first, in the following Section, we introduce the problem formally.

6.4. GREEN WPTN: ANALYSIS

Before we start with the introduction of the protocol to control the WPT chargers uptime we need to analyze the problem formally. For this we introduce a simplified WPTN model and subsequent performance metrics for the "green" WPTN.

6.4.1. WPTN MODEL

Let a WPTN be composed of $i \in \mathcal{M}, |\mathcal{M}| = m$ ERxs and $j \in \mathcal{N}, |\mathcal{N}| = n$ ETxs. The decision of ETx j is to switch itself on or off (to conserve ETx power), with the switch decision denoted as $c_j \in \{1,0\}$, respectively. We assume that the decision c_j is performed per time slot and that the state of WPTN (e.g. position of ETx and ERx, propagation conditions) is invariant within the time slot.

6.4.2. GREEN WPTN PERFORMANCE DESCRIPTORS

Based on the definition of Green WPTN from Section 6.1.1 we consider the following performance metrics of Green WPTN.

1. Received energy $\delta_{i,j} > 0$ (expressed in Watts) at ERx i from ETx j.
2. Charging efficiency
$$\xi_{i,j} \triangleq \begin{cases} \frac{\delta_{i,j}}{\mu_j}, & c_j = 1, \\ 1, & c_j = 0, \end{cases} \tag{6.1}$$
where μ_j (expressed in Watts) denotes the energy cost of running ETx j.
3. Charging accuracy, denoting the probability when the charging process is correct, defined as $A \triangleq \Pr[\vartheta_{i,j} = 1]$, where
$$\vartheta_{i,j} \triangleq \begin{cases} 1, & (c_j = 1 \wedge P^{(e)}_{r_{i,j}} \geq E^{(e)}_t) \\ & \vee (c_j = 0 \wedge P^{(e)}_{r_{i,j}} < E^{(e)}_t), \\ 0, & (c_j = 1 \wedge P^{(e)}_{r_{i,j}} < E^{(e)}_t) \\ & \vee (c_j = 0 \wedge P^{(e)}_{r_{i,j}} \geq E^{(e)}_t), \end{cases} \tag{6.2}$$
is the correct charging process state, in which $P^{(e)}_{r_{i,j}}$ (assuming that ETx j is on) is the signal strength of the received charge transferred from ETx j to ERx i rectified only if it is above $E^{(e)}_t$ W.
4. The probability of over-charging $X_o \triangleq \Pr[c_j = 1 \wedge P^{(e)}_{r_{i,j}} < E^{(e)}_t]$, which is used to evaluate the wasted charging energy by ETx.
5. The probability of mis-charging $X_m \triangleq \Pr[c_j = 0 \wedge P^{(e)}_{r_{i,j}} \geq E^{(e)}_t]$, which is used to evaluate the level of missed opportunity for charging the ERx.

6.4.3. GREEN WPTN: THEORETICAL ANALYSIS

WPTN CHARGE CONTROL PERFORMANCE

Let us assume that ERxs beacon charge request messages periodically and ETxs switch on charging for a beacon period once a beacon from ERx is received. As the charge switching

is related to the effectiveness of receiving charge request beacons, our aim is to analyze this dependency. In this section, for notation simplicity we remove the index j from c_j, and superscripts $^{(c)}$ and $^{(e)}$ denote calculations for request and energy, respectively.

Assume that the radio propagation follows a pathloss and log-normal shadowing model for both energy and beacon transmission with pathloss exponent n, log-normal random value $X \sim \mathcal{N}(0,\sigma)$ (where n and σ is assumed equal for both energy transmission and beacons, respectively). Furthermore, we assume that one static ETx is positioned at the center of a circular area and ERx is within the effective communication range R m of ETx. ERx is randomly deployed as static within an annulus between circles of $R_{\min}$ m and $R_{\max}$ m radius, with $R_{\min} < R_{\max}$ and $R_{\min}, R_{\max} \in [0, R]$. ETx has an omnidirectional range (for both charge request reception and energy transmission), so does the communication range of ERx. Consequently, the CDF of the distance d from ETx to ERx is $F_v(d) = \frac{d^2 - R_{\min}^2}{R_{\max}^2 - R_{\min}^2}$, for $d = [R_{\min}, R_{\max}]$ (see [17, (45)]), from which its PDF is $f_v(d) = \frac{2d}{R_{\max}^2 - R_{\min}^2}$ for $d = [R_{\min}, R_{\max}]$.

We now assume that ETx is able to receive a request from ERx at distance d only if $P_r^{(c)}(d)$ W, received power of a beacon signal at distance d between ETx and ERx, is greater than $E_t^{(c)}$ W. The received power provided from ETx to a random ERx at a distance d m is denoted as $P_r^{(e)}(d)$ W, which is rectified at ERx only if it is above $E_t^{(e)}$ W. Then, based on the definition $c = 0$ iff $P_r^{(c)}(d) < E_t^{(c)}$. For compactness, denote $\Pr[\Gamma_d^{(c)}] \triangleq \Pr[P_r^{(c)}(d) < E_t^{(c)}]$ and $\Pr[\Gamma_d^{(e)}] \triangleq \Pr[P_r^{(e)}(d) < E_t^{(e)}]$. Similarly, $\Pr[\Gamma^{(c)}] \triangleq \Pr[P_r^{(c)} < E_t^{(c)}]$, and $\Pr[\Gamma^{(e)}] \triangleq \Pr[P_r^{(e)} < E_t^{(e)}]$.

WPTN Charge Accuracy and Charging Error Based on the assumption above the evaluation parameters (charge accuracy, mis-charge error and over-charge error) obtain the new forms. Mis-charge error is $X_m = \Pr[\overline{\Gamma}^{(e)}\Gamma^{(c)}]$, over-charge error is $X_o = \Pr[\Gamma^{(e)}\overline{\Gamma}^{(c)}]$ and the charge accuracy is $A = \Pr[\Gamma^{(e)}\Gamma^{(c)}] + \Pr[\overline{\Gamma}^{(e)}\overline{\Gamma}^{(c)}]$, where $\overline{x}$ represents the complementary event.

We now calculate the probability $\Pr[\Gamma^{(e)}\Gamma^{(c)}]$, noting that the remaining expressions, i.e. $\Pr[\overline{\Gamma}^{(e)}\Gamma^{(c)}]$, $\Pr[\Gamma^{(e)}\overline{\Gamma}^{(c)}]$ and $\Pr[\overline{\Gamma}^{(e)}\overline{\Gamma}^{(c)}]$ can be calculated following the same steps. The probability that the two events $\Gamma^{(c)}$ and $\Gamma^{(e)}$ happen at the same time can be calculated as $\Pr[\Gamma^{(e)}\Gamma^{(c)}] = \Pr[\Gamma^{(e)}|\Gamma^{(c)}]\Pr[\Gamma^{(c)}]$. We need to calculate $\Pr[\Gamma^{(c)}]$ and $\Pr[\Gamma^{(e)}|\Gamma^{(c)}]$ separately.

To calculate charge request probability $\Pr[\Gamma^{(c)}]$ define received signal power of the charge request at ETx from ERx, $P_r^{(c)}$, as

$$P_r^{(c)} = \underbrace{\left[P_t^{(c)} - L^{(c)}(d_0) - X_\sigma\right]}_{\triangleq P_{r_1}^{(c)}} + \underbrace{\left[-10n\log(d/d_0)\right]}_{\triangleq P_{r_2}^{(c)}(d)}, \tag{6.3}$$

where $P_t^{(c)}$ defines the transmitted power of control data (charge request) from ERx (in dBm), $L^{(c)}(d_0)$ is the average pathloss at reference distance d_0 m (in dBm), and $X_\sigma \sim \mathcal{N}(0,\sigma)$ dBm.

Proposition 2. *The distributions of the received power $P_r^{(c)}(d)$ for ERx is*

$$f^{(c)}\left(P_r^{(c)}\right) = \eta \int_{\xi_{\min}}^{\xi_{\max}} e^{-\beta} 10^{-\rho} \mathrm{d}P_{r_1}^{(c)}, \tag{6.4}$$

where $\eta \triangleq \frac{{d_0}^2 \ln 10}{5\sqrt{2\pi}\sigma n(R_{\max}^2 - R_{\min}^2)}$, $\beta \triangleq \frac{\left(P_{r_1}^{(c)} - \varepsilon^{(c)}\right)^2}{2\sigma^2}$, $\rho \triangleq \frac{P_r^{(c)} - P_{r_1}^{(c)}}{5n}$, $\varepsilon^{(c)} \triangleq P_t^{(c)} - L^{(c)}(d_0)$, $\xi_{\min} \triangleq P_r^{(c)} + 10n\log\left(\frac{R_{\min}}{d_0}\right)$ *and* $\xi_{\max} \triangleq P_r^{(c)} + 10n\log\left(\frac{R_{\max}}{d_0}\right)$.

Proof. Consider the static ERx. First we observe that $f^{(c)}\left(P_{r_1}^{(c)}\right) = \mathcal{N}\left(\varepsilon^{(c)}, \sigma\right)$. To calculate the distribution of $P_{r_2}^{(c)}(d)$, using the technique of dependent variables to calculate joint PDF of ERx position and signal attenuation we have

$$\begin{aligned} f^{(c)}\left(P_{r_2}^{(c)}(d)\right) = & f_v\left(h\left(P_{r_2}^{(c)}(d)\right)\right) \\ & \times \left|\partial h\left(P_{r_2}^{(c)}(d)\right)/\partial P_{r_2}^{(c)}(d)\right|, \end{aligned} \tag{6.5}$$

where $h\left(P_{r_2}^{(c)}(d)\right) = d_0 10^{-\frac{P_{r_2}^{(c)}(d)}{10n}}$ is the inverse function of $P_{r_2}^{(c)}(d)$ and $\frac{\partial h\left(P_{r_2}^{(c)}\right)}{\partial d} = -\frac{d_0 \ln 10}{10n} 10^{-\frac{P_{r_2}^{(c)}}{10n}}$.

We assume that an ERx is always within the ETx transmission range $-10n\log\left(\frac{R_{\max}}{d_0}\right) \leqslant P_{r_2}^{(c)} \leqslant -10n\log\left(\frac{R_{\min}}{d_0}\right)$. Replacing $P_{r_2}^{(c)}(d)$ with $P_r^{(c)} - P_{r_1}^{(c)}$ we have $\xi_{\min} \leq P_{r_1}^{(c)} \leq \xi_{\max}$. We can now derive a joint PDF or $P_{r_1}^{(c)}$ and $P_{r_2}^{(c)}(d)$ in (6.3) through convolution as

$$\begin{aligned} f^{(c)}\left(P_r^{(c)}(d)\right) = & \int_{\xi_{\min}}^{\xi_{\max}} f^{(c)}\left(P_{r_1}^{(c)}\right) \\ & \times f^{(c)}\left(P_r^{(c)} - P_{r_1}^{(c)}\right) \mathrm{d}P_{r_1}^{(c)} \end{aligned} \tag{6.6}$$

leading to (6.4). □

Finally, the probability that the charge request signal $P_r^{(c)}$ is smaller than the communication threshold $E_t^{(c)}$ is

$$\Pr[\Gamma^{(c)}] = \int_{-\infty}^{E_t^{(c)}} f^{(c)}\left(P_r^{(c)}(d)\right) \mathrm{d}P_r^{(c)}(d). \tag{6.7}$$

Secondly, to calculate charge conditional probability $\Pr[\Gamma^{(e)}|\Gamma^{(c)}]$ we have the following proposition.

Proposition 3.

$$\Pr[\Gamma^{(e)}|\Gamma^{(c)}] = \int_{R_{\min}}^{R_{\max}} \frac{f_v(d)\Pr[\Gamma_d^{(c)}]\Pr[\Gamma_d^{(e)}]}{\int_{R_{\min}}^{R_{\max}} f_v(d)\Pr[\Gamma_d^{(c)}]\mathrm{d}d} \mathrm{d}d \tag{6.8}$$

Proof. The probability of ERx is at a position d given event $\Pr[\Gamma^{(c)}]$ happens is

$$\Pr[d|\Gamma^{(c)}] = \frac{f_v(d)\Pr[\Gamma_d^{(c)}]}{\int_{R_{\min}}^{R_{\max}} f_v(d)\Pr[\Gamma_d^{(c)}]\mathrm{d}d}. \tag{6.9}$$

The event that the ERx appears at distance d happens iff the event $\Gamma_d^{(e)}$ happens. Then the probability of event $\Gamma^{(e)}$ given event $\Gamma^{(c)}$ happens is calculated as the expected value of $\Pr[\Gamma_d^{(e)}]$ by

$$\Pr[\Gamma^{(e)}|\Gamma^{(c)}] = \int_{R_{\min}}^{R_{\max}} \Pr[d|\Gamma^{(c)}] \Pr[\Gamma_d^{(e)}] \mathrm{d}d \tag{6.10}$$

leading back to (6.8). □

Harvested Power and Charge Efficiency Denote $\varphi^{(c)}(d) = P_t^{(c)} - L^{(c)}(d_0) - 10n\log(d/d_0)$. Then the signal strength of the charge request message at distance d is $f_d^{(c)}(P_r^{(c)}(d)) \sim N(\varphi^{(c)}(d), \sigma)$, and $P[\overline{\Gamma}_d^{(c)}] = \int_{E_t^{(c)}}^{+\infty} f_d^{(c)}(P_r^{(c)}(d)) \mathrm{d}P_r^{(c)}(d)$. The received charge power $P_r^{(e)}$ at ERx from ETx can be calculated following the same distribution as presented in Section 6.4.3 with replacement of superscripts $^{(c)}$ to $^{(e)}$. The expected received charge power at distance d is $\mathbf{E}(P_r^{(e)}(d)) = \int_{E_t^{(e)}}^{+\infty} P_r^{(e)}(d) f_d^{(e)}(P_r^{(e)}(d)) \mathrm{d}P_r^{(e)}(d)$. Then the mean received charge power $\mathbf{E}(P_r^{(ec)}(d))$ triggered by signal level of charging request (beacon) message at d is calculated as $\mathbf{E}(P_r^{(ec)}(d)) = \mathbf{E}(P_r^{(e)}(d)) \Pr[\overline{\Gamma}_d^{(c)}]$. In the whole area the expected received power is

$$\mathbf{E}(P_r^{(ec)}) = \int_{R_{\min}}^{R_{\max}} f_v(d) E(P_r^{(ec)}(d)) \mathrm{d}d. \tag{6.11}$$

The mean charging power in the whole WPTN area is calculated as $\mathbf{E}(P_t^{(ec)}) = \Pr[\overline{\Gamma}^{(c)}] P_t^{(c)}$ and the WPTN charging efficiency is $\xi = \mathbf{E}(P_r^{(ec)}) / \mathbf{E}(P_t^{(ec)})$.

Numerical Example Numerical results of the above calculations are presented in Fig. 6.3, together with Matlab simulations to validate our analytical results. From this example it is clear that although signal strength of beacon (charging request) messages is easy to use, the mis-charging error and over-charging error are still high. Moreover we conjecture that signal strength of charge request beacons is not enough to accurately estimate the charging process and control the ETx uptime.

6.4.4. CONTROL COMPLEXITY

RF-based WPTN targets devices with low power consumption. Therefore, it is important to balance the power consumption at ERx for controlling the WPTN performance. In this Section we analyze the control complexity to achieve required performances.

Based on the definition of evaluation parameters from Section 6.4.2, we denote the error charging process as $1 - \vartheta_{i,j} \triangleq \eta_{i,j}$ and energy wasting rate from ETx j to ERx i as $\frac{1}{\xi_{i,j}} \triangleq \psi_{i,j}$. The user defined WPTN performance constraints are defined as follows. To achieve safe charging $\sum_{j=1}^{n} \delta_{i,j} \le \delta_t$ where δ_t is the exposure limit, see e.g. [34, Sec. III-B]. Note that, as in [34, Sec. III-A], we ignore the effect of destructive interference [190, /PDF/P2110-datasheet.pdf (p. 7)], i.e. $\sum_{\forall j: c_j=1} \delta_{i,j}$ increases with increasing $\sum_{j=1}^{n} c_j$. To achieve WPTN-wide charging error $\sum_{j=1}^{n} \eta_{i,j} \le \eta_t$, where η_t is the acceptable error

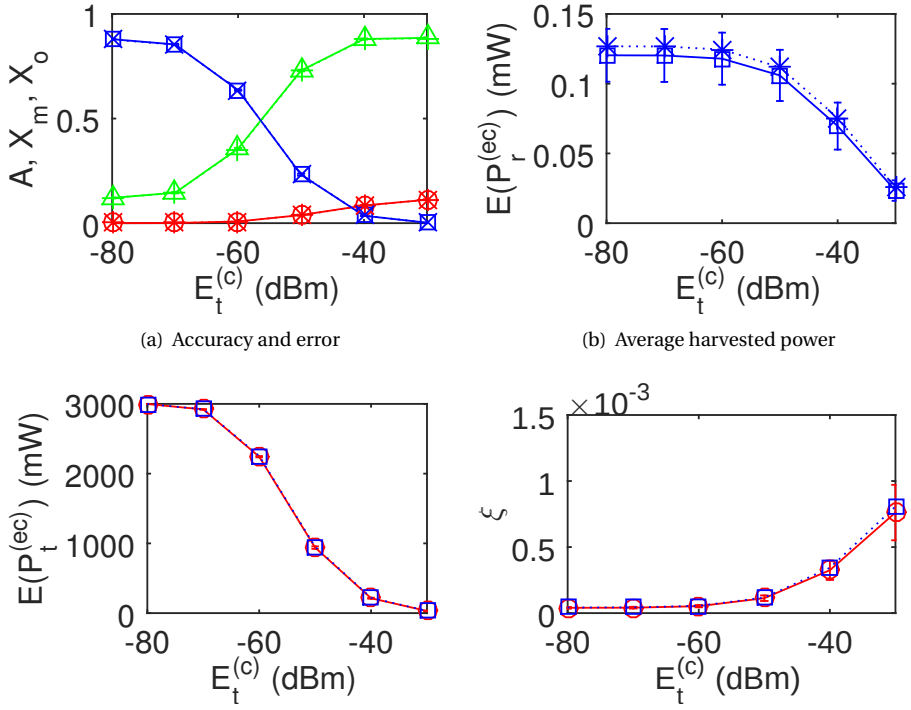

(a) Accuracy and error

(b) Average harvested power

(c) Average charged power

(d) Charge efficiency

Figure 6.3: Simulation (solid line) and analytical (dotted line) results of WPTN evaluation parameters: (a) charging accuracy (green triangle), over-charging error (blue square), mis-charging error (red circle); (b) average harvested power; (c) average charged power; and (d) charging efficiency. In the simulation the ERx is placed at 10000 random positions with 10 test rounds. The parameters are: $R_{\min} = 1$ m; $R_{\max} = 10$ m; $d_0 = 1$ m; $n = 3$; $\sigma = 7$; $f_p = 915$ MHz; $f_c = 2.4$ GHz; $E_t^{(e)} = -10$ dBm; $P_t^{(e)} = 3000$ mW; $P_t^{(c)} = 10$ mW.

limit. Finally, to achieve WPTN-wide energy wasting rate $\sum_{j=1}^{n} \psi_{i,j} \leq \psi_t$, where ψ_t is the allowed energy wasting limit.

In addition we introduce the following vectors: (i) $\mathbf{a}_{i,j} = [\delta_{i,j}, \vartheta_{i,j}, \xi_{i,j}]$ (vector of WPTN performance descriptors from ETx j to ERx i), (ii) $\mathbf{b}_{i,j} = [\delta_{i,j}, \eta_{i,j}, \psi_{i,j}]$ (alternative form of $\mathbf{a}_{i,j}$), (iii) $\mathbf{s}_t = [\delta_t, \eta_t, \psi_t]$ (vector of WPTN-wide constraints). In addition we introduce $\mathbf{w}_t = [w_\delta, w_\eta, w_\psi] \in \mathbb{R}^+ \cup \{0\}$ describing weights assigned to each WPTN performance descriptor.

We then define $o_{i,j} \triangleq \mathbf{w}_t \mathbf{a}_{i,j}^T$ (weighted sum of WPTN performance descriptors), $a_{i,j} \triangleq \mathbf{w}_t \mathbf{b}_{i,j}^T$ (weighted sum of alternative form of WPTN performance descriptors), and $s_t \triangleq \mathbf{w}_t \mathbf{s}_t^T$ (weighted sum of constraints). For $o_{i,j}$ we also define a total WPTN performance requirement o_q (user specified). We can now introduce two problems formally

$$\textbf{PI}: \sum_{j=1}^{n} \sum_{i=1}^{m} o_{i,j} c_j \geq o_q, \tag{6.12a}$$

$$\textbf{PII}: \max \sum_{j=1}^{n} \sum_{i=1}^{m} o_{i,j} c_j, \tag{6.12b}$$

$$\textbf{PI/PII} \text{ subject to } \sum_{j=1}^{n} a_{i,j} c_j \leq s_t. \tag{6.12c}$$

Proposition 4. ***PI*** *expressed as (6.12a) with subject to (6.12c) is NP-Complete.*

Proof. We will prove this proposition via restriction [48, Sec. 3.2.1]. By allowing only instances of **PI** where $m = 1$, $o_{i,j} = a_{i,j}$, $o_q = s_t = \frac{1}{2} \sum_{j=1}^{n} o_{i,j}$ and noting that $\sum_{j=1}^{n} \sum_{i=1}^{m} o_{i,j} c_j$ is a subset of all possible $o_{i,j}$ we restrict **PI** to the PARTITION problem which is NP-Complete [48, Sec. 3.1]. Therefore **PI** is NP-Complete. □

Corollary 4. ***PII*** *expressed as (6.12b) with subject to (6.12c) is NP-Hard.*

Proof. For $\sum_{j=1}^{n} \sum_{i=1}^{m} o_{i,j} c_j \triangleq S_{\textbf{PI}}$ in **PI**, to decide whether $S_{\textbf{PI}} \geq o_q$, we ask **PII** to find $\max S_{\textbf{PI}} \triangleq S_{\textbf{PII}}$, and then check whether $S_{\textbf{PII}} \geq o_q$. If $S_{\textbf{PII}} \geq o_q$, then $S_{\textbf{PI}} \in [o_q, S_{\textbf{PII}}]$. However, if $S_{\textbf{PII}} < o_q$, then there is no $S_{\textbf{PI}} \geq o_q$. Then we have **PI** $\leq_p$ **PII**, where $Y \leq_p X$ denotes "Y is polynomial time reducible to X" [95, Sec. 8.1]. From Proposition 4 **PI** is NP-Complete. Therefore Problem II is NP-Hard, following from its definition [84, pp. 80]. □

We remark that **PI** and **PII** is a generalized case of [34, (3)].

Less formally **PI** and **PII** can be looked at as the multi-dimensional 0–1 knapsack problem (MKP) [46]. That is, the number of ERx m with constraints s_t corresponds to the number of knapsack with capacities. The number of ETx n corresponds to the number of items. Each ETx j generates $a_{i,j}$ in ERx i and corresponds to each item consuming resources in the knapsack. Each ETx j yields $o_{i,j}$ profits in receiver i and corresponds to each item yielding profit in a knapsacks. Then, each ETx decides to turn on or off by assigning the values of c_j and corresponds to each item being selected or not. Now, (i)

the goal of **PI** is to decide whether the profit yielded by the ETx, i.e. $\sum_{j=1}^{n}\sum_{i=1}^{m} o_{i,j}c_j$, can be larger or equal to o_q while not exceeding constraint s_t in each receiver—while the decision goal of MKP is to decide whether the profit of the selected items can be larger or equal to the requirement and not exceeding the resource capacity of each knapsack. Similarly, (ii) the goal of **PII** is to make ETx yielding maximum profit from $\sum_{j=1}^{n}\sum_{i=1}^{m} o_{i,j}c_j$ while not exceeding constraint s_t in each ERx—while the optimization goal of MKP is to make selected items yield maximum profit and not exceeding the resource capacity of each knapsack.

To summarize, in WPTN it is difficult to find the best values of each of the parameters introduced in Section 6.4.2 at the same time. WPTN protocol must tradeoff among parameters, e.g. decrease harvested energy to save a large percent of charging energy.

6.5. GREEN WPTN: CHARGE CONTROL PROTOCOL PROPOSALS

Polynomial approximation schemes are used to solve MKP [46, Sec. 3.1]. Nevertheless, this does not help us designing an algorithm for maximizing $o_{i,j}$ in WPTN, as **PI**/**PII** are introduced for a very simple (per time slot) WPTN systems that does not consider other elements that increase the complexity of the problem (and the problem formulation), e.g. the mobility of ERxs, the communication rate between ERx and ETx, or path loss. This shows a need to design a protocol to control $\mathbf{a}_{i,j}$. Therefore, in this chapter we propose two simple protocols (heuristics) to solve (6.12) in a best effort way. The general high-level idea behind these is as follows.

- Protocol 1—*Beaconing*: when an ERx is in need of energy it broadcasts charging request packets periodically. If a charging request is received by an ETx, it turns itself on in order to charge the ERx. While the ETx is turned on, it expects that charging requests will arrive correctly at regular intervals from the ERx. This approach follows the beaconing mechanism available in many contemporary protocols, e.g. used for status broadcast in IEEE 802.11p [128].

- Protocol 2—*Probing*: Extending Protocol 1, if an ERx is in need of energy it measures harvested energy and reports it to the ETx. Then, the ETx decides if the ERx should be charged based on the information regarding energy harvested at the ERx. If the ETx does not receive any charge requests after a predetermined timeout, it will switch itself off. Just like the Beaconing, probing mechanism is widespread in many communication systems. For example it is successfully used in rate adaptation mechanism in many IEEE 802.11 versions, see e.g. [102, Sec. II-B].

To asses protocol 1 and 2 we propose a simple benchmark.

- Benchmark—*Freerun*: (i) there is no communication between ERx and ETx, i.e. no energy is consumed for communication, (ii) the ERx can freely harvest energy from each ETx, and (iii) the ETxs are awake and ready to charge all the time.

In the subsequent Sections we will describe and evaluate experimentally Protocol 1 and 2 in detail.

6.6. GREEN WPTN: CHARGE CONTROL PROTOCOL IMPLEMENTATION

6.6.1. WPTN HARDWARE, SOFTWARE AND MEASUREMENT PLATFORM

To evaluate the proposed protocols we have deployed the following WPTN emulator, together with the charging protocol measurement platform. Our green WPTN is composed of four Powercast TX91501-3W transmitters with integrated antennas [165, Powercast] and one P1110-EVB[7] receiver evaluation board with co-supplied 1 dBi omnidirectional antenna [165, /products/development-kits], see Fig. 6.4. Each ETx, see Fig. 6.4(a), is connected with the mains power through the transistor switch controlled by the Arduino Uno board [2, /arduinoBoardUno]. Analogically, the ERx emulator is controlled by the same Arduino board, see Fig. 6.4(b).

All Arduino Uno boards are equipped with Wireless Secure Digital (SD) Shields [2, /ArduinoWirelessShield] with Digi XBee IEEE 802.15.4 modules [218] attached (with 10EC version firmware and PCB antennas). XBee IEEE 802.15.4 modules are used to provide the communication layer for the emulated WPTN. Each XBee device is configured to work as an end node in a frame-based API mode and given a unique 16-bit address. The rest of XBee IEEE 802.15.4 configuration parameters have default values.

Each device logs its measurements and events to an SD card placed in the slot of the Wireless SD Shield. Both protocols introduced in Section 6.5, as well as a measurement collection process, has been implemented in C++ amassing to more than 2800 lines of code.

There are two remarks that need to be made about our WPTN deployment. first, we note that we use the word 'emulator' throughout, as the ERx is still connected to the power supply. This was dictated by (i) the simplicity of the WPTN design, and (ii) an extra energy burden on ERxs due to data collection. Therefore, our WPTN implementation should be considered as an evaluation testbed for various WPTN protocols. Second, we note that the Powercast ETx/ERx we have used operated in the 915 MHz center frequency channels (ISM Region 2), co-interfering with the Dutch KPN cellular operator and channels allocated to the Dutch Ministry of Defense.

6.6.2. GREEN WPTN: CHARGE CONTROL PROTOCOL DETAILS AND IMPLEMENTATION

PROTOCOL DESCRIPTORS

Before describing the operation of the two protocols in detail we introduce a set of support variables used by both protocols—messages and states—controlled by the timers provided in Table 6.6.2.

ERx/ETx Messages Each packet from/to an ERx/ETx is enclosed in an IEEE 802.15.4 frame, with the frame header encapsulating source and destination address. In the protocols implementation of WPTN, on the reception of the packet, we allow to read the

[7] Due to measurement simplicity we have chosen a harvester based on a continuous output power, P1110, rather than pulsed power, P2110.

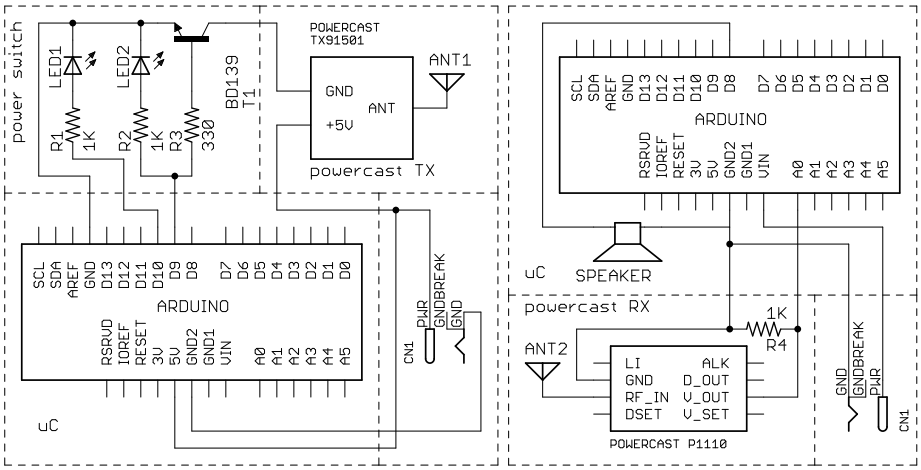

(a) ETx (b) ERx emulator

Figure 6.4: Components of the implemented WPTN: (a) ETx, and (b) ERx emulator and a charge measuring unit. Notes: LED1 and LED2 are used for ETx state indication purpose; value of resistor R4 is user-changeable allowing to test the effect of various ERx impedances on the WPTN performance.

received signal strength indicator of this particular packet. The following packet types used in our WPTN implementation are introduced:

- $\texttt{REQ}_{\texttt{CRG}}$: packet with charging request, broadcasted every $t_{\text{Ping}}^{\text{ERx}}$ s in Charging Request Phase (see Section 6.6.2) by ERx;
- $\texttt{REQ}_{\texttt{PWR}}$: power report packet request sent by ETx from ERx used in the Power Probing Phase (see Section 6.6.2);
- $\texttt{REP}_{\texttt{PWR}}$: packet containing two values: (i) voltage level on the load of the ERx—V and (ii) threshold level of the ERx—$\eta_{\text{PowerTh}}^{\text{ERx}}$[8]. $\texttt{REP}_{\texttt{PWR}}$ can be a response to $\texttt{REQ}_{\texttt{PWR}}$ (if in the Power Probing Phase) or sent by the ERx unsolicited (if in the Charging Phase, see again Section 6.6.2).

ERx/ETx States The ETx and ERx states are as follows.

ERx states: The following states are defined at the ERx:

- $\texttt{S}_{\texttt{IDLE}}$: The ERx is in need of energy and broadcasts $\texttt{REQ}_{\texttt{CRG}}$ every $t_{\text{Ping}}^{\text{ERx}}$ s. The ERx is in this state in the Charging Request Phase of the protocol;

[8] The reason for sending V and $\eta_{\text{PowerTh}}^{\text{ERx}}$ from ERx to ETxs is due to ease of experiment result collection (V) and debugging ($\eta_{\text{PowerTh}}^{\text{ERx}}$). The ETx uses $\eta_{\text{PowerTh}}^{\text{ERx}}$ extracted from the packet instead of a pre-programmed one, therefore only the ERx needs to be re-programmed in order to change this parameter of the experiment.

Table 6.2: Protocol parameter values used in the WPTN experiment implementation

Symbol	Type[a]		Description	Set value
$t^{\text{ETx}}_{\text{CrgReq}}$	B		In S_{ON} —feedback timer within which unsolicited $\texttt{REQ}_{\texttt{CRG}}$ packets from the ERx need to be received	8 s
$\eta^{\text{ETx}}_{\text{CommTh}}$	B	P	Received signal strength value below when a packet from the ERx is ignored when received[b]	–70 dBm
$t^{\text{ERx}}_{\text{Ping}}$	B	P	Time between two conSecutive $\texttt{REQ}_{\texttt{CRG}}$ packets being broadcasted by an ERx (if in S_{IDLE} for Probing)	4 s
$t^{\text{ETx}}_{\text{PwrProbeRsp}}$		P	Time the ETx waits for $\texttt{REP}_{\texttt{PWR}}$ after sending $\texttt{REQ}_{\texttt{PWR}}$	4 s
$t^{\text{ERx}}_{\text{RmvLast}}$		P	Time for which each ETx address is stored in Q_{TX} queue	30 s
$t^{\text{ETx}}_{\text{turnOff}}$		P	In S_{ON} —waiting time for the first (unsolicited) $\texttt{REP}_{\texttt{PWR}}$ (sent by an ERx on transition from S_{WAIT} to $S_{CHARGED}$)	2 s
$t^{\text{ETx}}_{\text{PwrProbe}}$		P	In S_{ON} —feedback timer within which unsolicited $\texttt{REP}_{\texttt{PWR}}$ packets from an ERx need to be received	8 s
$t^{\text{ERx}}_{\text{PwrProbe}}$		P	In $S_{CHARGED}$ —time between two $\texttt{REP}_{\texttt{PWR}}$ packets sent by an ERx to the ETx currently charging this ERx	4 s
$t^{\text{ETx}}_{\text{RandWait}}$		P	Maximum time the ETx waits before sending $\texttt{REQ}_{\texttt{PWR}}$ after receiving $\texttt{REQ}_{\texttt{CRG}}$ from an ERx[c]	0.5 s
$t^{\text{ERx}}_{\text{WaitForPwr}}$		P	Maximum time an ERx will wait for power from the ETx while being in state S_{WAIT}	4 s
$\eta^{\text{ERx}}_{\text{PowerTh}}$		P	Voltage threshold for a load being attached to the microcontroller[d]	0.5 V
t_{SYN}	n/a	n/a	Measurement synchronization interval[e]	2 s

[a] Protocol type: B—Beaconing, P—probing
[b] Parameter used to simulate different levels of communication layer power transmission/coverage
[c] Timer used to avoid collisions at the ERx when multiple ETx hear the same $\texttt{REQ}_{\texttt{CRG}}$ and send $\texttt{REQ}_{\texttt{PWR}}$ immediately
[d] If the voltage level is above this threshold the power level is considered to be sufficient to initiate charging
[e] Value chosen in order to ensure that synchronization happens more often than any events in the WPTN, see [52, Sec. 5.2] for detailed discussion

- S_{WAIT} : The ERx waits for the first power transmission from the ETx. If the power transmission is successful, the ERx will move to the $S_{CHARGED}$. Else, if the ERx does not receive any power for $t^{\text{ERx}}_{\text{WaitForPwr}}$ s the ERx moves back to S_{IDLE} [9];

- $S_{CHARGED}$: The state in which the ERx is being charged by a specific ETx. The ERx knows the address of the ETx (last one stored in Q_{TX} queue) and sends $\texttt{REP}_{\texttt{PWR}}$ to this ETx every $t^{\text{ERx}}_{\text{PwrProbe}}$ s. The ERx is in this state if the protocol is in the Charging Phase and the ERx harvests energy above $\eta^{\text{ERx}}_{\text{PowerTh}}$ V.

ETx states: The following states are defined at the ETx:

- S_{OFF} : The ETx does not transmit power;

- S_{ON} : The ETx does transmit power;

- S_{PROBE} : The ETx probes an ERx for power before deciding to move to S_{OFF} or S_{ON} ; the ETx waits in this state for $\texttt{REP}_{\texttt{PWR}}$ from an ERx for a maximum of $t^{\text{ETx}}_{\text{PwrProbeRsp}}$ s. The ETx is in this state when the protocol is in the Power Probing Phase.

[9] S_{IDLE} is a state in which the ERx is initially when the protocol is in the Charging Phase.

Algorithm 3 Beaconing—ETx and ERx events

1: **upon** $E_{\text{RxChrgReq}}$ () ▷ ERx event—Note (a)
2: BROADCAST($\texttt{REQ}_{\texttt{CRG}}$)
3: **upon** $E_{\text{TxChrgReq}}$ ($\texttt{REQ}_{\texttt{CRG}}$) ▷ ETx event
4: TURNONPOWERTRANSMISSION()
5: STATE $\leftarrow S_{ON}$
6: **upon** $E_{\text{TimeoutTxChrgReq}}$ () ▷ ETx event—Note (b)
7: TURNOFFPOWERTRANSMISSION()
8: STATE $\leftarrow S_{OFF}$

(a) Executed every $t^{\text{ERx}}_{\text{Ping}}$ s

(b) Executed in S_{ON} if $\texttt{REP}_{\texttt{PWR}}$ was not received for more than $t^{\text{ETx}}_{\text{PwrProbe}}$ s

BEACONING PROTOCOL DETAILS

The details of the protocol implementation is provided in Protocol 6.6.2. The set of the parameters describing the implementation are given in Table 6.6.2. As a worst case scenario, in the implementation we assume that the ERx is constantly in need of charging.

PROBING PROTOCOL DETAILS

The protocol executes in three phases described below. As in the case of Beaconing protocol, it is assumed that an ERx constantly requires charging.

Charging Request Phase In this phase all ERxs, every $t^{\text{ERx}}_{\text{Ping}}$ s, broadcast a $\texttt{REQ}_{\texttt{CRG}}$. At any time one or more ETx can receive a $\texttt{REQ}_{\texttt{CRG}}$ and initiate the Power Probing Phase.

Power Probing Phase Here the ETx tries to find out if an ERx is already being charged by another ETx. After the ETx received $\texttt{REQ}_{\texttt{CRG}}$ it will wait for random time interval distributed uniformly with a maximum $t^{\text{ETx}}_{\text{RandWait}}$ s (used as a simple collision avoidance scheme at the ERx) and then send $\texttt{REQ}_{\texttt{PWR}}$ to the ERx from which $\texttt{REQ}_{\texttt{CRG}}$ was received. After the ERx receives the first $\texttt{REQ}_{\texttt{PWR}}$ it will ignore all subsequent $\texttt{REQ}_{\texttt{PWR}}$ packets from other ETxs in the current Power Probing Phase. In return the ERx sends $\texttt{REP}_{\texttt{PWR}}$ containing the current level of harvested energy. After the ERx sends $\texttt{REP}_{\texttt{PWR}}$ in the Power Probing phase, it will wait a predefined time of $t^{\text{ERx}}_{\text{WaitForPwr}}$ s for the power transfer from the ETx after which (if no power was transferred) it concludes that power transfer from the ETx was unsuccessful.

If the $\texttt{REP}_{\texttt{PWR}}$ received by an ETx contains a power level lower than a power threshold, $\eta^{\text{ERx}}_{\text{PowerTh}}$, this means that the ERx is not currently harvesting energy and requires charging. Subsequently the ETx tries to charge the ERx and the Charging Phase starts. If no power is received, the ERx will go back to the Charging Request phase. In a process called blacklisting, the ERx saves the address of an ETx that was unsuccessful in the Charging Phase in its internal queue, denoted as the Q_{TX} . All the addresses are kept in the Q_{TX} for $t^{\text{ERx}}_{\text{RmvLast}}$ s. If the protocol is in a Power Probing state the ERx ignores all ETxs with addresses stored in the Q_{TX} . This is done to prevent an ETx that was not successful to initiate the Power Probing Phase with given ERx again before the network conditions change, e.g. the ERx moves to another position.

In consequence, in our current design the ETx that will charge the ERx will be (i) *the first* ETx that will respond with $\texttt{REQ}_{\texttt{PWR}}$ to $\texttt{REQ}_{\texttt{CRG}}$ from the ERx *and* (ii) the voltage on the

Algorithm 4 Probing—ERx events

1: **upon** $E_{\text{RXCHRGREQ}}$ () ▷ Note (a)
2: BROADCAST(REQ_{CRG})
3: **upon** $E_{\text{NEWPWRPROBE}}$ (REQ_{PWR}, ETx i) ▷ Note (b_1)
4: **if** STATE = S_{IDLE} **then**
5: $Q_{TX} \leftarrow$ ENQUEUE(ETx i address) ▷ Note (b_2)
6: SEND(REP_{PWR}, ETx i)
7: STATE $\leftarrow S_{\text{WAIT}}$
8: **upon** $E_{\text{VOLTAGEABOVE}}$ (ETx i) ▷ Note (c)
9: SEND(REP_{PWR}, ETx i)
10: STATE $\leftarrow S_{\text{CHARGED}}$
11: **upon** E_{RXPWRPR} () ▷ Note (d)
12: SEND(REP_{PWR}, ETx i=Q_{TX} (first))
13: **upon** $E_{\text{TIMEOUTWAITFORPWR}}$ () ▷ Note (e)
14: STATE $\leftarrow S_{\text{IDLE}}$
15: **upon** $E_{\text{RMVOLDEST}}$ () ▷ Note (f_1)
16: $Q_{TX} \leftarrow$ DEQUEUE(Q_{TX} (last)) ▷ Note (f_2)
17: **upon** $E_{\text{VOLTAGEBELOW}}$ () ▷ Note (g)
18: STATE $\leftarrow S_{\text{IDLE}}$

(a) Every $t^{\text{ERx}}_{\text{Ping}}$ s if ERx is in S_{IDLE}
(b_1) When REQ_{PWR} received from ETx i and ETx i address $\notin Q_{TX}$
(b_2) ENQUEUE method enqueues the element given as an argument in the Q_{TX} queue
(c) When ERx in S_{WAIT} receives power and load voltage exceeds $\eta^{\text{ERx}}_{\text{PowerTh}}$ V
(d) Every $t^{\text{ERx}}_{\text{PwrProbe}}$ s if ERx is in S_{CHARGED}
(e) When ERx in S_{WAIT} and no power from ETx for more than $t^{\text{ERx}}_{\text{WaitForPwr}}$ s
(f_1) When oldest address in Q_{TX} has been stored longer than $t^{\text{ERx}}_{\text{RmvLast}}$ s
(f_2) DEQUEUE methods takes of the element gven as an argument from the Q_{TX} queue
(g) When in S_{CHARGED} and attached load voltage drops below $\eta^{\text{ERx}}_{\text{PowerTh}}$ V

load of the ERx that appears as a result of the wireless power transmission from the ETx is above the threshold $\eta^{\text{ERx}}_{\text{PowerTh}}$.

Charging Phase After the ETx starts charging an ERx, there is a possibility that the ERx harvests energy that is above $\eta^{\text{ERx}}_{\text{PowerTh}}$ V. If this is the case the ERx will start sending unsolicited REP_{PWR} to the current ETx (as the ERx keeps track of the ETx devices that tried to charge it). If REP_{PWR} packets are received by the ETx at least every $t^{\text{ETx}}_{\text{PwrProbe}}$ s, the ETx will continue charging a given ERx. If the ERx does not receive enough power, it will not send a REP_{PWR} packet to the ETx within the specified time period, which will result in the ending of power transmission from the ETx to the ERx.

Pseudocode of the Probing protocol is described formally in Protocol 6.6.2 and in Protocol 6.6.2, for the ERx and the ETx side, respectively. Again, Table 6.6.2 summarizes all parameters of the protocol and their assumed values in the experiment.

6.6.3. SYNCHRONIZATION IN WPTN

For accurate collection of measurements a time synchronization is implemented as follows [52, Ch. 5]. An ERx broadcasts its timestamp every t_{SYN} s. On reception each ETx takes this timestamp as its own. After the experiment, timestamps received from an ERx are subtracted from the local ETx time. The result is the sum of transmission, processing

Algorithm 5 Probing—ETx events

1: **upon** $E_{\text{TxChrgReq}}$ ($\texttt{REQ}_{\texttt{CRG}}$, ERx i) ▷ Note (a)
2: **if** STATE = S_{OFF} **then**
3: WAITRANDOM($t^{\text{ETx}}_{\text{RandWait}}$) ▷ Uniform distribution
4: SEND($\texttt{REQ}_{\texttt{PWR}}$, i)
5: STATE ← S_{PROBE}

6: **upon** $E_{\text{PwrProbeAbove}}$ ($\texttt{REP}_{\texttt{PWR}}$, ERx i, V) ▷ Note (b)
7: **if** STATE = S_{PROBE} **then**
8: STATE ← S_{OFF}

9: **upon** $E_{\text{PwrProbeBelow}}$ ($\texttt{REP}_{\texttt{PWR}}$, ERx i, V) ▷ Note (c)
10: **if** STATE = S_{PROBE} **then**
11: TURNONPOWERTRANSMISSION()
12: STATE ← S_{ON}

13: **upon** $E_{\text{TimeoutPwrProbeRsp}}$ () ▷ Note (d)
14: STATE ← S_{OFF}

15: **upon** $E_{\text{TimeoutOnPwrProbe}}$ () ▷ Note (e)
16: TURNOFFPOWERTRANSMISSION()
17: STATE ← S_{OFF}

(a) When $\texttt{REQ}_{\texttt{CRG}}$ received from ERx i
(b) When $\texttt{REP}_{\texttt{PWR}}$ received from ERx i with $V \geq \eta^{\text{ERx}}_{\text{PowerTh}}$
(c) When $\texttt{REP}_{\texttt{PWR}}$ received from ERx i with $V < \eta^{\text{ERx}}_{\text{PowerTh}}$
(d) When in S_{PROBE} after sending $\texttt{REQ}_{\texttt{PWR}}$ the $\texttt{REP}_{\texttt{PWR}}$ from the ERx not received for more than $t^{\text{ETx}}_{\text{PwrProbeRsp}}$ s
(e) When in S_{ON} and no $\texttt{REP}_{\texttt{PWR}}$ from the ERx has been received for more than $t^{\text{ETx}}_{\text{PwrProbe}}$ s

and the actual clock time drift. Therefore time drift is the difference between the time of the reception of a $\texttt{REQ}_{\texttt{CRG}}$ at the ETx and the time of an ERx broadcasting it. As it is impossible to eliminate processing and transmission time from these measurements in a simple way all measurements were made with the assumption that these values are negligible compared with other events in WPTN.

6.6.4. WPTN DEPLOYMENT AND EXPERIMENT SCENARIOS

All ETxs and an the ERx emulator were placed on cardboard boxes 50 cm high—allowing for equal positioning in the vertical plane. Four ETxs were placed at the edges of a 1.5 m × 3.5 m rectangular plane. The angle of the front of the antennas were regulated and initially shifted 45 degrees to the border of the rectangular plane, with their center axis unchanged during the entire experiment. Conversely, the ERx emulator was allowed to be placed in ten different positions separated in vertical and horizontal axes by 1 m and 0.5 m, respectively. The front of the ERx emulator panel antenna was always vertical to the ground floor. A schematic representation of all ETxs and ERx emulator positions is presented in Fig. 7.3(a). The measurement setup has been built inside the master student office of the Delft University of Technology's Embedded Systems Lab, see Fig. 6.5(b), with movement of humans during the experiment minimized.

Within such a setup, the experiment simulated the random appearance/disappearance of the ERx in a controlled and replicable fashion. The experiment was started by placing the ERx emulator at position '1', see Fig. 7.3(a), and initializing a measurement by turning on or pressing the reset button of each device in the WPTN. From that moment the ERx emulator advertises itself to WPTN and starts collecting measurements. The ERx emulator

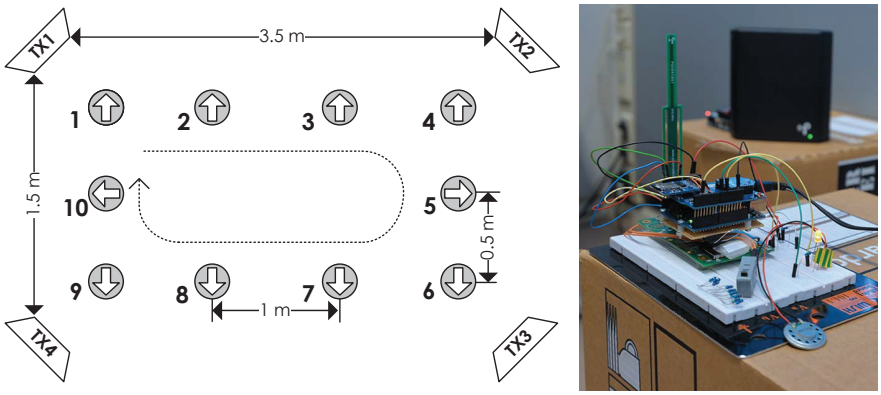

(a) Measurement setup (b) ERx emulator/ETx pair

Figure 6.5: WPTN experiment setup: (a) ERx—gray circles, with its position (marked as *1–10*) and its orientation (marked with arrows), where dashed arrow denotes the ERx movement direction; and ETx—white trapeziod, see also Section 6.6.4, (b) photograph of the ERx emulator/ETx pair in the laboratory setting—front: ERx emulator, back: one ETx.

is placed at this position for a random time chosen uniformly between 40 s and 44 s. This behavior is introduced to simulate random appearances and arrivals of the ERx emulator within one time period of sending $\texttt{REQ}_{\texttt{CRG}}$. After that time the end of the single measurement is signaled through a buzzer, see Fig. 6.4(b). Consequently, protocol execution is paused for 15 s allowing the experiment operator to move the ERx emulator to the next measuring position. One round of data collection is finished when the ERx emulator reaches position '10', with the movement pattern depicted in Fig. 7.3(a). Each round of movements has been repeated five times for statistical significance. The duration of a single experiment was ten minutes. Therefore, results presented in the following Section are based on approximately nine hours of constantly running measurements. The voltage at resistor R4 of an ERx, Fig. 6.4(b), was sampled with a period of 0.1 s.

EXPERIMENTAL RESULTS REPLICATION

For the results reproducibility measurement data, MATLAB post-processing scripts and Arduino-based charge control protocol implementation are available upon request or via `http://www.es.ewi.tudelft.nl/papers/2016-Liu-JSAC_source_code.zip`.

6.7. EXPERIMENT RESULTS

6.7.1. PERFORMANCE INDICATORS OF GREEN WPTN CONTROL

We will look at the following performance indicators for both protocols.

ERX ENERGY HARVESTED

Amount of energy harvested by an ERx during the entire experiment.

ETX ENERGY CONSUMPTION

Total energy consumed by all ETxs during the entire experiment.

Table 6.3: Variables used for ETx energy consumption calculation: ATmega328 (Arduino Uno's microcontroller) and Digi Xbee IEEE 802.15.4

Symbol	Description	Value
U_s	Voltage supply: ATmega328/Xbee	3.3 V
$I_{T,x}$	Current consumed: Xbee transmission	35 mA
$I_{R,x}$	Current consumed: Xbee reception	50 mA
$I_{S,x}$	Current consumed: Xbee sleep state	10 μA
$I_{S,a}$	Current consumed: ATmega328 sleep state	9 μA
$I_{A,a}$	Current consumed: ATmega328 active state	1.7 mA
R_d	Digi Xbee data rate	9.6 kb/s
S_p	Digi Xbee packet size	960 bits

ATmega328 DC characteristics follow from [8, Table 29-7]
Digi Xbee DC characteristics follow from [37]

WPTN CHARGING EFFICIENCY

Ratio of ERx energy harvested to the energy consumed by an ETx during charging.

ERX ENERGY CONSUMPTION

For a fair comparison of the two WPTN charge control protocols we take into consideration the energy consumed by the transmission/reception of packets from/to an ERx. Avoiding the extra burden of measuring the energy consumption of an ERx communication (refer e.g. to [26] for such studies) we directly calculated energy consumption values from the data sheet for the ERx emulator we built. The set of parameters used in the calculations are given in Table 6.3.

Although following Fig. 6.2 we assume that the passive wakeup radio is used to wake up an ERx from the off state to communication with the ETx state, in the calculation we nevertheless include the cost of the idle state of the microcontroller and the radio of the ERx. Therefore, we calculate the ERx's power consumption as $E_c = E_c^{(X)} + E_c^{(A)}$, where

$$\begin{aligned} E_c^{(X)} &\approx E_{T_x}^{(X)} + E_{R_x}^{(X)} + E_I^{(X)} \\ &= N_t \frac{S_p}{R_d}(U_s I_{T,x}) + N_r \frac{S_p}{R_d}(U_s I_{R,x}) + T_E U_s I_{S,x}, \end{aligned} \tag{6.13}$$

denoting total energy consumption of Digi Xbee board for T_E s total experiment time, composed of transmission energy ($E_{T_x}^{(X)}$), receive energy ($E_{R_x}^{(X)}$), and idle state energy ($E_I^{(X)}$), respectively, for and N_t and N_r are the number of packets that the ERx transmits and receives, and

$$\begin{aligned} E_c^{(A)} &\approx E_A^{(A)} + E_I^{(A)} \\ &= \left(N_t \frac{S_p}{R_d} + N_r \frac{S_p}{R_d} \right) U_s I_{A,a} + T_E U_s I_{S,a}, \end{aligned} \tag{6.14}$$

is the energy consumed by the Arduino Uno board composed of active state energy ($E_A^{(A)}$), and idle state energy ($E_I^{(A)}$), respectively[10].

[10] Note that (6.13) and (6.14) are worst case approximations, we assume for simplicity during transmission and reception Arduino was simultaneously in the sleep state—this is due to a small overhead of energy consumption by transmission and reception compared to the total time when the node was idle.

TIME TO CHARGE

Finally, we measure and analytically evaluate a protocol-specific parameter, i.e. time to charge—the time between transmission of a charge request by the ERx to the beginning of charge provision by the first-responding ETx.

We consider one ERx and N ETxs, as in the experiment. An ERx is in the charging range of K ETxs ($K \leq N$) and in communication range of all N ETxs. At a given moment of time (given ERx position) K and N is fixed. Our goal is to derive formulas for the expected time to charge an ERx in the WPTN.

Beaconing In Beaconing implementation we assumed only one round of charging, after which all ETxs within the communication range of an ERx will be turned on. The duration of this round is $T^{\mathrm{B}}_{\mathrm{opt}} = U(0, t^{\mathrm{ERx}}_{\mathrm{Ping}})$, where $U(a,b)$ denotes an uniform distribution from a to b.

If an ERx randomly starts to send charge requests in the WPTN, then the time to charge is $T^{\mathrm{B}}_{\mathrm{start}} = T^{\mathrm{B}}_{\mathrm{opt}}$. A cumulative distribution function (CDF) of $T^{\mathrm{B}}_{\mathrm{start}}$ under the assumption that $T^{\mathrm{B}}_{\mathrm{opt}}$ is not random but constant and equal to its mean value, $\overline{T}^{\mathrm{B}}_{\mathrm{opt}}$, is

$$F_{T^{\mathrm{B}}_{\mathrm{start}}}(t) \approx t / t^{\mathrm{ERx}}_{\mathrm{Ping}}, \tag{6.15}$$

where $t \in [0, t^{\mathrm{ERx}}_{\mathrm{Ping}}]$.

Probing Probing works in rounds. Successful round starts with a Charging Request, continues to the Power Probing Phase and ends in the Charging Phase, in which the protocol stays, successfully charging an ERx. However, if charging is not successful, the protocol goes back to the Charging Request phase. In the new Charging Request phase the previous ETx, that unsuccessfully attempted to charge an ERx, is excluded from the WPTN. Therefore, for the first round, there are N ETx and K ETx that could charge an ERx. If we choose one of $N-K$ ETxs that could not charge the ERx, we exclude it in the next round, which starts with $N-1$ ETx and K ETx that could charge the ERx. Considering random variable X_i—an ERx was charged in round i, then $\Pr[X_i] = K/N$ for $i = 1$ and $\Pr[X_i] = \frac{K}{N-(i-1)} \prod_{j=0}^{i-2} \frac{N-j-K}{N-j}$ for $i \in [2, N-K+1]$.

The length of a successful round, $T^{\mathrm{P}}_{\mathrm{opt}} = U(0, t^{\mathrm{ERx}}_{\mathrm{Ping}})$, is different from the unsuccessful round, $T^{\mathrm{P}}_{\mathrm{pes}} = U(0, t^{\mathrm{ERx}}_{\mathrm{Ping}}) + t^{\mathrm{ERx}}_{\mathrm{WaitForPwr}}$. Considering the average values of those variables, $\overline{T}^{\mathrm{P}}_{\mathrm{opt}}$ and $\overline{T}^{\mathrm{P}}_{\mathrm{pes}}$, respectively, as a consequence the CDF of $T^{\mathrm{P}}_{\mathrm{start}}$ assumes no randomness of $T^{\mathrm{P}}_{\mathrm{opt}}$ and $T^{\mathrm{P}}_{\mathrm{pes}}$, giving

$$F_{T^{\mathrm{P}}_{\mathrm{start}}}(t) \approx \sum_{i=1}^{f(t)} \Pr[X_i], t \in \{0, (N-K)\overline{T}^{\mathrm{P}}_{\mathrm{pes}} + \overline{T}^{\mathrm{P}}_{\mathrm{opt}}\}, \tag{6.16}$$

where $f(t) = \left\lfloor \frac{t - \overline{T}^{\mathrm{P}}_{\mathrm{opt}}}{\overline{T}^{\mathrm{P}}_{\mathrm{pes}}} - 1 \right\rfloor$.

WPTN CHARGE ACCURACY

Reference Measurement To calculate the accuracy for both protocols we need to measure the reference case first. The reference will denote whether an ETx should switch on during a particular time to charge an ERx. We measure the reference scenario as follows:

1. We mark the appearance time, $t_p^{(a)}$, and disappearance time, $t_p^{(d)}$, of the ERx at each position depicted in Fig. 7.3(a). The ERx stays at one location for 20 s and is allowed to move to a new position within 15 s from switch off, respectively[11];

2. During each round of movement of the ERx, one ETx is charging at a time. After position 10 was reached by the ERx as given in Fig. 7.3(a), a new ETx is turned on and a currently charging ETx is switched off;

3. We consider the following situation to be correct: if $V > \eta_{\text{PowerTh}}^{\text{ERx}}$ at a resistor R4 of ERx, then the ETx j should switch on to charge the ERx at this position, otherwise it should switch off. Each event of voltage crossing threshold is added to a vector $\mathbf{R_c} \triangleq [t_p^{(a,1)}, t_p^{(d,1)}, t_p^{(a,2)}, t_p^{(d,2)}, \ldots, t_p^{(a,x)}, t_p^{(d,x)}]$, where $t_p^{(d,x)} < T_E$ and $t_p^{(x,y)}$, $x \in \{a,d\}$ denote the start ($x = a$) and stop ($x = d$) of the reference charge and $y \in \mathbb{N}$ denote its successive number. We note that the voltage sampling period at resistor R4 of ERx is 0.1 s, similar to the experiments in Section 6.6.4.

Charge Accuracy Metric Having the reference case we can compare the actual working time sequence of each ETx j (for each protocol—Beaconing and Probing) with the reference vector R_c and calculate charge accuracy as[12]

$$\boxed{\overline{\vartheta} \triangleq (\mathbf{R_c} \Leftrightarrow \mathbf{R_c^{(x)}})/T_E}, \tag{6.17}$$

where $\mathbf{R_c^{(x)}}$ is the corresponding vector of for protocol x and $\Leftrightarrow$ denotes XNOR operation.

6.7.2. EXPERIMENTAL RESULTS: CASE 0—BENCHMARK

To obtain the metrics of interest from the measurements for the benchmark (Freerun protocol), see Section 6.5, we use the measured values in $\mathbf{R_c}$, described in Section 6.7.1, to calculate the harvested power at each position depicted in Fig. 7.3(a). We then sum up the harvested power of four ETxs, as the theoretical harvested power in the testing scenario where four ETxs are switched on all the time. Then we measure the same performance parameters for the other two protocols. Results are presented in Fig. 6.7 and Fig. 6.10 and discussed in the subsequent Sections. Note that all experimental results were plotted using MATLAB's boxplot function.

6.7.3. EXPERIMENTAL RESULTS: CASE 1—LINE OF SIGHT SCENARIO

We have performed the experiment for five different communication threshold values, $\eta_{\text{CommTh}}^{\text{ETx}}$, to measure the WPTN performance simulating various ETx/ERx link qualities. The result is presented in Fig. 6.7.

ERX HARVESTED ENERGY

Refer to Fig. 6.6(a). For every value of $\eta_{\text{CommTh}}^{\text{ETx}}$, the energy harvested by Beaconing is higher than for Probing. This is due to the restriction of Probing, where at most one ETx

[11] Note that these respective times were shorter than those during actual experiments, refer to Section 6.6.4.

[12] We refer the interested reader to [52, Ch. 5] where other types of accuracy metrics (including ETx accuracy and ERx accuracy) are introduced.

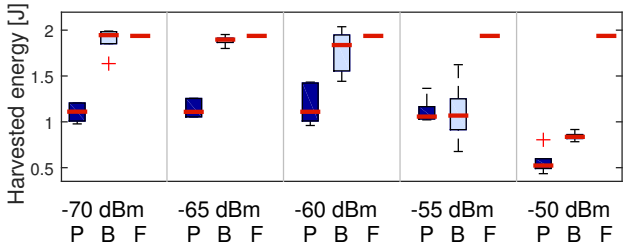

(a) ERx harvested energy

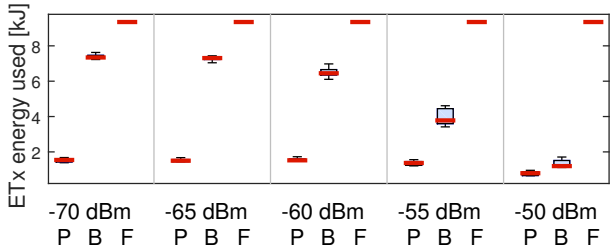

(b) ETx consumed energy

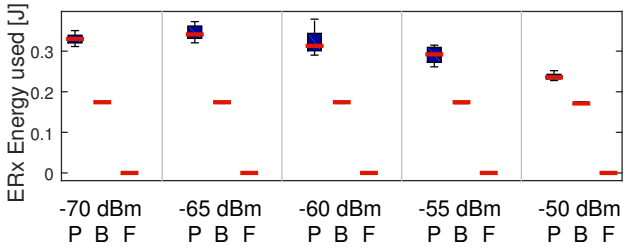

(c) ERx communication cost

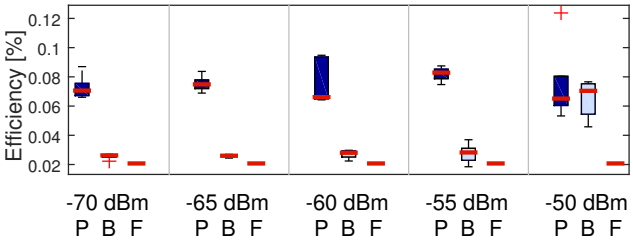

(d) WPTN Efficiency

Figure 6.6: WPTN experiment results: P—Probing, B—Beaconing, F—Freerun; Refer to Section 6.7.3 for more explanation. Observe large ETx energy consumption gain for Beaconing and Probing, compared to Freerun.

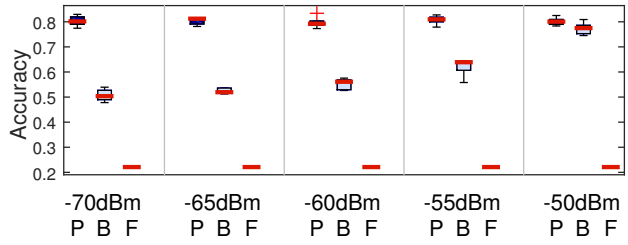

(a) WPTN Accuracy

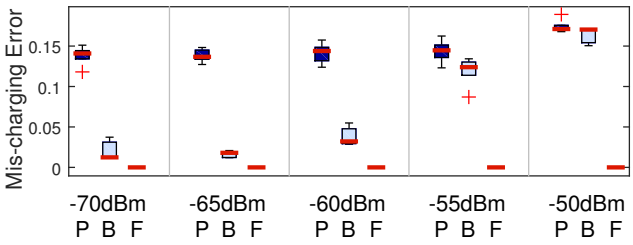

(b) Mis-scharging Error

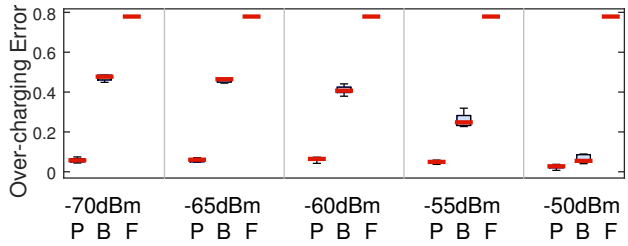

(c) Over-charging Error

Figure 6.7: WPTN experiment results for accuracy and mis- and over-charging error: P—Probing, B—Beaconing, F—Freerun; Refer to Section 6.7.3 for more explanation.

Table 6.4: Probability of receiving a beacon from ERx at each ETx during the whole experiment (Beaconing protocol)

η^{ETx}_{CommTh} (dBm)	% Prob. received beacons below η^{ETx}_{CommTh}
–70	0.96
–65	0.95
–60	0.84
–55	0.51
–50	0.17

can charge the ERx during a beacon period. The Beaconing protocol allows multiple ETxs to be turned on at the same time.

As the η^{ETx}_{CommTh} increases, the harvested energy decreases for both protocols—Beaconing and Probing. Naturally, the higher the threshold is, the less probability that the ETx would be triggered by neighboring ERxs—we refer to Table 6.4 where this relation has been shown clearly. As expected, the Freerun mode has the highest harvested energy in almost every testing point, because all ETxs are switched on all the time.

ETx Energy Consumption

We are now ready to present the fundamental result of this chapter, *proving the "green" aspect of the designed WPTN*. In addition to harvested energy we show total energy used (in kJ) by all ETxs during the whole experiment, refer to Fig. 6.6(b). We clearly see the power saved by the Beaconing and Probing protocol, compared with the Freerun mode (for Probing—by almost five times). Since the Freerun mode switches between ETxs all the time, the energy consumption by an ETx is highest and constant over η^{ETx}_{CommTh}. We discuss the reason behind this gain in detail in subsequent Sections.

ERx Energy Consumption

The power consumption of the Probing protocol is higher than for the Beacon protocol in our measurements. The main reason is that Probing needs an ERx to receive the probing command from the ETx, measure the signal strength and send feedback packets to the charger. The ETxs request an ERx to measure harvested power in every beacon round. Note that the Probing protocol uses three message types to trigger the charging Phase, see Protocol 6.6.2, while the Beaconing protocol uses only one message to trigger charging, see Protocol 6.6.2.

As the η^{ETx}_{CommTh} increases, the power consumption by the ERx using the Probing protocol decreases. The reason is that the larger the η^{ETx}_{CommTh} is, the smaller the probability that an ETx will accept charge request messages from the ERx. Then a larger η^{ETx}_{CommTh} causes fewer number of ETxs to associate with the ERx on probing, which further causes a smaller number of communication messages at the ERx.

WPTN Efficiency

Compared with the Beaconing protocol, the Probing protocol stays on a stable level for each η^{ETx}_{CommTh}. At –70 dBm, the efficiency of the Probing protocol is around three times larger than the Beaconing protocol. At –50 dBm, the efficiency of the Beaconing protocol increases. The main reason is that the η^{ETx}_{CommTh} represents the range that an ETx evaluates whether the ERx can be successfully charged or not. The larger the η^{ETx}_{CommTh} is,

the smaller the threshold range is, and the more energy an ERx can harvest. Therefore, a smaller $\eta^{\text{ETx}}_{\text{CommTh}}$ value results in a higher efficiency. The benefit of using a smaller threshold $\eta^{\text{ETx}}_{\text{CommTh}}$ is that the power transmission efficiency increases. The drawback is that a decreasing range causes a smaller amount of harvested energy, see Fig 6.6(a).

The Freerun mode always has the lowest charging efficiency because it cannot estimate whether an ERx is inside or outside the WPTN and what the possible harvesting power is. If the receiver is outside the WPTN or in the area with very low power radio, switching on the ETxs will waste a lot of power. In the experiment, the disappearing time of an ERx is 15 s. We conjecture that if the disappearing time increases the efficiency of the Freerun mode will be even lower.

WPTN ACCURACY

The Probing protocol has a relatively high and stable accuracy from –70 dBm to –50 dBm. The high accuracy explains the high efficiency in the probing based protocol as shown in Fig 6.6(d). In the Probing protocol, only one ETx is allowed to charge the ERx which potentially decreases the accuracy. We hypothesize that if multiple ETxs could exploit a Probing-like protocol at the same time the accuracy and efficiency could further increase.

The accuracy of the Beaconing protocol increases as the threshold increases from –70 dBm to –50 dBm—the higher the $\eta^{\text{ETx}}_{\text{CommTh}}$ value is, the closer the ERx must be to an ETx in order to trigger the charging. And the closer the ERx is to the charger, the higher the probability that the ETx can charge the ERx. The Freerun mode naturally has the worst charging accuracy—the ERx can hardly harvest sufficient energy at certain positions while the ETxs are continuously switched on.

OVER-CHARGING AND MIS-CHARGING ERROR

As $\eta^{\text{ETx}}_{\text{CommTh}}$ increases, mis-charging and over-charging error of Beaconing increases and decreases, respectively. For Freerun the mis-charging error is zero, however over-charging error reaches almost 80%. In comparison, Probing stays on a stable low level for each $\eta^{\text{ETx}}_{\text{CommTh}}$ and the over-charging error is less than 10%. This means that Probing protocol successfully minimizes the wasted charging power from ETx. The main reason which causes the mis-charging error of Probing being relatively high is that the probing protocol allows only one ETx to be used for charging the ERx.

ERX TIME TO CHARGE

To verify the theoretical analysis of the time to charge in both protocols, we have conducted an experiment, where we have placed an ERx less than 50 cm to each of the ETxs devices (to ensure an ERx is within charging range of all ETxs). To emulate an ERx being in the charging range of a given ERx, we would connect or disconnect the Powercast device from the Arduino microcontroller. For each value of K from $K = 1$ (one ETx connected) to $K = 4$ (four ETxs connected) we have performed an experiment where an ERx appears randomly in the network 50 times. Afterwards, we measured the time it takes from first appearing in the network to being charged. A CDF values of those experiments are presented in Fig. 6.8. In this figure experimental results (solid lines) are compared against theoretical results (dashed lines). For Fig. 6.8(a)–Fig. 6.8(d) additionally a CDF of $T^{\text{B}}_{\text{start}}$ is added.

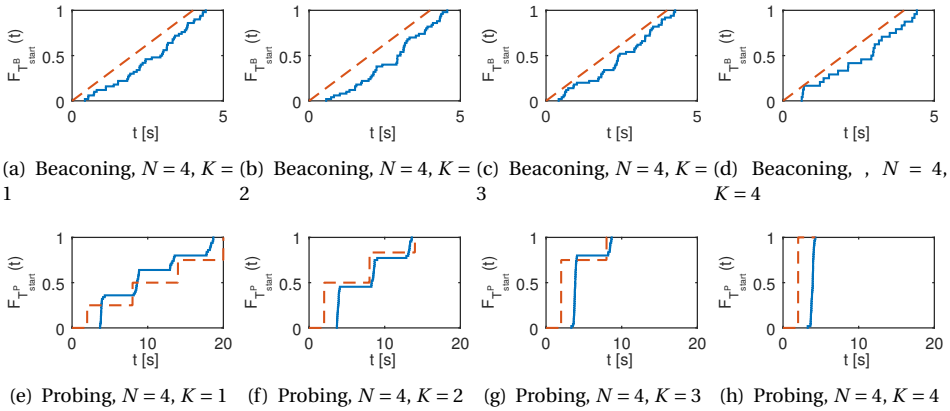

(a) Beaconing, $N = 4$, $K = 1$ (b) Beaconing, $N = 4$, $K = 2$ (c) Beaconing, $N = 4$, $K = 3$ (d) Beaconing, , $N = 4$, $K = 4$

(e) Probing, $N = 4$, $K = 1$ (f) Probing, $N = 4$, $K = 2$ (g) Probing, $N = 4$, $K = 3$ (h) Probing, $N = 4$, $K = 4$

Figure 6.8: WPTN time to charge CDF: P—Probing, B—Beaconing, solid line–experiment, dashed line–analysis.

We see that the Beaconing protocol is faster in reaching the ETx than the Probing protocol, however with increasing K the time to charge for the Probing protocol becomes very low as well (almost instant connection after approximately two Seconds). For the Beaconing protocol, irrespective of the number of ETxs, the time to charge stays constant. This discrepancy between experimental and numerical results is due to the approximation that does of not take the propagation and processing time into account. Nevertheless the analysis follow the trends of the experimental results in all cases reasonably well.

6.7.4. EXPERIMENTAL RESULTS: CASE 2—NON-LINE OF SIGHT SCENARIO

In this experiment, we have tested the performance of the WPTN, in which the ERx is inside the communication range while outside the charging range of an ETx. We change the experiment setup in Fig. 6.5 by turning ETx 1 and ETx 3 by 180 degrees around their axis. Results in this testing scenario and from the previous Section are depicted as *back*, and *normal*. The ETx $\eta^{\text{ETx}}_{\text{CommTh}}$ is set to –70 dBm.

ERX HARVESTED ENERGY

In both normal and back condition, the harvested energy of the Beaconing protocol is larger than the Probing protocol. Using the Beaconing protocol the harvested energy in the back condition decreases by 45% from the normal condition, which fits with the experiment setup by turning two chargers 180 degrees back. The decreasing percent in Probing from normal to back condition is 32%, which is smaller than in the Beaconing protocol. This can be explained because the Probing protocol only selects the ETx that can charge energy over the threshold $\eta^{\text{ETx}}_{\text{CommTh}}$.

ETX ENERGY CONSUMPTION

As expected, the power consumption of ETxs in the Beacon protocol and Freerun mode maintain at the same level in both normal and back conditions. The Beacon protocol does not give the ETxs the function to know whether the charging power is efficiently harvested

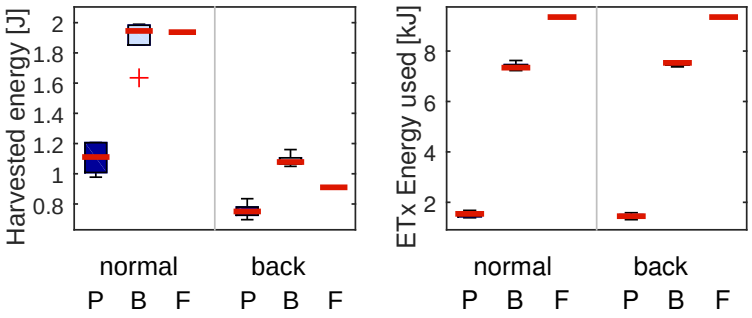

(a) ERx harvested energy

(b) ETx consumed energy

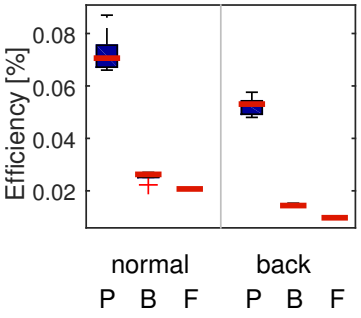

(c) WPTN Efficiency

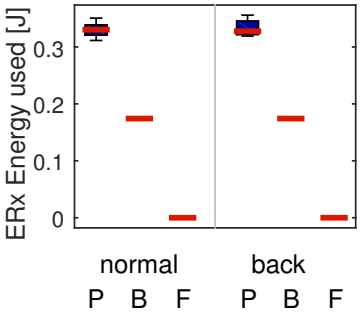

(d) ERx Communication cost

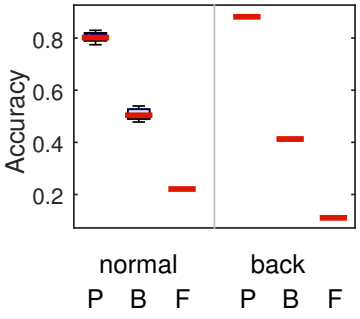

(e) WPTN Accuracy

Figure 6.9: WPTN experiment results: (a); B—Beaconing, P—Probing, F—Freerun; Refer to Section 6.7.4 for more explanation.

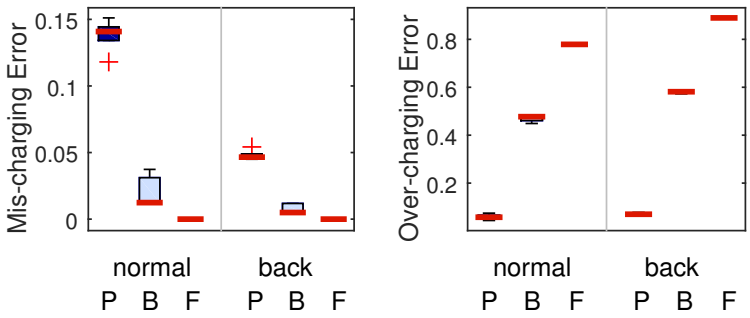

(a) Mis-scharging error (b) Over-charging error

Figure 6.10: WPTN experiment results: (a); B—Beaconing, P—Probing, F—Freerun; Refer to Section 6.7.4 for more explanation.

or not. Therefore, as in the back condition, even if the ERx is outside the charging range, the charger still switches on as it recieves the request message from the ERx. Lots of energy is wasted in the back condition by the Beaconing protocol. In the Probing protocol, the 'back' ETxs (ETx 1 and ETx 3) will switch off, after they evaluate that the potential harvested energy at the ERx is too low.

ERx Energy Consumption

For both protocols, Beaconing and Probing, the scheduling of the communication in the ERx are not influenced by the topology of the WPTN. So the power consumption used by communication in both normal and back conditions are almost the same.

WPTN Efficiency

Using the Beaconing protocol, the efficiency in the back condition decreases by 45% from the normal condition. The decrease in the Probing protocol from normal to back condition is 25%, which is much smaller than for Beaconing. This smaller decrease can be explained because the Probing protocol ensures that the ETxs work only when the charged energy is over a predefined $\eta^{\text{ETx}}_{\text{CommTh}}$. The 25% decrease mainly comes from the probing period when the ETx is turned on and asks the ERx to measure the harvested power. In our hardware implementation the probing period is very short (4 s) and we speculate that increasing the probing period can further increase the efficiency of probing based protocol in the back condition.

WPTN Accuracy

The accuracy trends in the non-line of sight scenario are the same as in the line-of-sight case, see Sec. 6.7.3. Also, as in the previous case the Probing protocol maintains the highest accuracy over the other two considered approaches.

OVER-CHARGING AND MIS-CHARGING ERROR

Compared with the over-charging error in a line-of-sight experiments in Section 6.7.3, the improvement in non-line-of-sight condition from Freerun and Beaconing protocols to Probing protocol becomes larger. Although in the non-line-of-sight the mis-charging error of Probing (≈0.04) is higher than for Beaconing (≈0.01) and Freerun (0), see Fig. 6.10(b), the improvement in over-charging error from Beaconing (≈0.6) and Freerun (≈0.9) to Probing (≈0.1), see Fig. 6.10(b), is much larger.

6.8. DISCUSSION: LIMITATIONS AND FURTHER RESEARCH DIRECTIONS

With these results we do believe we open up a new research direction within WPTN and we are aware of many points of improvement. We list the most important ones here.

1. Considering the Beaconing protocol, the charge request rate should be optimized with respect to power consumption and harvested energy of the ERx. For example, the beacon period can adapt to the number of ERxs in the WPTN. Since as long as one ERx calls the charger to switch on there is no need to trigger an ETXs for every ERx.

2. Considering the Probing protocol, the probing frequency should be optimized with respect to power consumption of probing as well. The ERxs should optimize the probing scheduling considering both static and dynamic conditions. For example, when the ERx is static, there is no need to make the receiver measure harvested power with a high frequency, since the harvested power is not expected to fluctuate much in this case.

3. The WPTN should optimize the combinations of the subset of switched on the ETxs in order to take advantage of the constructive signal combined at the ERx. Measuring all possible combinations of the subset of the neighboring ETxs to switch on consumes too much time and power at the ERx. Thus a novel charge control algorithm is required to enable green WPTN with multiple ETxs operating at the same time.

6.9. CONCLUSIONS

In this chapter we have introduced a new class of charging control protocols for wireless power transfer networks (WPTNs)—denoted as 'green'—that conserve energy of the chargers. The purpose of these protocols is to maximize three metrics of interest to WPTNs (that we introduced here for the first time): (i) ETx charge accuracy, (ii) ETx charge efficiency and (iii) ERx harvested power, which in-turn minimize unnecessary uptime of WPTN energy transmitters. We prove that this problem is NP-hard.

To solve it we propose two heuristics, denoted as 'beaconing' (where energy receivers simply request power from transmitters) and 'probing' (based on the principle of charge feedback from the energy receivers to the energy transmitters). The strength of our protocols lies in making few assumptions about the WPTN environment.

We conclude that each protocol performs its task best in two special cases. Experimentally we show that for large distances between chargers and receivers, probing is more efficient and accurate but harvests less energy than beaconing and has a higher communication cost. As the charger to receiver distance increases, the efficiency of the beaconing-based protocol increases (since the communication range is positively correlated with the charging range).

7

WiPLoc: Perpetual Indoor Localization with RF Wireless Power Transfer

This chapter [1] uses RF-based wireless power to support the energy requirement of localization networks. Together with Chapter 5 and Chapter 6, we design and implement mobile systems using wireless power transfer to research energy autonomy properties.

7.1. Introduction

Indoor localization is a topic that has been investigated for more than a decade [58, 124]. Yet, no single system exists that is widely adopted as the de facto localization standard. From a research perspective the goal is to obtain a solution that is general, simple and accurate [124]. But as the number of devices in the Internet of Things grow, a new set of challenges are appearing: (i) maintainability, (ii) low operational costs, and more importantly, (iii) energy autonomy.

7.1.1. Motivation: Indoor Localization with Wireless Power

In large-scale indoor localization scenarios [104] the cost of replacing the batteries of thousands of anchor nodes (devices sending location information) and mobile nodes (devices to be localized) is high.

Example: Amsterdam Schiphol Airport has roughy 10 000 Bluetooth Low Energy (BLE) beacons deployed to provide navigation services. In order to maintain the operation of all BLE beacons, battery status monitoring mechanism of the localization beacons must be implemented. These include measuring beacon signal strength by crossing the entire airport area [35] or beacon signal strength crowdsourcing.

[1] This chapter is based on the paper:
Qingzhi Liu, Wieger IJntema, Anass Drif, Przemysław Pawełczak, Marco Zuniga. *WiPLoc: Perpetual Indoor Localization with RF Wireless Power Transfer.*

The research community has recognized this autonomous energy challenge and therefore the area of Wireless Power Transfer (WPT) starts to gain momentum [220, 221]. In WPT systems a *charger* radiates energy in the form of electromagnetic or mechanical waves to *receivers* that harvest this energy. It would be thus valuable to combine the emerging area of WPT with the established area of indoor localization to propose a novel positioning system.

Challenges of RFID localization: The idea of battery-less localization is not new. Radio Frequency Identification (RFID) has been extensively researched for this purpose. Unfortunately, RFID-based localization has some inherent limitations. First, most RFID localization approaches, e.g. [173], require pre-deployed anchor tags, where portable RFID readers estimate their position by detecting nearby backscatter signals from tags. Although the RFID tags are batteryless, the mobile reader requires a lot of energy during tag scanning [114, Table I], and due to the fast attenuation of backscatter signals, the density of RFID tags must be high. Second, RFID technology is also used in tracking systems [225], where mobile nodes carry a passive tag and static readers are used to track their location. In principle, this system is similar to ours, with WPT chargers playing the role of RFID readers. But WiPLoc has the added advantage of having both the monitoring system and the tag itself being aware of the location. With RFID tracking, only the system knows the location of the tags, but the tags themselves are not aware of their own location.

7.1.2. WIRELESS POWERED INDOOR LOCALIZATION: RESEARCH CHALLENGE

Localization and WPT are well researched topics on their own, but using WPT for localization entails a substantial challenge. The problem is that WPT provides amounts of power that are too small for the operation of most radio-based localization systems. For example, experimenting with TX91501 power transmitter [166], due to the exponential decay of signal strength, the harvested power is 0.79 mW at 3 m. However, highly energy-efficient radios, such as BLE nodes, consume around 25 mW in receiving mode. This small amount of power is insufficient for not only receiving packets from many anchor nodes but also to synchronize the operation of the localization system.

Research Question: Based on the observation above we define the research problem as: *given the limited harvested energy from WPT, how should a system manage the indoor localization process to achieve continuous and perpetual localization?*

7.1.3. OUR CONTRIBUTIONS

Considering the research question described above we propose a unified set of solutions for wirelessly powered indoor localization. Namely:

Contribution 1: To minimize the radio transmission and receiving time of localization and meet the limited harvested energy supply, we propose a novel localization method where all anchors transmit localization messages *simultaneously* and the induced collisions are resolved via orthogonal codes. The key advantage of this approach is that the radios of all nodes, including anchor nodes and nodes requiring localization, are active only for the duration of a single message transmission.

Contribution 2: We implement and evaluate an operational system using off-the-shelf BLE motes [153] and WPT chargers and harvesters [166]. Based on systematic experiments in an office environment, we demonstrate that WiPLoc can achieve perpetual indoor

localization with room-level ($\approx$16 m^2) and cell-level ($\approx$ 4 m^2) accuracies of approximately 90% and 70%, respectively. To the best of our knowledge, WiPLoc is the first system that successfully achieves room-level localization using the energy of RF based WPT.

The rest of the chapter is organized as follows. The related work is discussed in Section 7.2. Our basic battery-less localization method achieving room-level accuracy, denoted as WiPLoc, is presented in Section 7.3, while its experimental evaluation is presented in Section 7.4. Approaches to further save power and increase localization accuracy, denoted as WiPLoc++, are presented in Section 7.5, with its detailed evaluation presented in Section 7.6. Finally, we present our conclusions in Section 7.7.

7.2. RELATED WORK

7.2.1. LOCALIZATION WITH WIRELESS POWER TRANSFER

The field of (indoor) localization has been researched for years [58, 124]. Interestingly engough to the best of our knowledge, we are not aware of any localization technique that uses WPT except for TOC [177]. TOC obtains location information based on the time of charge provided by mobile chargers to the static nodes being localized. Unfortunately TOC requires frequent position changes of mobile charger to obtain reasonable location accuracy and has been tested in outdoors only. TOC belongs to a static receiver/mobile charger WPT network type. Following the categorization of [114, Sec. III-A], none of three remaining categories have been applied for localization (either indoor or outdoor). Specifically, localization infrastructure where static charger (not obstructing the area of localization) and mobile receiver being localized, which is the most desired.

7.2.2. LOCALIZATION WITH RFID

Localization based on RFID technology is developing rapidly in recent years. These approaches can be classified into three categories [152, Sec.III]. In the first category, RFID reader-based localization system, e.g. [173, 231], allocates RFID reader in the object requiring localization to detect the pre-deployed anchor tags nearby. Although the deployment and maintenance cost of RFID tags are low, the localization lifetime depends on the limited battery of mobile readers. In the second category, RFID tag-based localization system, e.g. [151, 225], tracks the location of object attached with RFID tag by pre-deployed readers. The advantage of this approach is that the lifetime of tags is unlimited. However, the localization range is limited by the density of readers. Also, the tags cannot be localized once they are outside the range of readers. In the last category, RFID device-free localization system, e.g. [118], detects the position of target wearing no additional localization devices. The idea is to find the target location by detecting and comparing the change of RFID signal in the environment. Tag-based and device-free localization are both passive localization/tracking, which do not fall into the research area of this chapter.

7.3. WIPLOC: WIRELESSLY-POWERED LOCALIZATION

We propose a new indoor localization method for a freely moving device that trades-off accuracy for power consumption. The goal is to reduce the energy consumption of the localization system to a level allowing to power the localization infrastructure wirelessly

over large distances.

Selection of WPT technology. While many WPT techniques exist [221, Table 1] we chose the one based on Radio Frequency (RF) for two reasons. First, RF signals can serve the dual purpose of providing localization and energy. This simplifies the design, operation and cost of anchors and tags compared to systems using different signals for localization and energy transfer, such as sound or magnetic resonance. Secondly, it is the most promising WPT technology as it allows for long-range power transfer even with small receiver antennas, which is challenging with other WPT technologies such as induction-based WPT.

How WiPLoc enables WPT-based localization. The main idea behind WiPLoc's low power consumption is to exploit synchronous packet transmissions to reduce the radio activity time and, in-turn, collision resolution through improved packet capture. In the subsequent sections we will introduce two main WiPLoc processes: (i) localization (Section 7.3.1) and (ii) wireless energy supply (Section 7.3.2), in detail.

7.3.1. WIPLOC: LOCALIZATION PROTOCOL

To get a clear understanding of how WiPLoc localization works we introduce all localization building blocks in detail.

DEPLOYMENT AREA

The system is designed for indoor use. WiPLoc's aim is to find a location of the moving object within strictly defined localization areas, i.e. rooms of an office environment.

COMPONENTS

The WiPLoc system consist of two building blocks: (i) Anchor Nodes and (ii) Mobile Nodes that want to be localized.

- **Anchor Node:** This node is deployed as static in a room and placed at specific locations that maximize signal reception by the Mobile Node in that room. The Anchor Node is pre-programmed with a unique ID that correlates with that specific room. The Anchor Node is constantly powered via a cable and is always in a receiving mode. For deployment simplicity each room has only one Anchor Node.
- **Mobile Node:** This node can move between rooms and is powered by some form of wireless energy. The Mobile Node is constantly in sleeping mode and only wakes up after a pre-defined time after which it goes back to sleep. It has a pre-defined table with all anchor IDs to correlate the Anchors Nodes with a location (room).

LOCALISATION ALGORITHM

The network is consisting of Anchor Nodes and Mobile Nodes, where the Mobile Nodes are localized by receiving the ID of the strongest anchor. WiPLoc localization belongs therefore to the proximity-based methods of indoor localization systems [111, Sec. II-C].

Localization methods that use packet radio are usually asynchronous to avoid collisions among packets sent by other anchors. In WiPLoc however, all anchors send their packets at the same time, enforcing packet collisions. The mobile node leverages the capture effect [3, Sec. II-A] to decode the strongest signal and assigns its location to that

anchor. The key advantage of this method is its energy efficiency: Anchors and Mobile Nodes in the WiPLoc network only need to be active for a single packet transmission and reception time slot. A separate discussion is needed on packet synchronization, collision resolution and error correction.

Packet Synchronisation The packets from the anchors need to arrive at the Mobile Node at the same time. For example, in our protocol each packet consists of a preamble of one byte, a payload and a CRC of the whole packet. To leverage the capture effect the packets should arrive within each other's preamble at the Mobile Node. To achieve this synchronization the Mobile Node broadcasts a `location-request` packet. This is a synchronization packet that instructs all receiving anchors to immediately respond with their ID encoded in a payload. Leveraging the capture effect alone however has limitations [196, Sec. IV]. For the capture effect to work the strongest signal needs a certain minimum SINR. If this requirement is not satisfied, packets will collide and the anchor ID will not be retrieved.

Orthogonal Spreading Codes To overcome this limitation the Anchor Node ID is encoded with an orthogonal code to increase inter-packet distinction. Each bit of the Anchor Node ID is multiplied by an orthogonal code unique for each anchor. The encoded Anchor Node ID is then send in the payload of a packet. The decoding process at each mobile node is an XOR operation between the payload of received packet with a list of orthogonal codes. In this chapter a Hadamard matrix of size k is used to generate the codes[2], i.e.,

$$H_{2k} = \begin{bmatrix} H_{2^{k-1}} & H_{2^{k-1}} \\ H_{2^{k-1}} & -H_{2^{k-1}} \end{bmatrix} = H_2 \otimes H_{2^{k-1}}, \tag{7.1}$$

where $H_2 = \begin{bmatrix} 1 & 1 \\ 1 & -1 \end{bmatrix}$, $2 \leq k \in \mathbb{N}$ and $\otimes$ is the Kronecker product.

FEC layer Although orthogonal codes have a build-in tolerance for bit errors they are unable to decode them all. For this reason the Anchor Node ID is first encoded with a Forward Error Correcting (FEC) code, before it is multiplied by the orthogonal codes. The FEC layer is constructed of maximum minimum Hamming distance codes [125] i.e. codes having equal Hamming distance to each other. The decoding of the FEC layer uses minimum distance decoding.

Illustration—Eliminating Localization Dead Zone

To verify that the orthogonal codes are working correctly the following experiment was performed.

Experiment Hardware For convenience we select the nRF51822 SoC with a ARM Cortex M0 from Nordic Semiconductor with BLE support [153] as hardware platform to test the localization protocol. For WiPLoc however, we do not use the BLE protocol stack but use

[2] Any other method can be used as long as the codes all have zero cross-correlation with each other.

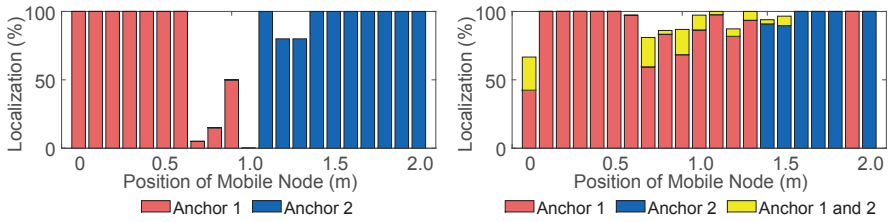

(a) Without orthogonal codes (b) With orthogonal codes

Figure 7.1: Localization accuracy experiment with two anchors placed two meters apart. We demonstrate the elimination of the packet reception *dead zone* with orthogonal codes, see Section 7.3.1 for details of the experiment setup.

the radio peripheral of the nRF51822 and introduce our own packet and communication protocol instead. We refer to [75] for the source code of the implementation.

- **Anchor Node:** The Smart Beacon Kit form Nordic Semiconductor [153] is used. This module has a coin size form factor with a PCB integrated antenna.
- **Mobile Node:** The Nordic Semicoductor PCA10005 [153] is used. It has an SMA connector with a connected quarter-wave helical monopole antenna of 1.6 dBi gain[3].

Experiment Setup Two anchors are placed two meters apart and the mobile node is placed at 20 points in a straight line between the anchors with each measurement point separated 10 cm from each other. The transmission power of the Anchor Nodes are set to 0 dBm. The mobile node stays at each point for around 30 s and sends localization request every second. First the localization experiment was performed without orthogonal codes. After that the same experiment was performed with orthogonal codes.

Experiment Results In Fig. 7.1(a) we observe that in-between anchors, we obtain a *dead zone*, i.e. area of no reception because in this region the SINR is insufficient to receive a correct packet and the packets collides which causes the packets to deform. Fig. 7.1(b) demonstrates that the dead zone is eliminated with orthogonal codes. Furthermore, we observe that multiple anchor IDs can be decoded from one packet. We call this phenomenon *multi-packet reception*. The reason for the larger coverage of Anchor 1 in Fig. 7.1(b) is due to use of antenna with a different coverage pattern in that experiment.

7.3.2. WIPLOC: WIRELESS ENERGY SUPPLY

Having low power features of WiPLoc implemented, we are ready to extend WiPLoc with wireless power localization features. As in Section 7.3.1 we describe all localization blocks with WPT enabled.

[3] In the rest of the chapter we will refer to both devices as nRF51822.

Algorithm 6 Location protocol at the Anchor and Mobile Node

Anchor Node:

```
1: loop
2:     if location-request packet is received then
3:         Send location-reply packet back
```

Mobile Node:

```
1: loop
2:     Sleep
3:     if timer ≥ t_m then                          ▷ See Section 7.3.2
4:         Broadcast location-request
5:         if location-reply packet received then
6:             Decode and calculate location
```

Components

The WiPLoc components described in Section 7.3.1 are in this section extended with WPT functionality.

- **Anchor Node:** As the anchor nodes are located at static and central in a room we combine them with a power transmitter. This transmitter should provide full coverage for one room.
- **Mobile node:** This node is combined with a power harvester that harvests RF power form the RF power transmitter. Note that the WPT channel is different than the communication channel.

Software Implementation

The localization algorithm is the same as in Section 7.3.1 however to enable it with WPT the following steps have been taken. To keep the power consumption at a minimum all the peripherals of the Mobile Node are turned off except for one hardware timer which is set to generate an interrupt[4] at each period t_m. The CPU of the nRF51822 is most of the time in *Wait For Interrupt (WFI)* state, which we denote as the *sleep state*. When the interrupt is executed the nRF51822 is woken up and begins a localization round. The localization round starts broadcasting a `location-request`. Next, the radio directly switches to receiving mode. If a valid location packet is received (meaning the CRC is correct) decoding the anchor ID is trivial. On the other hand, if the received packet is corrupted the orthogonal codes inside ensure that the anchor ID can still be decoded from the packets. After this the Mobile Node goes back to sleep. The complete program flow is depicted in Algorithm 6.

There are two types of packets sent by the WiPLoc protocol. Both types have a fixed payload length of 30 bytes. Next section will elaborate on how the payload of the packets is constructed for each type.

Location Request Packet The `location-request` packet contains in the first two bytes of the payload the group ID of anchors. The group ID of all anchors is the arbitrary integer j. The anchors are then programmed to accept all packets that contain this integer j in the first two bytes. The packet send back by the Anchor to the Mobile Node is a `location-reply` packet.

[4] We again refer to [75] for the source code of the implementation.

Location Reply Packet The `location-reply` packet contains in the payload the anchor ID encoded by the FEC layer which is then encoded by the orthogonal codes and this is stored in the payload of the packet.

Location Reply Encoding Process All the Anchor Nodes have an array $\mathbf{C}$, $|\mathbf{C}| = N$ with FEC codes having an equal Hamming distance d to each other. The anchor ID is then FEC encoded by replacing the anchor ID with a n-th FEC code from the array. The orthogonal codes are generated using the method described in Section 7.3.1. For the generated matrix each -1 symbol is replaced with a 0 and each row of the matrix represents a binary spreading code. Finally, every bit of the FEC code is represented by the n-th orthogonal code from the array. If the bit is zero, the bitwise NOT of the orthogonal code is used[5].

Location Reply Decoding Process As stated in Section 7.3.1 also the Mobile Node has an array of all orthogonal and FEC codes used by the anchors. For every entry in the orthogonal code array the Mobile Node tries to decode the packet. When a candidate anchor ID is found, the decoded code is compared to the correlating FEC code of the candidate ID. When the Hamming distance d_c of the candidate FEC code compared to a code from the FEC array follows $d_c < \frac{d}{2}$ we assume that the candidate ID is the correct one. The decoding stops when the last orthogonal code in the array is used to decode a packet. The source code accompanying this chapter is available at [75].

HARDWARE IMPLEMENTATION

The WiPLoc localization components are connected as follows, see Fig. 7.2:

- **Anchor Node:** This node is combined with the Powercast TX91501 Powercaster transmitter [166]. It has an Effective Isotropic Radiated Power (EIRP) of 3 W and operates at a RF center frequency of 915 MHz. There is no signal connecting the powercaster to the nRF51882. The Powercaster is always active and is always sending RF energy into the environment. In the rest of the chapter we will refer to this component as *powercaster*.
- **Mobile Node:** The Powercast P2110B power harverster [166] is used as power supply for the nRF51822. It is a development PCB with a SMA connector for connecting an antenna for harvesting power. Two antennas can be selected: (i) a vertical polarized omni-directional dipole antenna with 1.0 dBi gain and (ii) a vertical polarized patch antenna with a 6.1 dBi gain. We will refer to this component as the *harvester*.

7.4. WIPLOC: EXPERIMENT RESULTS

From [32] we know that the lower bound for harvested energy from a distance of four meters from the powercaster is –8 dBm. In order to operate within the powercaster range in our setup the average power consumption of the Mobile Node should be below 0.16 mW. More sensitive receiver [7] can further increase the operation range of the receiver.

[5] The size of the orthogonal codes is 16 bits and this results in a total message length of 30 bytes that fits in the payload of the radio packet.

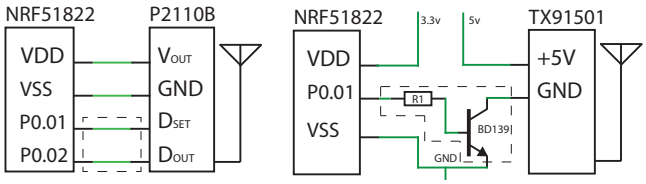

(a) Mobile Node implementation (b) Anchor Node implementation

Figure 7.2: Implementation of WiPLoc components: (a) Mobile Node: Nordic Semiconductors nRF51822 SoC [153] connected to Powercast energy harvester P2110B [166]; and (b) Anchor Node: nRF51822 connected to Powercast power transmitter [166]. Note that in case of nRF51822 only the relevant pin connections are shown as other pins are left as not connected. The connections inside the dotted line are only applicable for WiPLoc++, refer to Section 7.5. The value for $R_1 = 330\,\Omega$.

Table 7.1: Consumed power in each fundamental state of the WiPLoc localizarion protocol

State	Power (mW)		Time (ms)		Energy (μJ)	
Transmitting	35.88	35.88	0.80	0.80	28.7	28.7
Receiving	20.17	26.05	0.60	8.29	12.1	216.1
ADC	—	1.69	—	0.65	—	1.10
WFI	0.15	0.14	998.60	925.9	149.8	138.9
Average	0.19	0.49	1000.0	1000.0	190.6	493.4

Note: The left column denotes the power consumption of the Mobile Node, the right column denotes the WPA (See Section 7.5).

To verify the energy efficiency of the WiPLoc components the nRF51822 is measured with a Power Monitor [139]. The nRF51822 has three power states: *sleep* (WFI), *transmitting* (TX) and *receiving* (RX). The localization period $t_m = 1.0$ s and the transmit power is set to 4 dBm. A localization round starts with a TX followed by RX and WFI. We measured the energy consumption of each state separately, repeated each measurement ten times and averaged them. Table 7.1 presents the power consumption measurements. The measurements show that the average power consumption is 0.20 mW which is very close to the requirement of 0.16 mW. We are thus ready to implement WiPLoc.

7.4.1. Experiment Setup

Each location is divided in four of two by two meters cells. At the center of the cell is an test location for the mobile node. Each room has four test locations. Every device is placed 1.0 m above the floor and they are all in line of sight from each other.

For every experiment that is done the following yields. The mobile node is placed at every testing location in room one and two and the corridor. On every test location the mobile node initiates 50 localization rounds. The localization period is set to 1.0 s and the transmit power of the Anchor and Mobile Node is set at the maximum of 4 dBm.

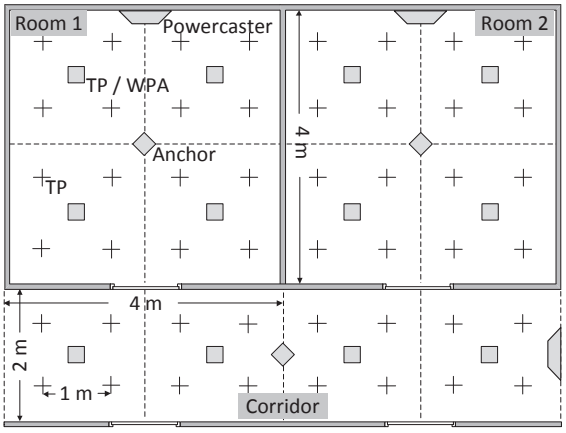

(a) Top view of WiPLoc deployment in the office environment

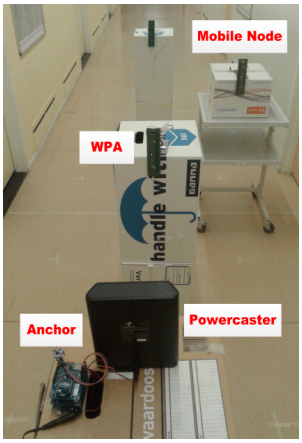

(b) A picture of corridor WiPLoc experiment setup

Figure 7.3: Experiment setup: **TP/WPA**: The places marked as "□" are used as the testing positions (TP) of Mobile Node in the room-level localization experiment of Section 7.4 and the deployment positions of WPA and in the cell-level localization experiment of Section 7.5, respectively. **TP**: places marked as "+" are the testing positions (TP) of Mobile Node in the cell-level localization experiment of Section 7.5.

EXPERIMENT SCENARIOS

The following three experiments were performed.

Experiment 1: One Anchor Node is placed in the center of one room and the Mobile Node is placed at every testing location in room one and two and the corridor. As there is only one Anchor Node in the area we consider all packets decoded with this anchor ID correctly localized.

Experiment 2: Two Anchor Nodes are deployed, each in the center of room one and two. Two Voronoi cells around the Anchor Nodes are defined and if the Anchor Node is localized in the Voronoi cell that corresponds to the Anchor ID that is decoded we consider it as correctly localized.

Experiment 3: Three Anchor Nodes are deployed, each in the center of room one, two and the corridor. The Mobile Node is correct if the localization result is in the correct room. We make use of the fact that the walls attenuate the RF signals from the nRF51822 and that the signal range will adjust to the room layout accordingly.

DATA ACQUISITION

As the Mobile Node is powered wirelessly interfacing with the nRF51822 would consume power which we then can not be used for localization. We overcome this problem by using a BLE USB dongle as a sniffer [153]. This sniffer monitors all packets sent by the Mobile Node. In our experiment the result of every localization round is send in the next localization round within the `location-request` packet. The sniffer then receives the data and saves it on to a text file on the PC for further data processing.

7.4.2. Experiment Results

For the evaluation of WiPLoc we introduce two metrics: *accuracy* and *Packet Reception Rate (PRR)*. We define accuracy as follows. When the Mobile Node is localized in the room where it is currently located we count the localization as successful. When the Mobile Lode is localized to another room then where it is currently located it is counted as unsuccessful. PRR is defined as the number of `location-request` packets send by the mobile node divided by the number of received `location-reply` packets.

At every test location 50 localization rounds were performed. For each test location PRR and the accuracy is computed and averaged. The results are shown in Table 7.2 where the accuracy is normalized to the PRR. We observe that if the number of anchors deployed increases the PRR decreases. The accuracy also decreases when the number of anchors increases. The PRR decreasing is mostly due the fact of packet collisions. Nevertheless, even in the worst case (Experiment 3) we demonstrate that we achieve (i) extremely low power consumption for localization using collision packets, and (ii) accurate room-level localization for Mobile Node using only WPT energy.

Table 7.2: WiPLoc localization experiment result

	PRR (%)	Accuracy (%)
Experiment 1	100	100
Experiment 2	99.3	95.5
Experiment 3	89.6	84.6

7.5. WiPLoc++: Extending WiPLoc to Cell-Level Localization Accuracy

So far we have demonstrated how WiPLoc allows us to accurately localize items per room. The question is how to improve localization accuracy from room-level to cell-level.

7.5.1. WiPLoc: Challenge of Cell-level Localization

WiPLoc is designed to cope with localization at a room-level ($\approx 16\,m^2$) accuracy but does not allow to improve the accuracy further down. We shall describe specific problems of WiPLoc related to this functionality and propose our improvements, which we collectively shall denote as WiPLoc++.

Problem 1—Limited Energy for Synchronization

Referring again to Table 7.1, we see the the power consumption of packet reception ($\approx$26 mW) is above the limit of harvested power ($\approx$0.8 mW at 3 m). Synchronization is needed when operating with multiple Anchor Nodes this requires idle listening continuously, However this is not possible if Anchor Nodes are required to operate under the harvested RF energy.

Solution to Problem 1: We propose a semi-passive wakeup scheme to allow Anchor Nodes listening to the synchronization signal only when there is a localization request. This solution will be described in Section 7.5.2.

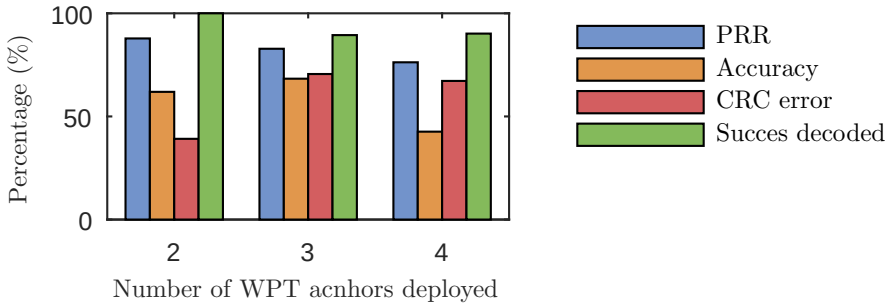

Figure 7.4: Cell-level localization as a function of number of Anchor Nodes deployed. The radio interference from multiple Anchor Nodes causes the increase of CRC error and the decrease of success decode rate.

PROBLEM 2—SCALABILITY OF WIPLOC

Normally, with more Anchor Nodes we obtain higher localization accuracy. To prove this assumption, we deploy 2, 3 and 4 Anchor Nodes, respectively, in room one and test the PRR and accuracy respectively. The deployment setup and localization testing positions are illustrated in Fig. 7.3(a) while the test results are shown in Fig. 7.4. The key observation is that the PRR and accuracy of cell-level localization decrease as the number of Anchor Nodes increase. This is mainly caused by the radio interference to the orthogonal code from multiple Anchor Nodes. It means that interference caused by multiple Anchor Nodes will limit the accuracy and scalability of WiPLoc in dense Anchor Nodes deployments.

Solution to Problem 2: We propose to restrict the number of Anchor Nodes used for cell-level localization by using WPT Receive Signal Strength (RSS) based distance estimation, which will be presented in Section 7.5.3.

7.5.2. ID BASED SEMI-PASSIVE WAKEUP

The collision based localization introduced in Section 7.3 requests the synchronization of packet transmission and reception among multiple nodes. The Anchor Node, also responsible for charging, has a fixed power supply, *ergo* enough energy to listen to the localization request and synchronization signal continuously. If we want to increase the number of Anchor Nodes without a fixed power supply, they also need to be be powered by wireless power.

EXTRA LOCALIZATION COMPONENT

Following from the above observation we introduce a new node aiding in localization.

- **Wirelessly-Powered Anchor Node (WPA):** This node is the same as Anchor Node, however it operates purely based on harvested RF energy from the Anchor Node.

Energy harvested from Anchor Node is not enough for WPAs to listen to the synchronization signal continuously. Therefore, we propose ID based semi-passive wakeup approach to wakeup WPAs from sleeping mode only when the localization request is sent from Mobile Nodes. The method works as follows.

Wakeup Process

As in WiPLoc, Anchor Nodes are deployed one per room and constantly switched on for wireless charging. Using the harvesting energy from neighbor Anchor Nodes, WPAs periodically wakeup from sleep mode and perform the measurement of the voltage of the harvested power with Analog to Digital Converter (ADC) port. Based on our measurements (see again Table 7.1), the power consumption of ADC measurement (≈ 1.5 mW) is of the same magnitude as the harvested power (from ≈ 3.2 mW at 1 m to ≈ 0.79 mW at 3 m). Although the power consumption of ADC measurement is larger than harvested power at the distance of 3 m. We only conduct one ADC measurement every period t_c and are in sleeping mode the rest of time. This ensures that the average power consumption low enough.

Now, suppose that the Mobile Node has initiated the room-level localization. Then Mobile Node broadcasts a `localization request` to the Anchor Nodes. The Anchor Node will send a `location reply` back and will send a passive wake up signal to all WPAs in the same room: switch off (the powercaster) charging for a short time and then switch back on again. Then the Anchor Node sends `sleep` commands to the WPAs that are required to stay a sleep for the cell-level localization.

At the WPA, Once a voltage falling of the harvested power is measured on D_{out}, the WPA wakes up from sleeping mode and starts listening to radio packets. If the WPA does receive a `sleep` it keeps listening for a `location-request` from the Mobile Node.

Meanwhile, the Mobile Node received the `location-reply` from the Anchor Node and then waits for t_c to broadcast the `location-request` to the WPAs. Then Mobile Node is localized based on the collision based localization approach as explained in Section 7.3. The whole process is described in Algorithm 7.

It is worth noting that the wake up time of each WPA and Mobile Node have small differences. The main reason for that is the time for measuring the semi-passive wake up signal at each WPA is not synchronized. To guarantee that all WPAs can hear the localization synchronization signal from Mobile Node, all WPAs wakeup immediately after receiving the semi-passive wakeup signal and listen a maximal period of t_c and sleep again if they receive nothing in that time frame.

Optimization

Although the power consumption of ADC is much lower than receiving according to the measurement results in Table 7.1, for efficiently using the limited WPT energy we optimize the ADC period t_c to further decrease the total power consumption of WPA. Assume that $i \in \mathbf{N}, |\mathbf{N}| = n$ WPAs are deployed around the semi-passive wakeup range of Anchor Node. The time that the semi-passive wakeup signal is detected by the ADC measurement at WPA i is denoted as t_a^i. After sending `passive-wakeup-request` to Anchor Node, the Mobile Node sleeps for t_c and then sends `localization-request`. Then each WPAs are waken up and listen for $t_{\text{rx}}^i = t_c - t_a^i$. To simplify the analysis we assume that t_a^i are independent and uniformly distributed in t_c with CDF $F(t_a^i) = \frac{t_a^i}{t_c}, t_a^i \in [0, t_c)$.

Proposition 5. *The value of t_c producing minimum expected power consumption at WPA, P_a, is*

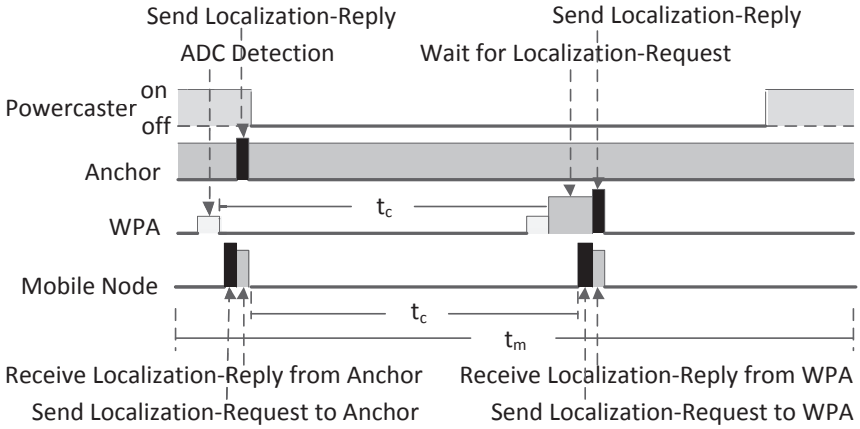

Figure 7.5: Semi-passive wakeup process during localization period t_m.

$$\arg\min_{t_c}[\mathrm{E}(P_a)] \approx \sqrt{\frac{2t_m t_{adc}(p_{adc}-p_{wfi})}{p_{rx}-p_{wfi}}}. \tag{7.2}$$

Proof. The average power consumption of a WPA during a localization period t_m is

$$P_{\mathrm{a}} = \frac{P_{\mathrm{rx}}t_{\mathrm{rx}} + P_{\mathrm{tx}}t_{\mathrm{tx}} + k_{\mathrm{adc}}P_{\mathrm{adc}}t_{\mathrm{adc}} + P_{\mathrm{wfi}}t_{\mathrm{wfi}}}{t_m}, \tag{7.3}$$

where the expected time of waiting for interruption during t_m is $t_{\mathrm{wfi}} = t_m - (k_{\mathrm{adc}}t_{\mathrm{adc}} + t_{\mathrm{rx}} + t_{\mathrm{tx}})$, where $k_{\mathrm{adc}} = \left\lfloor \frac{t_m}{t_c} \right\rfloor$ denotes the the number of ADC measurement during t_m and t_{adc}, t_{rx} and t_{tx} denote time spent in ADC measurement, packet reception and transmission, respectively. To calculate t_{rx} recall that the expectation of t_a^i is $\mathrm{E}(t_a^i) = \frac{t_c}{2}$. Then the expected waiting time is $t_{\mathrm{rx}} = t_c - \mathrm{E}(t_a^i) = \frac{t_c}{2}$.

As k_{adc} is discreet we replace it with a continuous value $k_{\mathrm{adc}}^c = \frac{t_m}{t_c}$ for estimating the range of the minimum value $\mathrm{E}(P_a)$. The value of t_c that minimizes the expectation of P_a can be calculated as $\arg\min_{t_c}[\mathrm{E}(P_a)] = \{t_c \,|\, \frac{\partial P_a}{\partial t_c} = 0,\ k_{\mathrm{adc}} = k_{\mathrm{adc}}^{\mathrm{c}}\}$ which results in (7.2). □

7.5.3. RANGE ESTIMATION USING RSS OF WPT SIGNAL

The purpose of this component is to narrow down the possible location of the Mobile Node, and restrict the number of WPAs used for collision-based localization. We shall now justify the selection of the range estimation process.

REASON FOR RANGE ESTIMATION USING WPT RRS

We select range estimation using WPT RSS for two reasons: (i) the charging radio of WPT covers the localization area already, which does not require any additional communication component; (ii) Fig. 7.6 illustrates the voltage measurement results using ADC (at D_{out} pin) for various distances. The figure also illustrates that the harvested power RSS is in much more stable then the RSS of the nRF51822 at the same distance. We take advantage

the attenuation of voltage over distances to estimate whether the Mobile Node is inside or outside a requested range.

Range Estimation Process

The RSS-based range estimation works as follows. Following the same deployment model as in Section 7.5.2, we define the cell of WPA i as Γ_i, and the voltage measurement results using ADC of a Mobile Node and WPAs as ξ and μ_i, respectively. The threshold RSS value, θ, is used to classify the cells of WPAs. The cells of WPAs are then categorized as (i) $\Delta_c = \{\Gamma_i \mid \mu_i \geq \theta\}$, (ii) $\Delta_f = \{\Gamma_i \mid \mu_i < \theta\}$, and (iii) $\overline{\Delta} = \{\Delta_f \mid \xi \geq \theta\}$ or $\{\Delta_c \mid \xi < \theta\}$.

The Mobile Node broadcasts a `localization-request` with ξ. If an Anchor Node receives a `localization-request` it will compare ξ with the threshold value θ. If $\xi \leq \theta$, then the Anchor Node sends a semi-passive wakeup signal to WPAs in Δ_f; otherwise, it wakes up WPAs in Δ_c for localization.

If the Mobile Node does receive a `localization-reply` from the WPAs, it will then request the Anchor Node to wake up the WPAs in other area for cell-level localization. The detailed process is presented in Algorithm 7.

Discussion

We need to point to certain limitations of the WiPLoc++ localization.

1. The value θ can calculated by $(\sum_{i=1}^{n} \mu_i) n^{-1}$. To simplify the implementation we use the pre-measured RSS $\theta = 3.7$ dBm at the geographic middle position of the deployment area of WPAs around the Anchor Node. Such approach however might not be always practical.

2. Values of ξ and μ can be affected by obstacles between powercaster and WPA / Mobile Node, relative direction of antennas between charger and harvester, etc. Therefore WPT RSS-based range estimation can only be used for estimating the Mobile Node location with a coarse resolution.

3. The transmission power of WPA messages is set to cover only the cell area which itself belongs to. If the Mobile Node is not inside the estimated range using ξ, it may not receive a `localization-reply` from WPAs belonging to the estimated range. To compensate this case, Anchor Node wakes up the WPAs in the other area for the next round of localization.

7.6. WiPLoc++: Implementation and Evaluation

We evaluate the overall performance of WipLoc++ through (i) PRR and localization accuracy (as in the case of WiPLoc) and (ii) the recharging period of WPA using harvested energy.

7.6.1. Hardware Implementation

To implement WiPLoc++ using existing WiPLoc hardware some modifications need to be made. We list them below.

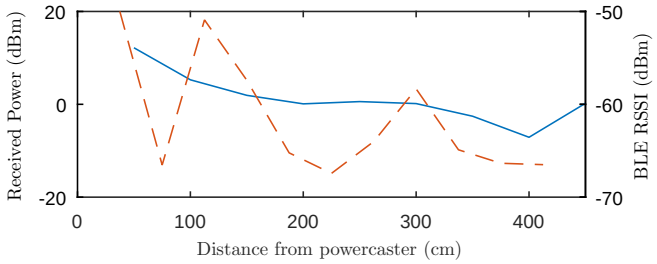

Figure 7.6: Signal strength of WPT and BLE communication signal. The solid line shows the received power calculated from the D_{out} from the harvester. The dotted line shows the RSSI from the nRF51822.

Algorithm 7 Cell-level localization protocol

Anchor Node (Fixed Powered Anchor Node):

loop
  if `location-request` received **then**
    Send `location-reply`
    Switch off and on powercaster as `passive-wakeup` signal
    if $\xi \leq \theta$ **then**
      Broadcast `sleep` command for WPAs in Δ_c
    else
      Broadcast `sleep` command for WPAs in Δ_f
  if `location-request` with `no-reply` received **then**
    Switch off and on powercaster as `passive-wakeup` signal
    Broadcast `sleep` command for WPAs in $\overline{\Delta}$

WPA (Wireless Powered Anchor Node):

loop
  Sleep
  Monitor D_{out} every t_c
  if `passive-wakeup` detected **then**
    Start receiving
    if `Sleep` command received **then**
      Goto Sleep
    if `location-request` received **then**
      Send `location-reply`

Mobile Node:

loop
  Sleep
  Monitor D_{out} every t_c.
  if timer $\geq t_m$ **then**
    Broadcast `location-request`
    if `location-reply` received **then**
      Wait for t_c
      Broadcast `location-request` to WPAs
      if `location-reply` received from WPAs **then**
        Decode `location-replys` and compute Room and Cell location.
      else
        Decode room-level `location-reply`
        Broadcast `location-request` with `no-reply` in next round

- **Anchor Node:** This node the nRF51822 is combined with the powercaster. A transistor is added to the power line of the powercaster so that the nRF51822 can control if the powercaster is on or off.
- **Mobile Node:** There are no modification to the hardware of the mobile node but two extra connections are made between the nRF51822 and the harverster. The

Table 7.3: Experiment results of WiPLoc++ in the room and the corridor

	PRR (%)	Accuracy (%)
Room	97.5	59.9
Corridor	100	82.2

D_{out} and the D_{set} are connected to P0.01 and P0.02 of the nRF51822, respectively.

- **Wirelessly-Powered Anchor Node:** This node uses the same combination of hardware and connections as the Mobile Node except for one difference. The development board for the nRF51822 is the Smart Beacon Kit and not the PCA10005.

All electrical connections of three nodes are given in Fig. 7.2.

7.6.2. EXPERIMENT SETUP

Due to the limited number of harvesters in our laboratory, we only deploy four WPAs around one Anchor Node. The cell-level localization experiments are performed in a room and corridor separately. The deployment of WPAs, Anchor Nodes in the rooms and the testing positions of Mobile Node are illustrated in Fig. 7.3(a). The Mobile Node sends 20 localization requests with period 1.0 s at each testing position. As the length of the corridor is larger than the effective charging range from Anchor Node to WPA we deploy two powercasters back-to-back in the middle of the corridor pointing to the begin and the end of the corridor, respectively.

7.6.3. EXPERIMENT RESULTS

Compared with the WiPLoc room-level results, (see Table 7.2), the average cell-level PRR and localization accuracy of WiPLoc++ in the room and corridor (see Table 7.3) are on the same level. Although the cell-level localization accuracy in the room is lower than the room-level accuracy, the localization cell is only 4 m^2 using WiPLoc++, which is much smaller than the 16 m^2 localization room using WiPLoc. The test results prove that WiPLoc++ is able to achieve cell-level localization using WPT in all deployed nodes except the Anchor Node.

On the other hand, we find that cell-level localization accuracy at some positions in Fig. 7.7 is much lower than the average value for the whole area. This is due to two reasons: (i) the radio pattern of powercaster has only 60° coverage in width and height, therefore some testing positions at the border of the room are not effectively covered and (ii) the threshold value θ uses the measured RSS value at the middle position of the charging area. However, the contour line of θ is not straight in the radio pattern of powercaster, which makes it difficult to categorize cells into strict squares.

7.7. CONCLUSION

In this chapter we presented an RF WPT-enabled indoor localization system denoted as **WiPLoc** (**Wi**reless **P**owered **Loc**alization system). The key innovations of WipLoc include: (i) leveraging collisions and orthogonal codes to build an extremely low power localization approach, and (ii) constructing a cell-level localization network by managing the limited

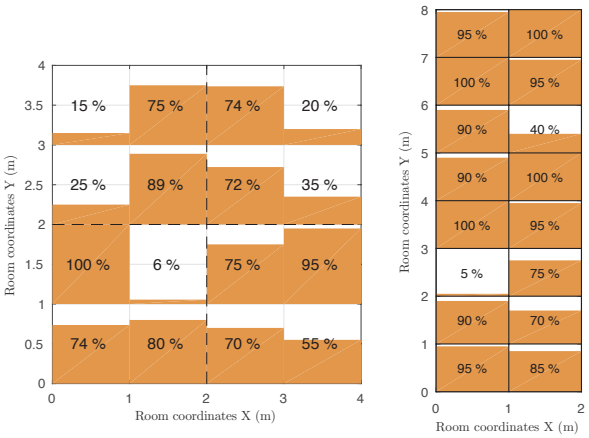

(a) Localization accuracy: room

(b) Localization accuracy: corridor

Figure 7.7: WiPLoc++ localization results. The values in orange rectangles of two figures represent the cell-level localization accuracy of WiPLoc++ measured per testing positions of (a) room two and (b) corridor as shown in Fig. 7.3(a).

harvested energy from RF-based WPT systems. Based on extensive indoor experiments, we showed that WiPLoc is capable of providing continuous cell-level localization to mobile nodes. To the best of our knowledge, WiPLoc is the first localization system powered by RF transmission.

8

Conclusion and Future Work

As mobile wireless devices are increasingly used in our daily life, the number of mobile devices and networks increase to unprecedented numbers. More application systems require the management of mobile devices and networks to be automatic and convenient. To achieve this goal, autonomic computing is widely researched. In this dissertation, autonomic computing systems were investigated by designing and implementing self-adaptive self-organizing systems and RF wireless power transfer systems. These systems demonstrate the potential to increase the autonomy of mobile systems.

8.1. Research Questions Revisited

In Chapter 3 to Chapter 7, we focused on five sub-research questions proposed in Chapter 1. In this section, we summarize our research results and answer these questions.

8.2. Sub Research Questions

- *Can local information exchange in mobile communication networks achieve self-organizing data aggregation?*

- *Can local information exchange in mobile communication networks achieve distance estimation?*

Chapter 3 and Chapter 4 investigated the self-adaptive self-organizing properties of distributed systems by designing data aggregation and distance estimation in mobile networks. Chapter 3 successfully evolved data aggregation algorithms in wireless networks to meet application requirements and adapt to changes in the application scenarios. The approach was automated in every node during runtime, and adaptive to the network topology in real-time. Chapter 4 introduced a distance-estimation algorithm in large-scale wireless networks, for the purpose of estimating the distances between nodes in both static and mobile scenarios with high accuracy. The global localization behavior is adaptive to network mobility, density, and topology.

One common property of both systems is that the global behavior of a network is designed by allowing each node only to broadcast local information to its direct neighbors. Compared to centralized control systems, this mechanism largely decreases the communication complexity of the proposed designs, although these algorithms require that networks wait for the convergence from the behavior of each local node to the global state of the whole system. The network can adapt to changes in the application scenarios, such as incoming new nodes and leaving existing nodes. Therefore, the two chapters showed that local broadcast communication can achieve complicated autonomic abilities in large-scale networks.

- *Can communication power efficiency be increased with backscatter radio?*

In Chapter 5, harvested energy was not used directly as a power supply for the mobile device, instead backscatter was used to save energy. To extend the possible application scenarios with the limited harvested energy of RF wireless power transfer systems, the requirement of using harvested energy directly as a power supply was relaxed. A hybrid radio platform BLISP composed of the Wireless Identification and Sensing Platform (WISP) and the Bluetooth Low Energy (BLE) was designed and implemented. The hybrid platform switches between the use of backscatter radio and active radio based on observations of the communication channel quality. BLISP improves the energy efficiency of communication compared to BLE when the device is close to the RFID reader. At the same time, the reliability of BLISP is higher than WISP when the device moves frequently far away from the RFID reader. The results of this chapter show that the combination of active and backscatter radio can be used to increase the amount of communication data using the equal amount of energy in mobile systems. Although the harvested energy is not directly used to charge a battery or as a power supply, it prolongs the lifetime of mobile devices by using backscatter radio for communication.

- *How can the performance of RF-based wireless power transfer networks be optimized?*

Chapter 6 introduced a charging control protocol for wireless power transfer networks (WPTNs). The system increases the charging efficiency while keeping the harvested energy at the required level. Advantages and disadvantages of beacon-based and probe-based control protocols were studied. This chapter showed that energy cannot only be saved on the harvester side, but also on the charger side. For mobile chargers, saving power means a longer life time to provide charging services, a smaller number of chargers to cover a specified area, and a larger coverage area of one charger with a fixed movement speed. All of these properties increase the energy autonomy of the whole system.

- *Can RF-based wireless power transfer supply enough energy to run a localization service?*

Chapter 7 presented an indoor localization system by using the limited harvested energy from a RF-based WPT system. In the algorithm design of Chapter 3 and Chapter 4, focusing on the network level, nodes are assumed to be in idle-listening mode all the time. This is not possible for devices that receive power using wireless power transfer. Since the harvested energy from RF is quite limited, it cannot support the additional

power consumption of a continuous idle-listening mode. In Chapter 7, we leveraged collision beacons and passive wakeup to decrease the power consumption of localization. Besides the innovation of combining WPT and indoor localization, another challenge was to provide the network with adaptive or autonomic properties. The proposed algorithm that selects the anchor node adapts its behavior. Although this adaptive characteristic is not strongly expressed in the algorithm, it improves the localization accuracy and saves energy. Based on the results of Chapter 7, we conclude that wireless power transfer can support the energy requirements of indoor localization systems using simple adaptive operations.

8.3. MAIN RESEARCH QUESTION

Can self-organization based on local information exchange achieve global control of energy-autonomous systems?

The common goal of self-organization and energy autonomy is autonomic management. We use local information exchange for decreasing communication complexity in distributed systems. The research of self-adaptive self-organization focuses on the global and local behavior of distributed mobile networks. Through the study of distributed data aggregation (Chapter 3) and distance estimation (Chapter 4), we demonstrated that local information exchange and management can achieve the desired global behavior of the networks. The research of energy-autonomous systems addressed the challenge of power supply in mobile systems. We studied merging backscatter and active radio (Chapter 5), wireless power transfer networks (Chapter 6), and indoor localization with wireless charging (Chapter 7). The three research points respectively represent harvester side, charger side, and a complete mobile system using wireless charging. The results show that RF-based wireless power transfer systems with optimized control can extend the lifetime of mobile devices. Finally, the research of Chapters 5 to 7 illustrates that self-adaptive self-organization can be used to control the operation of energy-autonomous systems.

8.4. FUTURE WORK

This section presents an overview of the future work of this dissertation from the perspectives of self-adaptive self-organization and energy-autonomous systems.

8.4.1. FUTURE SELF-ADAPTIVE SELF-ORGANIZATION RESEARCH

We summarize the future work of Chapter 3 and Chapter 4 as three main points.

Firstly, compared to centralized control, self-adaptive self-organizing networks are more adaptive to changes in application scenarios. However, the number of operations supported by the self-adaptive self-organizing networks is limited. For example, the algorithm in Chapter 4 is only used for distance estimation. Chapter 3 addresses this limitation by means of an evolutionary algorithm, but the number of function combinations and the element functions must be predefined according to the proposed application scenarios. Therefore, a promising direction for future work of self-adaptive self-organizing networks is to explore adaptation of multiple operations.

Secondly, the algorithms in Chapter 3 and Chapter 4 use broadcast for communication. The power consumption of the idle-listening mode is high, especially for devices that use harvested energy from wireless power transfer. So the power consumption of communication in broadcast-based autonomic computing networks must be decreased.

Thirdly, the proposed algorithms have only been evaluated using simulations. Some simulation models are not precise enough compared with real deployment scenarios. For example, both algorithms assume the transmission range to be a round disk, which is hard to implement, especially indoors using wearable devices. It is important to explore whether the algorithms works, once they are implemented on real hardware.

8.4.2. FUTURE WIRELESS POWER TRANSFER RESEARCH

Wireless power transfer is an emerging research area. We summarize the future work based on this dissertation as follows.

Firstly, the application scenarios of implemented wireless power transfer systems in Chapter 5, Chapter 6 and Chapter 7 have not been fully tested. In Chapter 5 and Chapter 6, the communication protocols claim to save energy on the harvester and charger side, respectively. Although the experimental results confirm this, all tests are based on predefined scenarios. It is unknown whether the system operates properly when deployed in the real world. Although the system in Chapter 7 claims to target localization for mobile devices, the testing points in the deployment area are static without obstacles. It is unknown whether the indoor localization system still works well with real-world parameters, such as real world mobility or obstacles. Therefore, future work for RF wireless power transfer systems is to observe the performance of such systems in real-world deployment scenarios.

Secondly, Chapter 5, Chapter 6 and Chapter 7 target application scenarios using multiple-charger networks. However, all the testing scenarios only involve a limited number of chargers. Although the experimental results illustrate the feasibility of the system, there will be other problems as the number of chargers increases. For example, Chapter 7 uses semi-passive wakeup to avoid idle listening of anchor nodes. As the density of chargers increases, the semi-passive wakeup signal from one charger may wakeup the anchor nodes belonging to other chargers, and this unnecessary wakeup will waste energy in the anchor nodes. It is unknown how to coordinate chargers to schedule their wakeup signal to minimize the wasted power consumption of anchor nodes. Chapter 5 saves energy by merging backscatter radio and active radio. The chapter implements experiments with one reader as data aggregator. It is unknown how to deploy a larger number of readers in an area to minimize the communication power consumption of the device. Therefore, future work is needed to analyze the system performance in large-scale wireless power transfer networks.

LIST OF PUBLICATIONS

1. **Qingzhi Liu**, Wieger IJntema, Anass Drif, Przemysław Pawełczak, Marco Zuniga. *WiPLoc: Perpetual Indoor Localization with RF Wireless Power Transfer.* (Under preparation)

2. **Qingzhi Liu**, Kasım Sinan Yıldırım, Przemysław Pawełczak, Martijn Warnier. *Safe and Secure Wireless Power Transfer Networks: Challenges and Opportunities in RF-Based Systems.* IEEE Communication Magazine, 54:(9) 74 - 79, 2016.

3. **Qingzhi Liu**, Ivar in't Veen, Przemysław Pawełczak. *Joint Control of Computational RFID and Bluetooth Low Energy Motes.* Patent, TUDelft Application No. 2015432, filed in 14.09.2015.

4. Ivar in 't Veen, **Qingzhi Liu**, Przemyslaw Pawelczak, Aaron N Parks, Smith Joshua. *BLISP: Enhancing Backscatter Radio with Active Radio for Computational RFIDs.* In Proceedings of the IEEE RFID, Orlando, FL, May 3-5, 2016.

5. **Qingzhi Liu**, Michal Golinski, Przemyslaw Pawelczak, Martijn Warnier. *Green Wireless Power Transfer Networks.* IEEE Journal on Selected Areas in Communications, 34(5): 1740 - 1756, 2016.

6. Thomas C King, **Qingzhi Liu**, Gleb Polevoy, Mathijs de Weerdt, Virginia Dignum, M Birna van Riemsdijk, Martijn Warnier. *Request Driven Social Sensing.* In Proceedings of the AAMAS, Paris, May 5-9, 2014.

7. Venkatraman Iyer, **Qingzhi Liu**, Stefan Dulman, Koen Langendoen. *Adaptive Online Estimation of Temporal Connectivity in Dynamic Wireless Networks.* In Proceedings of the IEEE SASO, Philadelphia, USA, Sep. 9-13, 2013.

8. **Qingzhi Liu**, Stefan Dulman, Martijn Warnier. *AREA: an Automatic Runtime Evolutionary Adaptation Mechanism for Creating Self-Adaptation Algorithms in Wireless Networks.* In Proceedings of the Spatial Computing Workshop colocated with AAMAS, Saint Paul, Minnesota, USA, May 6-10, 2013.

9. **Qingzhi Liu**, Andrei Pruteanu, Stefan Dulman. *Gradient-Based Distance Estimation for Spatial Computers.* Computer Journal, 56(12):1469-1499, 2013.

10. **Qingzhi Liu**, Andrei Pruteanu, Stefan Dulman. *GDE: a Distributed Gradient-Based Algorithm for Distance Estimation in Large-Scale Networks.* In Proceedings of the ACM MSWiM, Miami Beach, FL, USA, Oct. 31- Nov. 4, 2011.

REFERENCES

[1] Adafruit Technology (2015). Slim sticker-type GSM/cellular quad-band antenna datasheet.

[2] Arduino (2014). *Arduino Homepage*. http://arduino.cc/en/Main/.

[3] Arnbak, J. C. and van Blitterswijk, W. (1987). Capacity of slotted aloha in rayleigh-fading channels. *IEEE J. Sel. Areas Commun.*, 5(2):261–269.

[4] Artemis (2014). *Artemis Home Page*. http://www.artemis.com.

[5] Ashby, W. R. (1991). Principles of the self-organizing system. In *Facets of Systems Science*, pages 521–536. Springer.

[6] Assimonis, S. D., Daskalakis, S.-N., and Bletsas, A. (2014). Efficient rf harvesting for low-power input with low-cost lossy substrate rectenna grid. In *RFID Technology and Applications Conference (RFID-TA)*, pages 1–6. IEEE.

[7] Assimonis, S. D., Daskalakis, S.-N., and Bletsas, A. (2016). Sensitive and efficient rf harvesting supply for batteryless backscatter sensor networks. *IEEE Transactions on Microwave Theory and Techniques*, 64(4):1327–1338.

[8] Atmel Corp. (2015). Atmel 8-bit microcontroller with 4/8/16/32 kbytes in-system programmable flash.

[9] Awad, A., Frunzke, T., and Dressler, F. (2007). Adaptive distance estimation and localization in wsn using rssi measures. In *Proceedings DSD*, pages 471 –478.

[10] Back, T., Fogel, D. B., and Michalewicz, Z. (1997). *Handbook of evolutionary computation*. IOP Publishing Ltd.

[11] Barroca, N., Borges, L. M., Velez, F. J., Monteiro, F., Górski, M., and Castro-Gomes, J. (2013). Wireless sensor networks for temperature and humidity monitoring within concrete structures. *Construction and Building Materials*, 40:1156–1166.

[12] Beal, J. and Schantz, R. (2010). A spatial computing approach to distributed algorithms. In *45th Asilomar Conference on Signals, Systems, and Computers*.

[13] Beeby, S. P., Torah, R., Tudor, M., Glynne-Jones, P., O'Donnell, T., Saha, C., and Roy, S. (2007). A micro electromagnetic generator for vibration energy harvesting. *Journal of Micromechanics and microengineering*, 17(7):1257.

[14] Beeby, S. P., Tudor, M. J., and White, N. M. (2006). Energy harvesting vibration sources for microsystems applications. *Measurement science and technology*, 17(12):R175.

[15] Belleville, M., Fanet, H., Fiorini, P., Nicole, P., Pelgrom, M., Piguet, C., Hahn, R., Van Hoof, C., Vullers, R., Tartagni, M., et al. (2010). Energy autonomous sensor systems: Towards a ubiquitous sensor technology. *Microelectronics Journal*, 41(11):740–745.

[16] BENARROCH, E. E. (1993). The central autonomic network: functional organization, dysfunction, and perspective. In *Mayo Clinic Proceedings*, volume 68, pages 988–1001. Elsevier.

[17] Bettstetter, C., Hartenstein, H., and Pérez-Costa, X. (2004). Stochastic properties of the random waypoint mobility model. *Wireless Networks*, 10(5):555–567.

[18] Bi, S., Ho, C. K., and Zhang, R. (2014). Wireless powered communication: Opportunities and challenges. accepted for publication.

[19] BLE (2016). *BLE Homepage*. https://www.bluetooth.com/.

[20] Bluetooth SIG Inc. (2015). Bluetooth low energy technical overview.

[21] Bouchouicha, D., Dupont, F., Latrach, M., and Ventura, L. (2010). Ambient rf energy harvesting. In *International Conference on Renewable Energies and Power Quality*, pages 1–4.

[22] Brideglall, R. (2007). RFID device, system and method of operation including a hybrid backscatter-based RFID tag protocol compatible with RFID, Bluetooth and/or IEEE 802.11x infrastructure.

[23] Byun, J., Jeon, B., Noh, J., Kim, Y., and Park, S. (2012). An intelligent self-adjusting sensor for smart home services based on zigbee communications. *IEEE Transactions on Consumer Electronics*, 58(3):794–802.

[24] Cannon, B. L., Hoburg, J. F., Stancil, D. D., and Goldstein, S. C. (2009). Magnetic resonant coupling as a potential means for wireless power transfer to multiple small receivers. *IEEE Transactions on Power Electronics*, 24(7):1819–1825.

[25] Caprarescu, B. A. and Petcu, D. (2009). A self-organizing feedback loop for autonomic computing. In *Future Computing, Service Computation, Cognitive, Adaptive, Content, Patterns*, pages 126–131. IEEE.

[26] Casilari, E., Cano-Garcia, J. M., and Campos-Garrido, G. (2010). Modeling of current consumption in 802.15.4/ZigBee sensor motes. *Sensors*, 10(6):5443–5468.

[27] Cattani, M. and Protonotarios, I. (2015). Gondola: a parametric robot infrastructure for repeatable mobile experiments.

[28] Champrasert, P., Suzuki, J., and Lee, C. (2012). Exploring self-optimization and self-stabilization properties in bio-inspired autonomic cloud applications. *Concurrency and Computation: Practice and Experience*.

[29] Cherry, S. (2004). Edholm's law of bandwidth. 41(7):58–60.

[30] Chiu, T.-C., Shih, Y.-Y., Pang, A.-C., Jeng, J.-Y., and Hsiu, P.-C. (2012). Mobility-aware charger deployment for wireless rechargeable sensor network. In *Proc. APNOMS*, Seoul, South Korea.

[31] Chiu, T.-C., Shih, Y.-Y., Pang, A.-C., Jeng, J.-Y., and Hsiu, P.-C. (2012). Mobility-aware charger deployment for wireless rechargeable sensor networks. In *The 14th Asia-Pacific Network Operations and Management Symposium*, pages 1–7. IEEE.

[32] Cirstea, C., Petrita, T., Popescu, V., and Gontean, A. (2013). Performance analysis and modelling of a radio frequency energy harvesting system. *Advances in Electrical and Computer Engineering*, 13(1):27–32.

[33] Dai, H., Chen, G., Wang, C., Wang, S., Wu, X., and Wu, F. (2014a). Quality of energy provisioning for wireless power transfer. accepted for publications.

[34] Dai, H., Liu, Y., Chen, G., Wu, X., and He, T. (2014b). Safe charging for wireless power transfer. In *Proc. IEEE INFOCOM*, Toronto, Canada.

[35] de Moes, A. (2015). personal communication.

[36] Dementyev, A. and Smith, J. R. (2013). A wearable UHF RFID-based EEG system. In *Proc. IEEE RFID*, Orlando, FL, USA.

[37] Digi International Inc. (2015). Xbee 802.15.4 module specification.

[38] Dong, Y., Wickramasinghe, A., Xue, H., Al-Sarawi, S., and Ranasinghe, D. C. (2015). A novel hybrid powered RFID sensor tag. In *Proc. IEEE RFID*, San Diego, CA, USA.

[39] Dorigo, M., Bonabeau, E., and Theraulaz, G. (2000). Ant algorithms and stigmergy. *Future Generation Computer Systems*, 16(8):851–871.

[40] Ducatelle, F., Di Caro, G. A., and Gambardella, L. M. (2010). Cooperative self-organization in a heterogeneous swarm robotic system. In *Proceedings of the 12th annual conference on Genetic and evolutionary computation*, pages 87–94. ACM.

[41] Duckham, M. Decentralized spatial algorithm design. *Spatial Computing 2012 colocated with AAMAS*, pages 13–18.

[42] Energous (2014). *Energous Homepage*. http://energous.com.

[43] Ensworth, J. F. and Reynolds, M. S. (2015). Every smart phone is a backscatter reader: Modulated backscatter compatibility with bluetooth 4.0 devices. In *Proc. IEEE RFID*, San Diego, CA, USA.

[44] Erturk, A., Hoffmann, J., and Inman, D. (2009). A piezomagnetoelastic structure for broadband vibration energy harvesting. *Applied Physics Letters*, 94(25):254102.

[45] Fonseca, R., Dutta, P., Levis, P., and Stoica, I. (2008). Quanto: Tracking energy in networked embedded systems. In *Proc. USENIX OSDI*, volume 8, San Diego, CA, USA.

[46] Fréville, A. (2004). The multidimensional 0-1 knapsack problem: An overview. *European Journal of Operational Research*, 155(1):1–21.

[47] Fu, L., Cheng, P., Gu, Y., Chen, J., and He, T. (2013). Minimizing charging delay in wireless rechargeable sensor network. In *Proc. IEEE INFOCOM*, Turin, Italy.

[48] Garey, M. R. and Johnson, D. S. (1979). *Computers and Intractability: A Guide to the Theory of NP-Completeness*. Bell Telephone Labolatories, New York, NY, USA.

[49] Garlan, D., Cheng, S.-W., Huang, A.-C., Schmerl, B., and Steenkiste, P. (2004). Rainbow: Architecture-based self-adaptation with reusable infrastructure. *Computer*, 37(10):46–54.

[50] Gartner (2016). *Gartner, Inc.* http://www.gartner.com/newsroom/id/3165317.

[51] Ghosh, D., Sharman, R., Rao, H. R., and Upadhyaya, S. (2007). Self-healing systems—survey and synthesis. *Decision Support Systems*, 42(4):2164–2185.

[52] Goliński, M. (2015). Wireless power transfer networks. Master's thesis, Delft University of Technology, Delft, the Netherlands.

[53] Gollakota, S., Reynolds, M. S., Smith, J. R., and Wetherall, D. J. (2014). The emergence of RF-powered computing. 47(1):32–39.

[54] Gomez, C., Oller, J., and Paradells, J. (2012a). Overview and evaluation of Bluetooth Low Energy: An emerging low-power wireless technology. *Sensors*, 12(9):11734–11753.

[55] Gomez, K., Riggio, R., Rasheed, T., Miorandi, D., and Granelli, F. (2012b). Energino: a hardware and software solution for energy consumption monitoring. In *Proc. International Workshop on Wireless Network Measurements*, Paderborn, Germany.

[56] GS1 EPCglobal (2013). EPC radio-frequency identitiy protocols generation-2 UHF RFID. Version 2.0.1.

[57] GSMA (2016). *GSMA Intelligence*. https://gsmaintelligence.com.

[58] Gu, Y., Lo, A., and Niemegeers, I. (2009). A survey of indoor positioning systems for wireless personal networks. *IEEE Commun. & Surveys Tuts.*, 11(1):13–32.

[59] Gummeson, J., Ganesan, D., Corner, M. D., and Shenoy, P. (2010). An adaptive link layer for heterogeneous multi-radio mobile sensor networks. 28(7):1094–1104.

[60] Gummeson, J., Zhang, P., and Ganesan, D. (2012). Flit: a bulk transmission protocol for RFID-scale sensors. In *Proc. ACM MobiSys*, Low Wood Bay, Lake District, UK.

[61] Guo, S., Wang, C., and Yang, Y. (2013). Mobile data gathering with wireless energy replenishment in rechargeable sensor networks. In *INFOCOM*, pages 1932–1940. IEEE.

[62] Guo, Y., Poulton, G., Corke, P., Bishop-Hurley, G., Wark, T., and Swain, D. L. (2009). Using accelerometer, high sample rate GPS and magnetometer data to develop a cattle movement and behaviour model. *Ecological Modelling*, 220(17):2068–2075.

[63] Gupta, G. and Younis, M. Load-balanced clustering of wireless sensor networks. In *Proceedings IEEE ICC*, volume 3, pages 1848–1852. IEEE.

[64] Hasan, Z., Boostanimehr, H., and Bhargava, V. K. (2011). Green cellular networks: A survey, some research issues and challenges. *IEEE Communications Surveys & Tutorials*, 13(4):524–540.

[65] He, S., Chen, J., Jiang, F., Yau, D. K., Xing, G., and Sun, Y. (2013). Energy provisioning in wireless rechargeable sensor networks. 12(10):1931–1942.

[66] He, T. and all (2004). Energy-efficient surveillance system using wireless sensor networks. In *The 2nd International Conference on Mobile Systems*. ACM.

[67] Ho, J. S., Kim, S., and Poon, A. S. Y. (2013). Midfield wireless powering for implantable systems. 101(6):1369–1378.

[68] Holleman, J., Yeager, D., Prasad, R., Smith, J. R., and Otis, B. (2008). NeuralWISP: An energy-harvesting wireless neural interface with 1-m range. In *Proc. IEEE BioCAS*, Baltimore, MD, USA.

[69] Horn, P. (2001). Autonomic computing: Ibm\'s perspective on the state of information technology.

[70] Huang, J., Farritor, S. M., Qadi, A., and Goddard, S. (2006). Localization and follow-the-leader control of a heterogeneous group of mobile robots. *IEEE/ASME Transactions on Mechatronics*, 11(2):205–215.

[71] Huang, K. and Lau, V. K. (2014). Enabling wireless power transfer in cellular networks: architecture, modeling and deployment. *IEEE Transactions on Wireless Communications*, 13(2):902–912.

[72] Huang, K. and Lau, V. K. N. (2012). Enabling wireless power transfer in cellular networks: Architecture, modeling and deployment. submitted to IEEE Trans. Wireless Commun.

[73] Huang, X., Han, T., and Ansari, N. (2015). On green-energy-powered cognitive radio networks. *IEEE Communications Surveys & Tutorials*, 17(2):827–842.

[74] Hui, S. Y. R., Zhong, W., and Lee, C. K. (2014). A critical review of recent progress in mid-range wireless power transfer. 29(9):4500–4511.

[75] IJntema, W., Drif, A., Liu, Q., Pawelczak, P., and Zuniga, M. (2015). Source code of wiploc system. http://bit.ly/1PaTcZk.

[76] Impinj (2015). Impinj Speedway Revolution readers. http://www.impinj.com/products/readers/speedway-revolution/.

[77] Impinj Inc. (2015a). Impinj speedway R1000 RFID reader data sheet.

[78] Impinj Inc. (2015b). Impinj speedway r1000 rfid reader data sheet.

[79] in 't Veen, I., Liu, Q., and Pawelczak, P. (2016). Source code of BLISP.

[80] Islam, A. B. M. A. A., Hossain, M. S., Raghunathan, V., and Hu, Y. C. (2014). Backpacking: Energy-efficient deployment of heterogeneous radios in multi-radio high-data-rate wireless sensor networks. *IEEE Access*, 2:1281–1306.

[81] Jabbar, H., Song, Y. S., and Jeong, T. T. (2010). Rf energy harvesting system and circuits for charging of mobile devices. *Transactions on Consumer Electronics*, 56(1):247–253.

[82] JFW Industries (2015). Benchtop rotary attenuators. http://www.jfwindustries.com/catalog/Benchtop_Rotary_Attenuators_L_Bracket-143-1.html.

[83] Jin, Y. and Branke, J. (2005). Evolutionary optimization in uncertain environments : A survey. *IEEE Transactions on Evolutionary Computation*, 9(3):303–317.

[84] Johnson, D. S. (1990). Catalog of complexity classes. In van Leeuwen, J., editor, *Handbook of Theoretical Computer Science: Algorithms and complexity*, volume A. Elsevier.

[85] Ju, H. and Zhang, R. (2014). Throughput maximization for wireless powered communication networks. 13(1):418–428.

[86] Ju, H. and Zhang, R. (2014). User cooperation in wireless powered communication networks. In *Global Communications Conference*, pages 1430–1435. IEEE.

[87] Kalp, C. G. D. H. D. and Tauche, W. (2010). Making wireless sensor networks truly wireless using RF power.

[88] Kamath, S. and Lindh, J. (2010). Measuring Bluetooth Low Energy power consumption. *Texas Instruments Application Note AN092*.

[89] Kampianakis, E., Kimionis, J., Tountas, K., and Bletsas, A. (2014). A remotely programmable modular testbed for backscatter sensor network research. In Langendoen, K., Hu, W., Ferrari, F., Zimmerling, M., and Mottela, L., editors, *Real-World Wireless Sensor Networks*, volume 281, pages 153–161. Springer International Publishing.

[90] Kanjo, E. (2010). Noisespy: a real-time mobile phone platform for urban noise monitoring and mapping. *Mobile Networks and Applications*, 15(4):562–574.

[91] Kansal, A., Hsu, J., Zahedi, S., and Srivastava, M. B. (2007). Power management in energy harvesting sensor networks. *Transactions on Embedded Computing Systems*, 6(4):32.

[92] Kennedy, J. (2006). Swarm intelligence. *Handbook of nature-inspired and innovative computing*, pages 187–219.

[93] Kephart, J. O. and Chess, D. M. (2003). The vision of autonomic computing. *Computer*, 36(1):41–50.

[94] Keyrouz, S., Visser, H. J., and Tijhuis, A. (2013). Multi-band simultaneous radio frequency energy harvesting. In *The 7th European Conference on Antennas and Propagation (EuCAP)*, pages 3058–3061. IEEE.

[95] Kleinberg, J. and Tardos, É. (2005). *Algorithm Design*. Addison Wesley.

[96] Kleinrock, L. and Silvester, J. (1978). Optimum transmission radii for packet radio networks or why six is a magic number. In *Proc. of the IEEE National Telecom. Conference*, volume 4, pages 1–4.

[97] Krikidis, I. (2014). Simultaneous information and energy transfer in large-scale networks with/without relaying. *Transactions on Communications*, 62(3):900–912.

[98] Krikidis, I. (2014). Simultaneous information and energy transfer in large-scale networks with/without relaying. 62(3):900–912.

[99] Kurose, J., Lyons, E., McLaughlin, D., Pepyne, D., Philips, B., Westbrook, D., and Zink, M. (2006). An end-user-responsive sensor network architecture for hazardous weather detection, prediction and response. In *Technologies for Advanced Heterogeneous Networks II*, pages 1–15. Springer.

[100] Kurs, A., Karalis, A., Moffatt, R., Joannopoulos, J. D., Fisher, P., and Soljačić, M. (2007). Wireless power transfer via strongly coupled magnetic resonances. *Science*, 317(5834):83–86.

[101] Laird Technology (2015). S9028PCR RFID panel antenna.

[102] Lakshmanan, S., Sanadhya, S., and Sivakumar, R. (2011). On link rate adaptation in 802.11n WLANs. In *Proc. IEEE INFOCOM*, Orlando, FL, USA.

[103] Lang, H.-D., Ludwig, A., and Sarris, C. D. (2014). Convex optimization of wireless power transfer systems with multiple transmitters. 62(9):4623–4636.

[104] Lazik, P., Rajagopal, N., Shih, O., Sinopoli, B., and Rowe, A. (2015). ALPS: A bluetooth and ultrasound platform for mapping and localization. In *Proc. ACM SenSys*, Seoul, South Korea.

[105] Le, T., Mayaram, K., and Fiez, T. (2008). Efficient far-field radio frequency energy harvesting for passively powered sensor networks. *IEEE Journal of Solid-State Circuits*, 43(5):1287–1302.

[106] Leabman, M. A. and Brewer, G. S. (2015). Social power sharing for mobile devices based on pocket-forming.

[107] Lee, C., Suzuki, J., and Vasilakos, A. (2012). An evolutionary game theoretic framework for adaptive, cooperative and stable network applications. *BIONETICS*, pages 189–204.

[108] Lee, U., Zhou, B., Gerla, M., Magistretti, E., Bellavista, P., and Corradi, A. (2006). Mobeyes: smart mobs for urban monitoring with a vehicular sensor network. *Wireless Communication*, 13(5):52–57.

[109] Lettieri, P. and Srivastava, M. B. (1998). Adaptive frame length control for improving wireless link throughput, range, and energy efficiency. In *Proc. IEEE INFOCOM*, San Francisco, CA, USA.

[110] Li, N. and Hou, J. C. (2005). Localized topology control algorithms for heterogeneous wireless networks. *IEEE/ACM Transactions on Networking (TON)*, 13(6):1313–1324.

[111] Liu, H., Darabi, H., Banerjee, P., and Liu, J. (2007). Survey of wireless indoor positioning techniques and systems. *IEEE Trans. Syst., Man, Cybern. C, Appl. Rev.*, 37(6):1067–1080.

[112] Liu, L., Zhang, R., and Chua, K.-C. (2013). Wireless information and power transfer: a dynamic power splitting approach. *Transactions on Communications*, 61(9):3990–4001.

[113] Liu, L., Zhang, R., and Chua, K.-C. (2013). Wireless information and power transfer: A dynamic power splitting approach. 61(9):3990–4001.

[114] Liu, Q., Golinński, M., Pawełczak, P., and Warnier, M. (2016a). Green wireless power transfer networks. *IEEE Journal on Selected Areas in Communications*, 34(5):1740–1756.

[115] Liu, Q., Pruteanu, A., and Dulman, S. (2011a). Gde: a distributed gradient-based algorithm for distance estimation in large-scale networks. In *MSWiM*, pages 151–158. ACM.

[116] Liu, Q., Yıldırım, K. S., Pawełczak, P., and Warnier, M. (2016b). Safe and secure wireless power transfer networks: challenges and opportunities in rf-based systems. *IEEE Communications Magazine*, 54(9):74–79.

[117] Liu, X., Wang, P., Niyato, D., and Han, Z. (2014). Resource allocation in wireless networks with RF energy harvesting and transfer. accepted for publication.

[118] Liu, Y., Zhao, Y., Chen, L., Pei, J., and Han, J. (2011b). Mining frequent trajectory patterns for activity monitoring using radio frequency tag arrays. *IEEE Trans. Parallel Distrib. Syst.*, 23(11):2138–2149.

[119] Long, J. R., Wu, W., Dong, Y., Zhao, Y., Sanduleanu, M. A. T., Gerrits, J., and van Veenendaal, G. (2008). Energy-efficient wireless front-end concepts for ultra lower power radio. In *Proc. IEEE CICC*, San Jose, CA, USA.

[120] LoRa Alliance (2015). LoRa alliance – wide area networks for IoT.

[121] Lorincz, K., Malan, D. J., Fulford-Jones, T. R., Nawoj, A., Clavel, A., Shnayder, V., Mainland, G., Welsh, M., and Moulton, S. (2004). Sensor networks for emergency response: challenges and opportunities. *Pervasive Computing*, 3(4):16–23.

[122] Lu, X., Niyato, D., Wang, P., Kim, D. I., and Han, Z. (2014a). Wireless charger networking for mobile devices: Fundamentals, standards, and applications.

[123] Lu, X., Wang, P., Niyato, D., Kim, D. I., and Han, Z. (2014b). Wireless networks with RF energy harvesting: A contemporary survey.

[124] Lymberopoulos, D., Liu, J., Yang, X., Choudhury, R. R., Handziski, V., and Sen, S. (2015). A realistic evaluation and comparison of indoor location technologies: Experiences and lessons learned. In *Proc. ACM IPSN*, Seattle, WA, USA.

[125] MacDonald, J. E. (1960). Design methods for maximum minimum-distance error correcting codes. *IBM Journal of Research and Development*, 4(1):43–57.

[126] Malan, D., Fulford-Jones, T., Welsh, M., and Moulton, S. (2004). Codeblue: An ad hoc sensor network infrastructure for emergency medical care. In *International workshop on wearable and implantable body sensor networks*, volume 5.

[127] Mao, G., Fidan, B., and Anderson, B. (2007). Wireless sensor network localization techniques. *Computer Networks*, 51(10):2529–2553.

[128] Martelli, F., Renda, M. E., Resta, G., and Santi, P. (2012). A measurement-based study of beaconing performance in IEEE 802.11p vehicular networks. In *Proc. IEEE INFOCOM*, Orlando, FL, USA.

[129] Martinez, K., Hart, J. K., and Ong, R. (2004). Environmental sensor networks. *Computer*, 37(8):50–56.

[130] Massa, A., Oliveri, G., Viani, F., and Rocca, P. (2013). Array designs for long-distance wireless power transmission: State-of-the-art and innovative solutions. 101(6):1464–1481.

[131] Meignan, D., Koukam, A., and Créput, J.-C. (2010). Coalition-based metaheuristic: a self-adaptive metaheuristic using reinforcement learning and mimetism. *Journal of Heuristics*, 16(6):859–879.

[132] Melanie, M. (1999). An introduction to genetic algorithms. *Cambridge, Massachusetts London, England, Fifth printing*.

[133] Mercier, P. P. and Chandrakasan, A. P. (2011). A supply-rail-coupled eTextiles transciever for body-area networks. 46(6):1284–1295.

[134] Michel, J.-B., Shen, Y. K., Aiden, A. P., Veres, A., Gray, M. K., Brockman, W., The Google Books Team, Pickett, J. P., Hoiberg, D., Clancyand Peter Norvig, D., Orwant, J., Pinker, S., Nowak, M. A., and Aiden, E. L. (2011). Quantitative analysis of culture using millions of digitized books. *Science*, 331(6014):176–182.

[135] Microelectronics Technology Inc. (2015). MINI ME – smartphone RFID-reader.

[136] Mieghem, P. V. (2005). *Performance Analysis of Communications Networks and Systems*. Cambridge University Press, New York, NY, USA.

[137] Mishra, D., De, S., and Chowdhury, K. R. (2015a). Charging time characterization for wireless RF energy transfer. 62(4):362–366.

[138] Mishra, D., De, S., Jana, S., Basagni, S., Chowdhury, K., and Heinzelman, W. (2015b). Smart RF energy harvesting communications: challenges and opportunities. 53(4):70–78.

[139] Monsoon (2014). *Monsoon Power Monitor Homepage*. http://www.msoon.com/LabEquipment/PowerMonitor/.

[140] Mun, M., Reddy, S., Shilton, K., Yau, N., Burke, J., Estrin, D., Hansen, M., Howard, E., West, R., and Boda, P. (2009). Peir, the personal environmental impact report, as a platform for participatory sensing systems research. In *Proceedings of the 7th international conference on Mobile systems, applications, and services*, pages 55–68. ACM.

[141] Murphy, R. R., Lisetti, C. L., Tardif, R., Irish, L., and Gage, A. (2002). Emotion-based control of cooperating heterogeneous mobile robots. *Transactions on Robotics and Automation*, 18(5):744–757.

[142] Murty, R. N., Mainland, G., Rose, I., Chowdhury, A. R., Gosain, A., Bers, J., and Welsh, M. (2008). Citysense: An urban-scale wireless sensor network and testbed. In *IEEE Conference on Technologies for Homeland Security*, pages 583–588. IEEE.

[143] Muruganathan, S. D., Ma, D. C., Bhasin, R. I., and Fapojuwo, A. O. (2005). A centralized energy-efficient routing protocol for wireless sensor networks. *Communications Magazine*, 43(3):S8–13.

[144] Naderi, M. Y., Chowdhury, K. R., Basagni, S., Heinzelman, W., De, S., and Jana, S. (2014a). Experimental study of concurrent data and wireless energy transfer for sensor networks. In *Proc. IEEE GLOBECOM*, Austin, TX, USA.

[145] Naderi, M. Y., Nintanavongsa, P., and Chowdhury, K. R. (2014b). RF-MAC: A medium access control protocol for re-chargeable sensor networks powered by wireless energy harvesting. 13(7):3926–3937.

[146] Nagpal, R., Shrobe, H., and Bachrach, J. (2003). Organizing a global coordinate system from local information on an ad hoc sensor network. In *Information Processing in Sensor Networks*, pages 553–553. Springer.

[147] Nakano, T. and Suda, T. (2005). Self-organizing network services with evolutionary adaptation. *IEEE Transactions on Neural Networks*, 16(5):1269–1278.

[148] Nam, I., Dougal, R., and Santi, E. (2012). Novel control approach to achieving efficient wireless battery charging for portable electronic devices. In *Proc. IEEE Energy Conversion Congress and Exposition*, Raleigh, NC, USA.

[149] Nanas, N. and De Roeck, A. (2009). Autopoiesis, the immune system, and adaptive information filtering. *Natural Computing*, 8(2):387–427.

[150] Ng, D. W. K. and Schober, R. (2014). Resource allocation for coordinated multipoint networks with wireless information and power transfer. In *Proc. IEEE GLOBECOM*, Austin, TX, USA.

[151] Ni, L. M., Liu, Y., Lau, Y. C., and Patil, A. P. (2004). LANDMARC: indoor location sensing using active RFID. *Springer Wireless Networks*, 10(6):701–710.

[152] Ni, L. M., Zhang, D., and Souryal, M. R. (2011). RFID-based localization and tracking technologies. *IEEE Wireless Commun.*, 18(2):45–51.

[153] Nordic (2015). Bluetooth low energy products. https://www.nordicsemi.com/eng/Products/Bluetooth-Smart-Bluetooth-low-energy.

[154] Nordic Semiconductor (2012). NRF51822 Bluetooth Smart and 2.4GHz proprietary SoC.

[155] Nordic Semiconductor (2013). NRF51822 product anomaly notice v2.0.

[156] Nowak, M. (2006). *Evolutionary Dynamics: exploring the equations of life*. Belknap Press.

[157] Ossia (2014). *Ossia Homepage*. http://www.ossiainc.com.

[158] Parashar, M. and Hariri, S. (2005). Autonomic computing: An overview. In *Unconventional Programming Paradigms*, pages 257–269. Springer.

[159] Park, J. and Clerckx, B. (2014). Joint wireless information and energy transfer with reduced feedback in mimo interference channels.

[160] Patel, M. and Wang, J. (2010). Applications, challenges, and prospective in emerging body area networking technologies. 17(1):80–88.

[161] Peng, Y., Li, Z., Zhang, W., and Qiao, D. (2010). Prolonging sensor network lifetime through wireless charging. In *The 31st Real-Time Systems Symposium*, pages 129–139. IEEE.

[162] Philipose, M., Smith, J. R., Jiang, B., Mamishev, A., Roy, S., and Sundara-Rajan, K. (2005). Battery-free wireless identification and sensing. 4(1):37–45.

[163] Piñuela, M., Mitcheson, P. D., and Lucyszyn, S. (2013). Ambient RF energy harvesting in urban and semi-urban environments. 61(7):2715–2726.

[164] Poojary, N., Krishnamurthy, S. V., and Dao, S. (2001). Medium access control in a network of ad hoc mobile nodes with heterogeneous power capabilities. In *IEEE International Conference on Communications*, volume 3, pages 872–877. IEEE.

[165] Powercast (2014). *Powercast Corp. Homepage*. http://www.powercastco.com.

[166] Powercast (2015). Power harvesters and receivers. http://www.powercastco.com/products/powerharvester-receivers.

[167] Proxi (2014). *Proxi Homepage*. http://powerbyproxi.com.

[168] Qiu, Y., Van Liempd, C., Op het Veld, B., Blanken, P. G., and Van Hoof, C. (2011). 5μw-to-10mw input power range inductive boost converter for indoor photovoltaic energy harvesting with integrated maximum power point tracking algorithm. In *Solid-State Circuits Conference Digest of Technical Papers*, pages 118–120. IEEE.

[169] Raghunathan, V., Kansal, A., Hsu, J., Friedman, J., and Srivastava, M. (2005). Design considerations for solar energy harvesting wireless embedded systems. In *The 4th international symposium on Information processing in sensor networks*, page 64. IEEE.

[170] Ransford, B. (2015). Llrp library controller.

[171] Rao, A. and all (2003). Geographic routing without location information. In *Proceedings Mobicom*, pages 96–108. ACM.

[172] Rudafshani, M. and Datta, S. (2007). Localization in wireless sensor networks. In *Proceedings IPSN*, pages 51–60. ACM.

[173] Saab, S. S. and Nakad, Z. S. (2011). A standalone RFID indoor positioning system using passive tags. *IEEE Trans. Ind. Electron.*, 58(5):1961–1970.

[174] Sample, A. P., Waters, B. H., Wisdom, S. T., and Smith, J. R. (2013). Enabling seamless wireless power delivery in dynamic environments. 101(6):1343–1358.

[175] Sample, A. P., Yeager, D. J., Powledge, P. S., Mamishev, A. V., and Smith, J. R. (2008). Design of an RFID-based battery-free programmable sensing platform. 57(11):2608–2615.

[176] Seah, W. K., Eu, Z. A., and Tan, H.-P. (2009). Wireless sensor networks powered by ambient energy harvesting (wsn-heap)-survey and challenges. In *1st International Conference on Wireless Communication, Vehicular Technology, Information Theory and Aerospace & Electronic Systems Technology*, pages 1–5. IEEE.

[177] Shu, Y., Cheng, P., Gu, Y., Chen, J., and He, T. (2014). TOC: Localizing wireless rechargeable sensors with time of charge. In *Proc. IEEE INFOCOM*, Toronto, ON, Canada.

[178] Siekkinen, M., Hiienkari, M., Nurminen, J. K., and Nieminen, J. (2012). How low energy is Bluetooth low energy? comperative measurement with Zigbee/802.15.4. In *Proc. IEEE WCNC Workshops*, Paris, France.

[179] SigFox (2015). SigFox – global cellular connectivity for the internet of things.

[180] SLLURP (2015). *SLLURP Library Repository*. https://github.com/ransford/sllurp.

[181] Strassner, II, B. and Chang, K. (2013). Microwave power transmission: Historical milestones and system components. 101(6):1379–1396.

[182] Sun, M.-q., Liew, R. J., Zhang, M.-H., and Li, W. (2014). Development of cement-based strain sensor for health monitoring of ultra high strength concrete. *Construction and Building Materials*, 65:630–637.

[183] Talla, V., Kellogg, B., Ransford, B., Naderiparizi, S., Gollakota, S., and Smith, J. R. (2015). Powering the next billion devices with Wi-Fi.

[184] Tan, K., Peng, X., So, P., Chu, Y. C., and Chen, M. (2012). Centralized control for parallel operation of distributed generation inverters in microgrids. *IEEE Transactions on Smart Grid*, 3(4):1977–1987.

[185] Tan, Y. K. and Panda, S. K. (2011). Energy harvesting from hybrid indoor ambient light and thermal energy sources for enhanced performance of wireless sensor nodes. *IEEE Transactions on Industrial Electronics*, 58(9):4424–4435.

[186] Tanenbaum, A. S. and Van Steen, M. (2007). *Distributed systems*. Prentice-Hall.

[187] Tektronix (2015). MDO4000B mixed domain oscilloscope.

[188] Texas Instruments (2015). MSP EnergyTrace Technology.

[189] Thomas, S. J., Harrison, R. R., Leonardo, A., and Reynolds, M. S. (2012). A battery-free multichannel digital Neural/EMG telemetry system for flying insects. *IEEE Trans. Biomed. Circuits Syst.*, 6(5):424–435.

[190] TI (2014). *Texas Instruments Homepage*. http://www.ti.com.

[191] Timotheou, S., Krikidis, I., Zheng, G., and Ottersten, B. (2014). Beamforming with MISO interference channels with QoS and RF energy transfer. 13(5):2646–2658.

[192] Tong, B., Li, Z., Wang, G., and Zhang, W. (2010). How wireless power charging technology affects sensor network deployment and routing. In *IEEE 30th International Conference on Distributed Computing Systems*, pages 438–447. IEEE.

[193] Tsikalakis, A. G. and Hatziargyriou, N. D. (2011). Centralized control for optimizing microgrids operation. In *Power and Energy Society General Meeting*, pages 1–8. IEEE.

[194] Turgut, A. E., Çelikkanat, H., Gökçe, F., and Şahin, E. (2008). Self-organized flocking in mobile robot swarms. *Swarm Intelligence*, 2(2-4):97–120.

[195] uBeam (2014). *uBeam Homepage*. http://www.ubeam.com.

[196] van Velzen, J. and Zuniga, M. (2013). Let's collide to localize: Achieving indoor localization with packet collisions. In *Proc. IEEE PerCom Workshop*, San Diego, CA, USA.

[197] Vannucci, G., Bletsas, A., and Leigh, D. (2007). Implementing backscatter radio for wireless sensor networks. In *2007 IEEE 18th International Symposium on Personal, Indoor and Mobile Radio Communications*, pages 1–5. IEEE.

[198] Vannucci, G., Bletsas, A., and Leigh, D. (2008). A software-defined radio system for backscatter sensor networks. *IEEE Transactions on Wireless Communications*, 7(6):2170–2179.

[199] Vesanto, J. and Alhoniemi, E. (2000). Clustering of the self-organizing map. *IEEE Transactions on Neural Networks*, 11(3):586–600.

[200] Viroli, M., Casadei, M., Montagna, S., and Zambonelli, F. (2011). Spatial coordination of pervasive services through chemical-inspired tuple spaces. *ACM Trans. Auton. Adapt. Syst.*, 6(2):14:1–14:24.

[201] Visser, H. J. and Vullers, R. J. (2013). Rf energy harvesting and transport for wireless sensor network applications: Principles and requirements. *Proceedings of the IEEE*, 101(6):1410–1423.

[202] Visser, H. J. and Vullers, R. J. M. (2013). RF energy harvesting and transport for wireless sensor network applications: Principles and requirements. 101(6):1410–1423.

[203] Vougioukas, G., Daskalakis, S.-N., and Bletsas, A. (2016). Could battery-less scatter radio tags achieve 270-meter range? In *Wireless Power Transfer Conference (WPTC)*, pages 1–3. IEEE.

[204] Wang, C., Li, J., and Yang, Y. (2014). NETWRAP: An NDN based real-time wireless recharging framework for wireless sensor network. 13(6):1283–1297.

[205] Wang, C., Yang, Y., and Li, J. (2013). Stochastic mobile energy replenishment and adaptive sensor activation for perpetual wireless rechargeable sensor networks. In *Wireless Communications and Networking Conference*, pages 974–979. IEEE.

[206] Wei, H., Chen, Y., Tan, J., and Wang, T. (2011). Sambot: A self-assembly modular robot system. *IEEE/ASME Transactions on Mechatronics*, 16(4):745–757.

[207] Werner-Allen, G., Johnson, J., Ruiz, M., Lees, J., and Welsh, M. (2005a). Monitoring volcanic eruptions with a wireless sensor network. In *Wireless Sensor Networks*, pages 108–120. IEEE.

[208] Werner-Allen, G., Tewari, G., Patel, A., Welsh, M., and Nagpal, R. (2005b). Firefly-inspired sensor network synchronicity with realistic radio effects. In *Proceedings of the 3rd international conference on Embedded networked sensor systems*, pages 142–153. ACM.

[209] Wicaksono, R. P., Tran, G. K., Sakaguchi, K., and Araki, K. (2011). Wireless grid: Enabling ubiquitous sensor networks with wireless energy supply. In *Proc. IEEE VTC-Spring*, Yokohama, Japan.

[210] Wifi (2016). *Wifi Homepage*. http://www.wi-fi.org/.

[211] Wilensky, U. (1999). Netlogo, center for connected learning and computer-based modeling. *Northwestern University*.

[212] WISP (2014). *WISP 5.0 Wiki*. http://wisp5.wikispaces.com.

[213] WISP (2015a). *WISP 5.0 Firmware Repository*. https://github.com/wisp/wisp5.

[214] WISP (2015b). WISP 5.0 wiki.

[215] WiTricity (2014). *WiTricity Homepage*. http://www.witricity.com.

[216] WPAN (2013). *802.15.4k-2013 IEEE Standard for Local and metropolitan area networks*. http://standards.ieee.org/findstds/standard/802.15.4k-2013.html.

[217] Wu, H. H., Gilchrist, A., Sealy, K., Israelsen, P., and Muhs, J. (2011). A review on inductive charging for electric vehicles. In *2011 IEEE International Electric Machines & Drives Conference (IEMDC)*, pages 143–147. IEEE.

[218] XBee (2014). *Digi International Homepage*. http://www.digi.com/xbee/.

[219] Xiang, L., Han, J. L. K., and Shi, G. (2013). Fueling wireless networks perpetually: A case of multi-hop wireless power distribution. In *Proc. IEEE PIRMC*, London, UK.

[220] Xiao, L., Wang, P., Niyato, D., Kim, D., and Han, Z. (2014). Wireless networks with rf energy harvesting: A contemporary survey. *IEEE Commun. Surveys Tuts.*, 17(2):757–789.

[221] Xie, L., Shi, Y., Hou, Y. T., and Lou, W. (2013a). Wireless power transfer and applications to sensor networks. *IEEE Wireless Commun.*, 20(9):140–145.

[222] Xie, L., Shi, Y., Hou, Y. T., and Lou, W. (2013b). Wireless power transfer and applications to sensor networks. 20(3):140–145.

[223] Xu, J., Liu, L., and Zhang, R. (2014). Multiuser miso beamforming for simultaneous wireless information and power transfer. *Transactions on Signal Processing*, 62(18):4798–4810.

[224] Yang, G., Ho, C. K., and Guan, Y. L. (2013). Dynamic resource allocation for multiple-antenna wireless power transfer. submitted to IEEE Trans. Signal Processing.

[225] Yang, L., Chen, Y., Li, X.-Y., Xiao, C., Li, M., and Liu, Y. (2014). Tagoram: Real-time tracking of mobile rfid tags to high precision using COTS devices. In *Proc. ACM MobiCom*, Hawaii, USA.

[226] Yeager, D. J., Powledge, P. S., Prasad, R., Wetherall, D., and Smith, J. R. (2008). Wirelessly-charged UHF tags for sensor data collection. In *Proc. IEEE RFID*, Las Vegas, NV, USA.

[227] Yoon, S. K., Kim, S. J., and Kwon, U. K. (2013). Energy relaying in mobile wireless sensor networks. In *Proc. IEEE CCNC*, Las Vegas, NV, USA.

[228] Younis, O. and Fahmy, S. (2004). Heed: a hybrid, energy-efficient, distributed clustering approach for ad hoc sensor networks. *IEEE Transactions on Mobile Computing*, pages 366–379.

[229] Zhang, P., Gummeson, J., and Ganesan, D. (2012). Blink: A high throughput link layer for backscatter communication. In *Proc. ACM MobiSys*, Low Wood Bay, Lake District, UK.

[230] Zhao, M., Li, J., and Yang, Y. (2014). A framework of joint mobile energy replenishment and data gathering in wireless rechargeable sensor networks. 3(12):2689–2705.

[231] Zhu, W., Cao, J., Xu, Y., Yang, L., and Kong, J. (2014). Fault-tolerant rfid reader localization based on passive rfid tags. *IEEE Trans. Parallel Distrib. Syst.*, 25(8):2065–2076.

[232] Zigbee (2016). *Zigbee Homepage*. http://www.zigbee.org/.

[233] Zink, M., Westbrook, D., Abdallah, S., Horling, B., Lakamraju, V., Lyons, E., Manfredi, V., Kurose, J., and Hondl, K. (2005). Meteorological command and control: An end-to-end architecture for a hazardous weather detection sensor network. In *Proceedings of the 2005 workshop on End-to-end, sense-and-respond systems, applications and services*, pages 37–42. USENIX Association.